


5-2013

Molecular Mechanisms of Vascular Disease in Patients with Rare Variants in MYH11

Callie Kwartler

Follow this and additional works at: http://digitalcommons.library.tmc.edu/utgsbs_dissertations

 Part of the [Cell Biology Commons](#), and the [Medicine and Health Sciences Commons](#)

Recommended Citation

Kwartler, Callie, "Molecular Mechanisms of Vascular Disease in Patients with Rare Variants in MYH11" (2013). *UT GSBS Dissertations and Theses (Open Access)*. Paper 329.

This Dissertation (PhD) is brought to you for free and open access by the Graduate School of Biomedical Sciences at DigitalCommons@The Texas Medical Center. It has been accepted for inclusion in UT GSBS Dissertations and Theses (Open Access) by an authorized administrator of DigitalCommons@The Texas Medical Center. For more information, please contact laurel.sanders@library.tmc.edu.

MOLECULAR MECHANISMS OF VASCULAR DISEASE IN PATIENTS WITH
RARE VARIANTS IN *MYH11*

by

Callie Savannah Kwartler, B.A.

APPROVED:

Dianna M. Milewicz, M.D., Ph.D., Advisor

Rebecca Berdeaux, Ph.D.

Dorothy Lewis, Ph.D.

Yi-Ping Li, Ph.D.

Heinrich Taegtmeyer, M.D., D.Phil

APPROVED:

Dean, The University of Texas Graduate School of Biomedical Sciences at Houston

MOLECULAR MECHANISMS OF VASCULAR DISEASE IN PATIENTS WITH
RARE VARIANTS IN *MYH11*

A THESIS

Presented to the Faculty of
The University of Texas
Health Science Center at Houston

And

The University of Texas
M.D. Anderson Cancer Center
Graduate School of Biomedical Sciences

in Partial Fulfillment

of the Requirements

for the Degree of

DOCTOR OF PHILOSOPHY

by

Callie Savannah Kwartler, B.A.

Houston, TX

May 2013

Acknowledgements

I would like to thank my advisor, Dianna Milewicz. Dianna, my time in your lab has unequivocally helped me grow as a scientist and as a person, and your faith in me has played a huge role in that. Thank you for trusting me with these projects, and for supporting me intellectually and emotionally for the past five and a half years.

I would like to thank all of the faculty who have served on my various committees and put up with my constant requests for help. In particular, I would like to thank my Supervisory Committee members: Rebecca Berdeaux, Yi-Ping Li, Dorothy Lewis, and Heinrich Taegtmeier. Thank you for your time and your feedback.

I would like to thank Henry Epstein, who advised me on my SM1 project and taught me so much about myosin. I would like to thank James Stull, Kristine Kamm, and Jian Huang who let me come learn about contractility and force in the aorta.

I would like to thank my labmates over the past several years for some unforgettable shared times. To Christina, Amy, Carlos, and Jiumei for their support and friendship, and for listening to me vent at various times over the years. To Limin and Shao-Qing for their willingness to help at any time. To Jiyuan for the last month of very late nights helping me pull this thesis together. And to everyone else for making this lab feel like my home.

I would like to thank Kedryn Baskin, who listened to my ideas and helped me through the rough parts of my project. I would like to thank Dhananjay Thakur for his help with the calcium imaging, and for putting up with me on the many long days we spent together. I would like to thank everyone else in the Cell and Regulatory Biology program for making the hard parts of graduate school just a little easier.

Of course, I would like to thank my family and friends: my mother, who has supported me every day of my life, and has been there throughout this process trying to understand, my father, who knows just the right time to remind me how amazing I am, my sisters, who distract me and frustrate me and make me laugh, Eric's family, who have embraced me and given me a true second family, Caroline for being my constant cheerleader, Nupur for her pragmatic wisdom and great conversations, Katerina for being the only person in the world who understands exactly what I am going through, and, of course, my husband, whose love and support for the past eleven years have made me who I am. I am extremely lucky to have so many people who love and support me. Thank you.

MOLECULAR MECHANISMS OF VASCULAR DISEASE IN PATIENTS WITH
RARE VARIANTS IN *MYH11*

Publication No. _____

Callie Savannah Kwartler, B.A.

Advisor: Dianna M. Milewicz, M.D., Ph.D.

Thoracic aortic aneurysms and dissections (TAAD) are the primary disease affecting the thoracic ascending aorta, with an incidence rate of 10.4/100,000. Although about 20% of patients carry a mutation in a single gene that causes their disease, the remaining 80% of patients may also have genetic factors that increase their risk for developing TAAD. Many of the genes that predispose to TAAD encode proteins involved in smooth muscle cell (SMC) contraction and the disease-causing mutations are predicted to disrupt contractile function. SMCs are the predominant cell type in the ascending aortic wall. Mutations in *MYH11*, encoding the smooth muscle specific myosin heavy chain, are a rare cause of inherited TAAD. However, rare but recurrent non-synonymous variants in *MYH11* are present in the general population but do not cause inherited TAAD. The goal of this study was to assess the potential role of these rare variants in vascular diseases. Two distinct variants were selected: the most commonly seen rare variant, *MYH11* R247C, and a duplication of the chromosomal region spanning the *MYH11* locus at 16p13.1. Genetic analyses indicated that both of these variants were significantly enriched in patients with TAAD compared with controls.

A knock-in mouse model of the *Myh11* R247C rare variant was generated, and these mice survive and reproduce normally. They have no structural abnormalities of the aorta or signs of aortic disease, but do have decreased aortic contractility.

Myh11^{R247C/R247C} mice also have increased proliferative response to vascular injury *in vivo* and increased proliferation of SMCs *in vitro*. *Myh11*^{R247C/R247C} SMCs have decreased contractile gene and protein expression and are dedifferentiated. In fibroblasts, myosin force generation is required for maturation of focal adhesions, and enhancers of RhoA activity replace enhancers of Rac1 activity as maturation occurs. Consistent with these previous findings, focal adhesions are smaller in *Myh11*^{R247C/R247C} SMCs, and there is decreased RhoA activation. A RhoA activator (CN03) rescues the dedifferentiated phenotype of *Myh11*^{R247C/R247C} SMCs.

Myh11^{R247C/R247C} mice were bred with an existing murine model of aneurysm formation, the *Acta2*^{-/-} mouse. Over time, mice carrying the R247C allele in conjunction with heterozygous or homozygous loss of *Acta2* had significantly increased aortic diameter, and a more rapid accumulation of pathologic markers. These results suggest that the *Myh11* R247C rare variant acts as a modifier gene increasing the risk for and severity of TAAD in mice.

In patients with 16p13.1 duplications, aortic *MYH11* expression is increased, but there is no corresponding increase in smooth muscle myosin heavy chain protein. Using SMCs that overexpress *Myh11*, we identified alterations in SMC phenotype leading to excessive protein turnover. All contractile proteins, not just myosin, are affected, and the proteins are turned over by autophagic degradation. Surprisingly, these cells are also more contractile compared with wild-type SMCs.

The results described in this dissertation firmly establish that rare variants in *MYH11* significantly affect the phenotype of SMCs. Further, the data suggests that these rare variants do increase the risk of TAAD via pathways involving altered SMC phenotype and contraction. Therefore, this study validates that these rare genetic variants alter vascular SMCs and provides model systems to explore the contribution of rare variants to disease.

Table of Contents

Acknowledgements.....	iii
Abstract.....	v
Table of Contents.....	viii
List of Illustrations.....	x
List of Tables.....	xiii
List of Abbreviations.....	xiv
CHAPTER ONE: Introduction.....	1
The Aorta.....	2
Smooth muscle contractile function.....	4
Smooth muscle myosin isoforms and contractile function.....	10
Smooth muscle cell phenotypic plasticity.....	11
Thoracic Aortic Aneurysms and Dissections.....	13
Genetic Basis of TAAD.....	16
TGF- β Signaling and TAAD.....	19
Smooth muscle cell dysfunction and TAAD.....	21
Sporadic TAAD.....	23
Rare Variants, <i>MYH11</i> , and TAAD.....	24
CHAPTER TWO: Rare Nonsynonymous Variant in Smooth Muscle Myosin, <i>Myh11</i>	
R247C, Alters SMC Phenotype.....	26
Introduction.....	27
Materials and Methods.....	32
Results.....	36

Discussion	46
CHAPTER 3: <i>Myh11</i> R247C allele modifies the aneurysm phenotype of <i>Acta2</i> ^{-/-}	
mice	51
Introduction.....	52
Materials and Methods.....	55
Results	60
Discussion.....	67
CHAPTER 4: 16p13 Duplications Lead to Increased Contractile Protein Turnover	70
Introduction.....	71
Materials and Methods.....	75
Results	78
Discussion.....	93
CHAPTER 5: DISCUSSION.....	99
SMC proliferation drives genetically triggered vascular occlusive disease...	100
Decreased contractility and aneurysm formation.....	104
Aortic dissection: the black box.....	110
References.....	115
Vita.....	155

List of Illustrations

Figure 1.1: Arterial Structure.....	2
Figure 1.2: Elastin-Contractile Unit.....	3
Figure 1.3: Myosin monomer ultrastructure	5
Figure 1.4: Schematic of signaling events leading to SMC contraction.....	6
Figure 1.5: Myosin head domain structure.....	7
Figure 1.6: Actin-Myosin kinetic cycle.....	8
Figure 1.7: Isoforms of smooth muscle myosin heavy chain.....	9
Figure 1.8: Smooth muscle cell phenotypic switching.....	11
Figure 1.9: Thoracic aortic aneurysms and dissections.....	13
Figure 1.10: Medial degeneration.....	15
Figure 1.11: Contractile dysfunction in familial TAAD.....	22
Figure 2.1: Generation of <i>Myh11</i> ^{R247C/R247C} knockin mice.....	28
Figure 2.2: Decreased contractility without aortic disease in <i>Myh11</i> ^{R247C/R247C} mice	30
Figure 2.3: Increased vascular injury response in <i>Myh11</i> ^{R247C/R247C} mice.....	31
Figure 2.4: <i>Myh11</i> ^{R247C/R247C} SMCs are dedifferentiated.....	36
Figure 2.5: The SRF:MRTF axis drives dedifferentiation in <i>Myh11</i> ^{R247C/R247C} SMCs	38
Figure 2.6: Altered focal adhesions in <i>Myh11</i> ^{R247C/R247C} SMCs.....	40
Figure 2.7: CN03 treatment drives actin polymerization in <i>Myh11</i> ^{R247C/R247C} SMCs	41

Figure 2.8: CN03 treatment drives SMC differentiation in <i>Myh11</i> ^{R247C/R247C} SMCs	43
.....	
Figure 2.9: Focal adhesion kinase activation in <i>Myh11</i> ^{R247C/R247C} SMCs	44
Figure 2.10: <i>Myh11</i> ^{R247C/R247C} SMCs within the aortic wall are not dedifferentiated	46
.....	
Figure 2.11: Proposed model of phenotypic alteration in <i>Myh11</i> ^{R247C/R247C} SMCs	50
Figure 3.1: Aneurysm formation in <i>Acta2</i> ^{-/-} mice	53
Figure 3.2: No aortic dilation in <i>Acta2</i> ^{-/-} <i>Myh11</i> ^{R247C/R247C} mice at 4 weeks of age	59
Figure 3.3: <i>Myh11</i> R247C allele modifies <i>Acta2</i> ^{-/-} aortic phenotype at 8 weeks of age	60
.....	
Figure 3.4: <i>Myh11</i> R247C allele increases <i>Acta2</i> ^{-/-} aortic diameter at 12 weeks of age	61
.....	
Figure 3.5: <i>Myh11</i> R247C allele does not affect medial degeneration in <i>Acta2</i> ^{-/-} aortas at 12 weeks of age	62
.....	
Figure 3.6: <i>Myh11</i> R247C allele increases <i>Acta2</i> ^{-/-} aortic diameter at 24 weeks of age	64
.....	
Figure 3.7: <i>Myh11</i> R247C allele increased proteoglycan deposition in <i>Acta2</i> ^{-/-} aortas at 24 weeks of age	65
.....	
Figure 3.8: <i>Myh11</i> R247C allele does not affect contractility of <i>Acta2</i> ^{-/-} aortas	66
Figure 4.1: Transgenic overexpression of myosin isoforms alters aortic contractility	73
.....	
Figure 4.2: Unc45 overexpression drives myosin degradation in <i>C. elegans</i>	74

Figure 4.3: Changes in contractile gene expression and Unc45 isoform expression in tissue from 16p13 duplication patients.....	79
Figure 4.4: SM1 transgenic cells recapitulate phenotype of patient tissue.....	80
Figure 4.5: Increased protein turnover in SM1 SMCs.....	82
Figure 4.6: Autophagy, not the proteasome, drives protein degradation in SM1 SMCs	83
Figure 4.7: Increased autophagy markers in SM1 cells.....	85
Figure 4.8: Altered signaling pathways in SM1 cells.....	87
Figure 4.9: Increased contractility of SM1 SMCs.....	89
Figure 4.10: Changes in calcium in SM1 SMCs.....	91
Figure 4.11: Treatment with 4-PBA reduces autophagy in SM1 cells.....	92
Figure 4.12: Model of cellular pathways in SM1 cells.....	95
Figure 5.1: Co-occurrence of vascular occlusive disease with TAAD in <i>ACTA2</i> and <i>MYH11</i> families.....	102
Figure 5.2: Loss of SMC differentiation with <i>TGFBR2</i> mutations.....	107
Figure 5.3: Treatment with doxycycline, losartan, or a combination improves survival in <i>Fbn1</i> ^{mgR/mgR} mice.....	111

List of Tables

Table 2.1: Enzymatic activity of WT and R247C myosin.....	27
Table 2.2: Antibodies used in Chapter 2.....	34
Table 2.3: Buffer compositions used in Chapter 2.....	35
Table 3.1: n numbers of mice per genotype for each aspect of the study	55
Table 4.1: Antibodies used in Chapter 4	75

List of Abbreviations

4-PBA	4-phenylbutyric acid
<i>Acta2/ACTA2</i>	smooth muscle α -actin gene (mouse/human)
Agtr1	angiotensin II type 1 receptor
Agtr2	angiotensin II type 2 receptor
AMPK	AMP-associated protein kinase
<i>Cnn1/CNN1</i>	calponin gene (mouse/human)
CNV	copy number variant
ER	endoplasmic reticulum
FAK	focal adhesion kinase
<i>Fbn1</i>	fibrillin-1 gene
fTAAD	familial thoracic aortic aneurysms and dissections
GFP	green fluorescent protein
LC3	Microtubule-associated proteins 1A/1B light chain 3A
L-NAME	L-NG-Nitroarginine Methyl Ester
MLCK	myosin light chain kinase
MMP	matrix metalloproteinase
MRTF	myocardin related transcription factor
mTOR	mammalian target of rapamycin
<i>Myh11/MYH11</i>	smooth muscle myosin heavy chain gene (mouse/human)
NTG	non-transgenic
PERK	PKR-like ER-localized eIF2 α kinase

RFP	red fluorescent protein
RLC/MLC ₂₀	myosin regulatory light chain
SM1	cells with transgenic overexpression of the SM1A myosin isoform
SM2	cells with transgenic overexpression of the SM2A myosin isoform
SM-actin	smooth muscle α -actin protein
SMC	smooth muscle cell
SM-MHC	smooth muscle myosin heavy chain protein
SNP	single nucleotide polymorphism
SRF	serum response factor
TAAD	thoracic aortic aneurysms and dissections
<i>TGFBRI/2</i>	transforming growth factor β receptor 1 or 2 gene
<i>TGFB2</i>	transforming growth factor β 2 gene
TGF- β	transforming growth factor β
<i>Unc45a</i>	Unc45a gene
<i>Unc45b</i>	Unc45b gene

Chapter 1: Introduction

The Aorta

The aorta is the largest blood vessel in the body, and it carries blood directly from the left ventricle of the heart to feed the rest of the body. Like other vessels, there are three distinct layers of the aorta: the *tunica intima*, *tunica media*, and *tunica adventitia* [1,2]. A single cell layer of endothelial cells lining the vessel lumen forms the intimal layer of the vessel. The intimal layer acts as a barrier between the luminal blood and the vessel wall. The adventitial layer, on the external side of the vessel, is comprised of extracellular matrix collagens, fibroblasts, progenitor cells, and, in the case of the aorta, the *vasa vasorum* or “vessels of the vessels” which feed blood to the external portion of the aortic wall [3]. Most important for vascular function is the medial layer, which in the aorta and other elastic arteries consists of concentric layers of smooth muscle cells (SMCs) separated by rings of elastin fibers (**Figure 1.1A**) [1,2,4]. In smaller, “muscular” arteries, there are only two elastin rings at the borders separating the

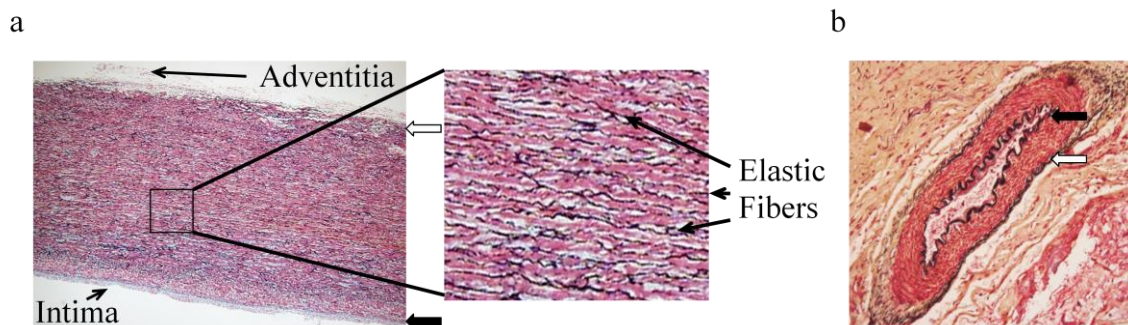


Figure 1.1 Arterial structure. A) Movat pentachrome stain of normal human aorta showing the aortic media comprised of concentric layers of smooth muscle cells (red) interspersed with elastic fibers (black). B) Movat pentachrome stain of human muscular artery from the *vasa vasorum*. Black arrows indicate internal elastic lamina, white arrows indicate external elastic lamina. Reprinted with permission from Genetics in Medicine [Genetic variants promoting smooth muscle cell proliferation can result in diffuse and diverse vascular diseases: Evidence for a hyperplastic vasculomyopathy. Milewicz DM, Kwartler CS, Papke CL, Regalado E, Cao J, Reid A. 2010.]

media from the intima and the adventitia (**Figure 1.1B**). In all vessels, elastic or muscular, the elastin ring separating the intimal and medial layers is termed the internal elastic lamina and the elastin ring separating the adventitial and medial layers is termed the external elastic lamina [2,4].

Elastin rings are laid down during development; no additional layers are added during adulthood in response to biomechanical forces or injury. The number of elastic lamellae is fixed and highly regulated for each portion of the vessel wall and each organism [4,5]. Increased numbers of elastin layers increase the tensile force that can be

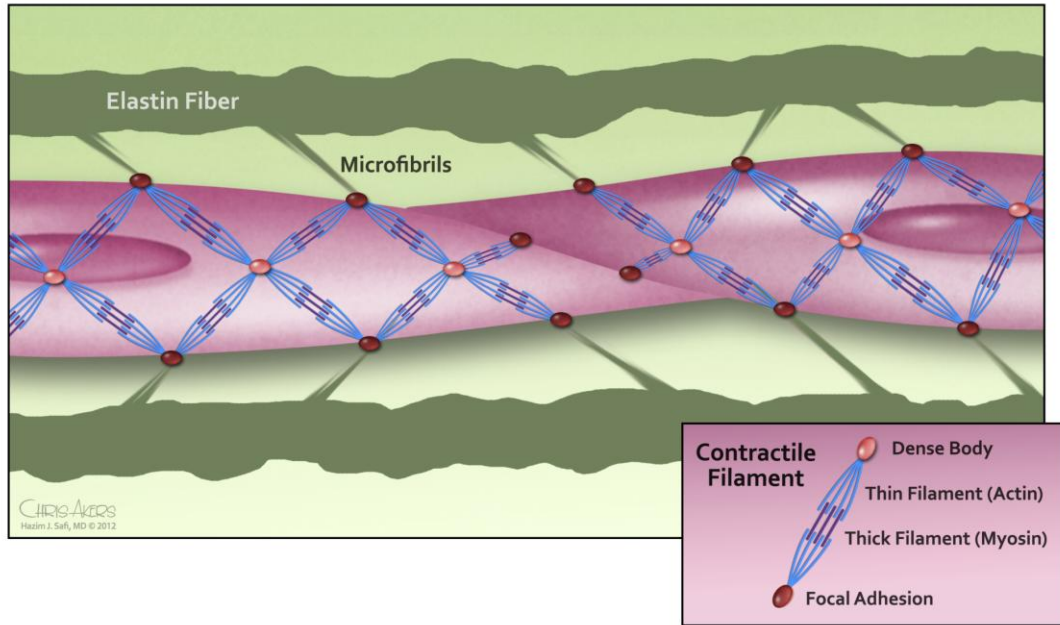


Figure 1.2 Elastin-contraction unit. Illustration shows the lamellar unit of the aortic wall, with linear connections between the smooth muscle cell contractile units and the elastic fibers formed by microfibrils. Reprinted with permission Elsevier Books [MuscleFundamental Biology and Mechanisms of Disease, Volume 2 , Chapter 97 “Genetic Variants in Smooth Muscle Contraction and Adhesion Genes Cause Thoracic Aortic Aneurysms and Dissections and Other Vascular Diseases”. Milewicz DM, Kwartler CS.]

generated by the vessel walls, so generally vessels that experience increased pulsatile pressures, like the thoracic ascending aorta, have the highest numbers of elastic layers [6,7].

In the aortic wall, individual layers of SMCs surrounded by two elastin rings are termed “lamellar units” (**Figure1.2**). The elastin fibers connect to the SMCs via microfibrils, composed predominantly of fibrillin-1 with other supporting extracellular matrix proteins like fibronectin [1,8]. Contact between the microfibrils and the cell body occurs at points on the cell surface known as dense plaques, also known as focal adhesions in single layered cell cultures. Dense plaques or focal adhesions are large and dynamic protein complexes that directly link with the contractile apparatus within the SMC. Thin filaments, comprised of smooth muscle specific α -actin, slide against thick filaments, whose backbone is formed by smooth muscle specific β -myosin heavy chain, to make up the contractile unit in SMCs. Additional adaptor proteins, like calponin, tropomyosin, and smoothelin, stabilize the structure and enhance the function of the contractile unit.

Smooth muscle contractile function

Like all muscle cells, SMCs depend on the motor function of myosin to drive contraction [9]. Filaments of myosin contain units of 6-protein complexes: two heavy chains, two regulatory light chains, and two essential light chains. Each myosin heavy chain has a globular head domain that contains actin-binding and ATP-binding sites, a linker domain which contains the sites of light chain binding, and a coiled-coil domain which enables interaction with other myosin heavy chain monomers to form first dimers,

then filamentous multimers (**Figure 1.3**). SMCs do not have a rigidly structured sarcomere like cardiac and skeletal muscle cells, but rather have dynamic contractile filaments arranged in a lattice-like structure spanning the cell body [10].

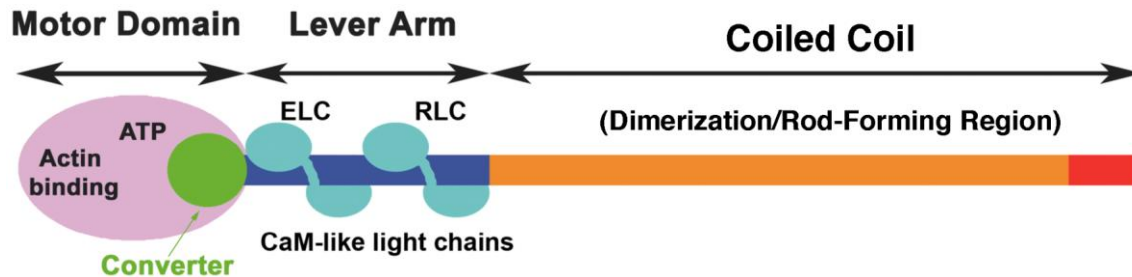


Figure 1.3 Myosin monomer ultrastructure. Illustration shows overall structure of the myosin molecule with a globular catalytic head domain, a lever arm where binding of light chain occurs, and a coiled coil domain for filament formation. Figure prepared by H. Lee Sweeney, Ph.D. and reprinted with permission.

Some studies suggest that the myosin thick filaments in SMCs actually form in response to contractile stimuli [11]. Although there are some stable filaments within the resting SMC, stimulation of contraction drives the number of thick filaments to increase, suggesting that monomeric pools of myosin may exist in a relaxed SMC [11,12].

Phosphorylation of the myosin regulatory light chain (RLC) is responsible for both the formation of thick filaments and also the activation of filamentous myosin through activating cross-bridges with actin in thin filaments [13]. The phosphorylation of the RLC is controlled by a specific kinase, myosin light chain kinase (MLCK), and a phosphatase (**Figure 1.4**). MLCK is primarily activated by increased intracellular calcium ion concentration and binding of calcium ions to calmodulin. The calcium-calmodulin complex dramatically upregulates the activity of MLCK to phosphorylate RLC at serine 19 [14]. Adrenergic receptor stimulation leads to release of calcium ions from the sarcoplasmic reticulum, which in turn activates a number of ion channels on the cell surface, magnifying the ionic excitation within the cell [15]. After stimulation ends,

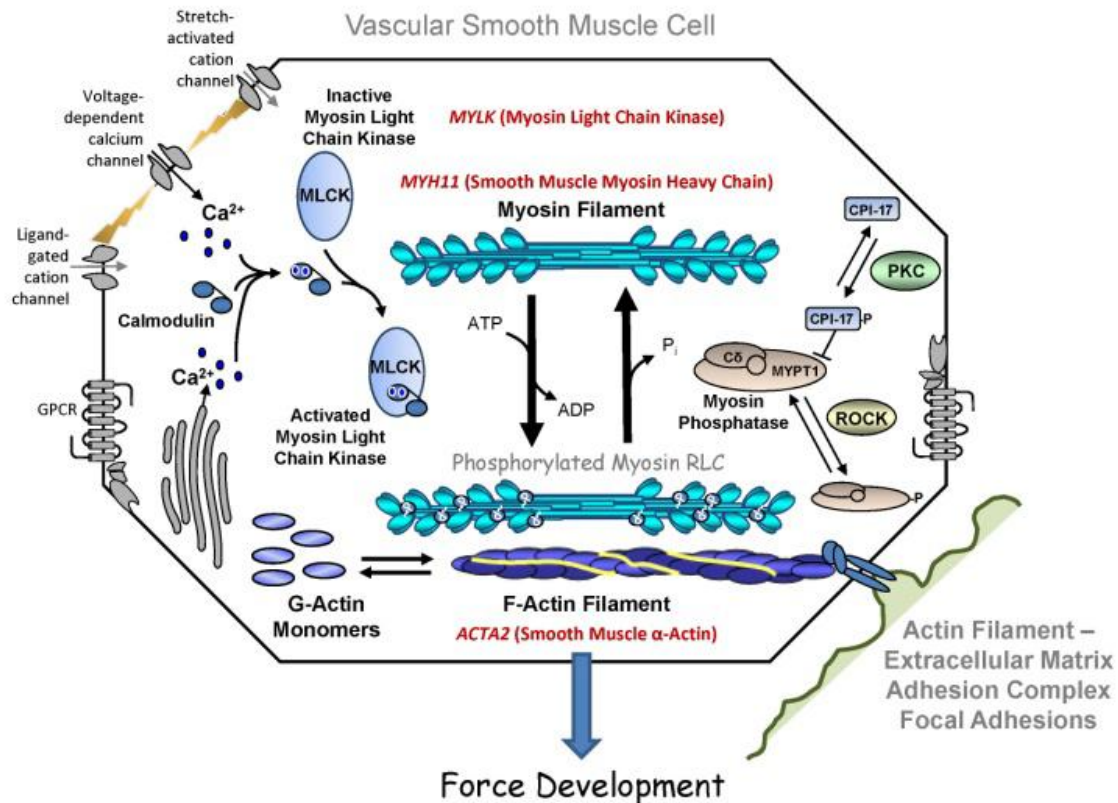


Figure 1.4 Schematic of signaling events leading to SMC contraction. Illustration shows signaling events in vascular SMCs leading to contraction. The key event driving contraction is phosphorylation of the myosin light chain. Figure prepared by James T. Stull, Ph.D., and Kristine Kamm, Ph.D., and reprinted with permission.

loss of intracellular calcium leads to a decrease in MLCK activity, and the myosin light chain phosphatase is able to de-phosphorylate RLC. The phosphatase is a protein complex comprised of three units: a catalytic unit (PP1C), a targeting subunit (MYPT), and a protein of unknown function (M20); its activity can be modulated by a variety of cellular signaling events, including activation of Rho-associated protein kinase (ROCK) or phospho-lipase C γ , which lead to downregulation of phosphatase activity and sensitizes the SMC to pro-contractile stimuli [16,17].

Myosin is by definition an actin-activated ATPase, with a nucleotide binding pocket and catalytic activity allowing the hydrolysis of ATP into ADP + Pi. There are three major globular domains of the head, of which one (the 50kD domain) is split by a

large cleft known as the 50kD cleft. The two sides of the cleft are separated by a loop known as “switch II.” Actin binds to a series of loops on the external surface of both the upper 50kD domain and the lower 50kD domain. Nucleotide binding occurs near the switch II loop at the joint of the two halves of the 50kD domain. Two flexible linkers, a relay loop and the SH1 helix connect the 50kD domain to the converter domain, which is adjacent to the lever arm (**Figure 1.5**) [18,19].

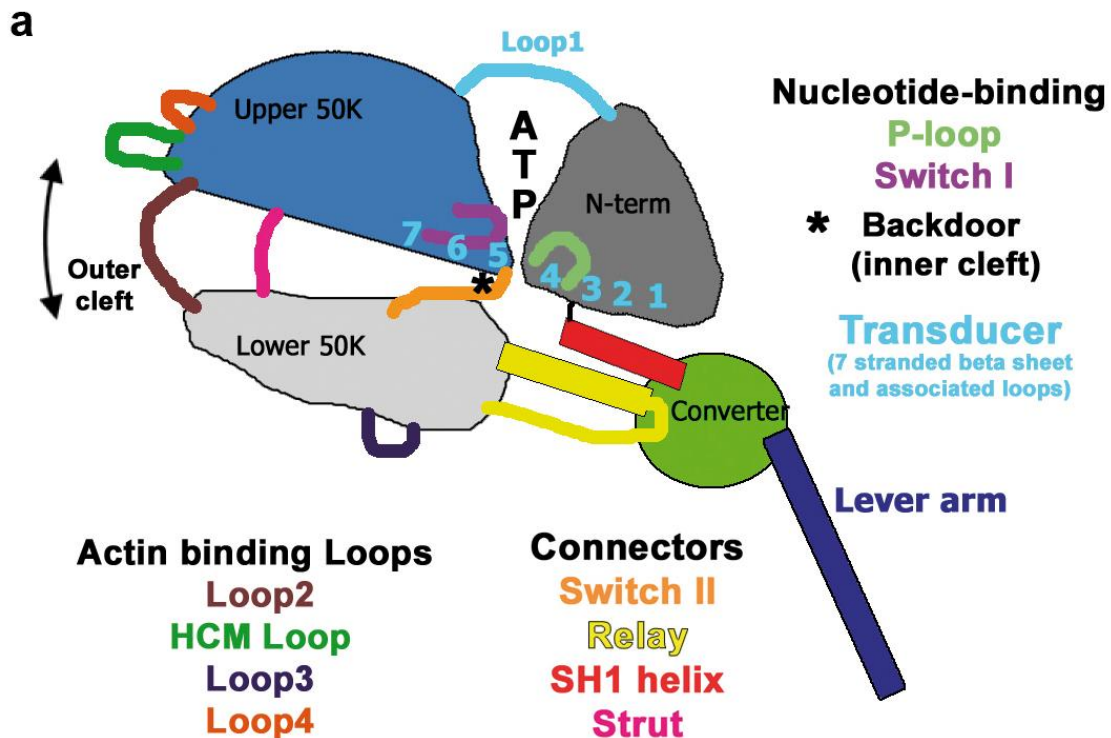


Figure 1.5 Myosin head domain structure. Illustration shows subdomains within the myosin head domain that are crucial for motor function. Actin binds between the upper 50K domain and the lower 50K domain. Figure prepared by H. Lee Sweeney, Ph.D. and reprinted with permission.

The myosin kinetic cycle involves a number of conformational rearrangements of the subdomains of the head (**Figure 1.6**). In the prepowerstroke structure, the 50kD cleft is partially closed at the site of nucleotide binding [20]. Actin is either unbound or

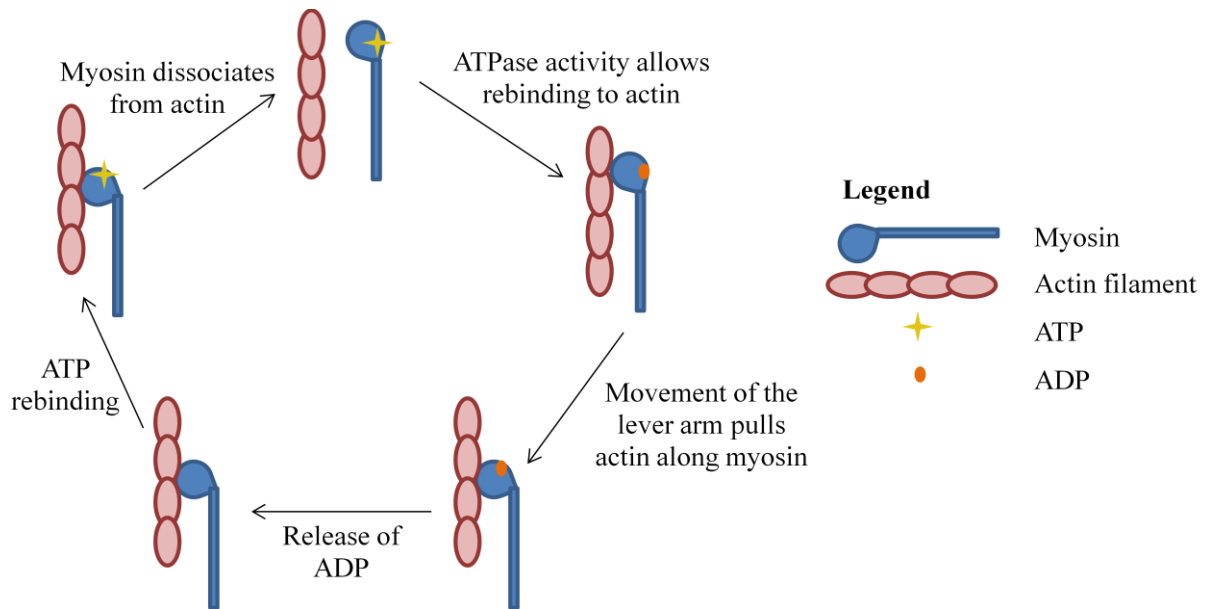


Figure 1.6 Actin-Myosin kinetic cycle. Illustration of the basic steps in the actin-myosin kinetic cycle.

weakly bound, and as ATP is hydrolyzed the gamma phosphate is trapped at the binding site [21]. This leads to full closure of the cleft, allowing all the actin-binding loops to be brought together for strong actin binding, and the “back door” of switch II opens to release the phosphate group [22]. These relatively small motions in the 50kD domain are transduced through the converter domain and the lever arm swings around to provide the full range of force-generating motion of the powerstroke [23]. After the stroke, the molecule is in a rigor-like state where the cleft is completely closed. The cycle is completed when ADP is released, ATP is rebound, actin dissociates from myosin, and the lever arm is reprimed for the next stroke.

Within the vessel wall, SMC contraction is regulated by blood flow from the heart and autonomic nervous cues, like the release of contractile agonist epinephrine. However, elastic fibers produce the majority of the tensile force within the aortic wall, and the role of SMCs in vascular contractility is debated [7]. In one study, vascular rings

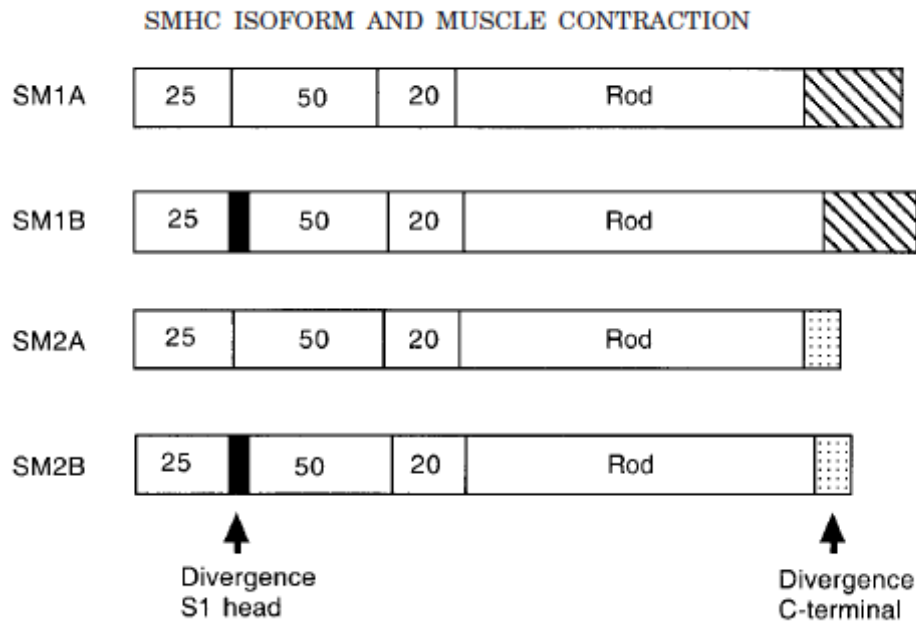


Figure 1.7 Isoforms of smooth muscle myosin heavy chain. Illustration shows the four isoforms of smooth muscle myosin heavy chain encoded by *MYH11*. -A and -B differ from each other by inclusion of a seven amino acid insertion in the head domain. -1 and -2 harbor distinct c-terminal exons. Reprinted with permission from John Wiley and Sons [Smooth muscle myosin heavy chain isoforms and their role in muscle physiology. Babu GJ, Warshaw DM, Periasamy M. *Microscopy Research and Technique*. 2000].

were subjected to pressure, and contractility was measured, both before and after administration of a substance that killed the SMCs. Both measurements revealed the same distensibility and contractile force generation, suggesting that the cells do not contribute to the mechanical properties of the vessel [24]. Other studies have alternately shown a role for SMC contraction in large arteries during acclimation to increased biomechanical forces [25,26]. Currently, consensus in the field suggests that SMCs act as biomechanical sensors in small arteries, responding to stimuli and regulating contraction in response to changes in pressure, but the role of SMCs in large, elastic arteries has not been determined.

Smooth muscle myosin isoforms and contractile function

The gene encoding smooth muscle myosin heavy chain (*MYH11*) actually encodes four separate mRNA transcripts which are translated into distinct isoforms of myosin heavy chain. The four isoforms are designated as SM1A, SM2A, SM1B, and SM2B; the designation of A vs. B is determined by the presence (B) or absence (A) of a seven amino acid insertion within the myosin head region, while the designation of 1 vs. 2 is determined by inclusion of distinct N-terminal exons (**Figure 1.7**). SM-B isoforms are predominantly expressed in the bladder and intestines; although some SM-B expression is observed in smaller arteries it is absent from the mature aorta [27]. In mice, knockout of the SM-B isoforms results in decreased shortening velocity but increased force generation in the smaller arteries and significantly reduced force generation in the bladder [28].

SM1A and SM2A are each expressed highly within the aorta, though vascular injury or atherosclerotic remodeling results in a decrease in specific expression of SM2A [29,30]. *In vitro* studies show that SM2 myosin has a higher critical concentration for filament assembly than SM1 myosin [31]. Specific knockout of the SM2 isoforms similarly resulted in increased contractile responses to stimuli, and additionally caused lethality by 4 weeks of age due to multiorgan failure [32]. These results suggest the importance of regulating smooth muscle contractile function in maintaining a healthy and viable mouse. Furthermore, transgenic overexpression of either SM1A or SM2A lead to dramatically different physiologic changes: SM1A overexpression increases force generation in both the aorta and bladder smooth muscle, whereas SM2A

overexpression decreases force generation in both tissues [33]. However, in both transgenic models, the ratio of expression of SM1 to SM2 was unaltered by specific overexpression of one isoform [33]. The latter strongly suggests that myosin isoform ratios are tightly controlled within each tissue, and that very small changes in those isoform ratios may result in highly significant changes in the contractile properties of the muscle tissue.

Smooth muscle cell phenotypic plasticity

Smooth muscle cells, unlike cardiac or skeletal muscle cells, retain phenotypic plasticity even in the mature vessel. Quiescent SMCs, such as those that populate the

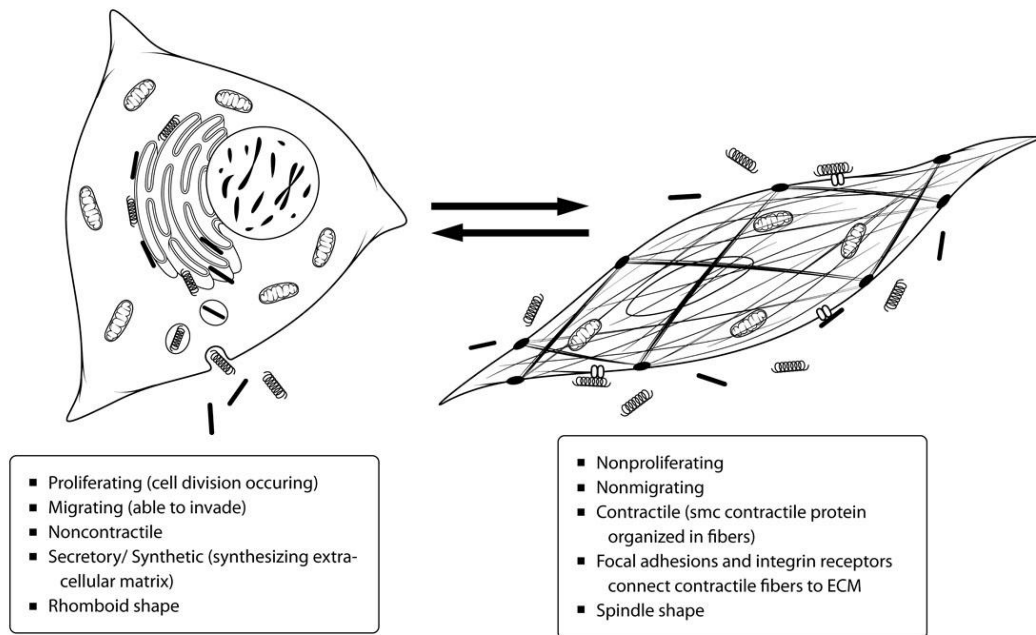


Figure 1.8 Smooth muscle cell phenotypic switching. Illustration shows two distinct phenotypes of vascular smooth muscle cells: on the left, the synthetic cell and on the right the contractile cell. Reprinted with permission from Genetics in Medicine [Genetic variants promoting smooth muscle cell proliferation can result in diffuse and diverse vascular diseases: Evidence for a hyperplastic vasculomyopathy. Milewicz DM, Kwartler CS, Papke CL, Regalado E, Cao J, Reid A. 2010.]

healthy aortic wall, are spindle shaped, do not proliferate or migrate, and express high levels of contractile proteins [34]. In these cells, the contractile proteins are assembled into the lattice-like filament structures; this phenotype is therefore termed “contractile.” However, in response to stimuli such as injury, growth factor signaling, or changes in mechanical force, SMCs can switch from expression of contractile genes to expression of growth-related and extracellular matrix-related genes [35]. The contractile filaments disassemble, and the cells proliferate, migrate, and secrete large quantities of matrix proteins to help repopulate damaged areas of the vessel wall or improve the strength of the wall in response to increased biomechanical pressures (**Figure 1.8**).

The dogma in SMC biology holds that SMCs can take on either a “contractile” or a “proliferative” phenotype, which are mutually exclusive. A canonical pathway, known as the serum response factor (SRF): myocardin related transcription factor (MRTF) axis, is thought to control the switch between the two phenotypes [36]. SRF is a promiscuous, and ubiquitously expressed, transcription factor, which can drive transcription of over 200 genes, and specificity for particular target genes is conferred via the binding of transcriptional coactivators [34,37,38]. Three members of the MRTF family of coactivators are specifically expressed in cardiomyocytes and SMCs: myocardin, MRTF-A, and MRTF-B [39]. Myocardin, which is constitutively localized to the nucleus, plays a key role in cardiac development; knockout of the *Myocd* gene leads to embryonic lethality at E10.5 due to heart and vascular development defects [40]. MRTF-A and -B, however, can move within the cell between the nucleus and the cytoplasm, and are predominantly expressed in SMCs [38,41]. Within the cytoplasm, monomeric or G-actin can bind to MRTFs, so as the contractile filaments disassemble in response to

growth factor or mechanical signals, MRTFs become sequestered in the cytoplasm. SRF is thus available to bind other coactivators, such as ternary complex factor (TCF), and drive expression of growth-related genes [38,39]. Differentiation of SMCs is accompanied by actin polymerization, as driven by the small G-protein RhoA. As actin polymerizes, MRTFs are free to move back into the nucleus, where they bind SRF and drive transcription of contractile genes [42].

Thoracic aortic aneurysms and dissections

Aortic aneurysms and dissections have an incidence of 10.4/100,000, and result in approximately 15,000 deaths per year [43]. An aneurysm is an enlargement of the vessel wall, and the natural history of thoracic aortic aneurysms is to progress to a

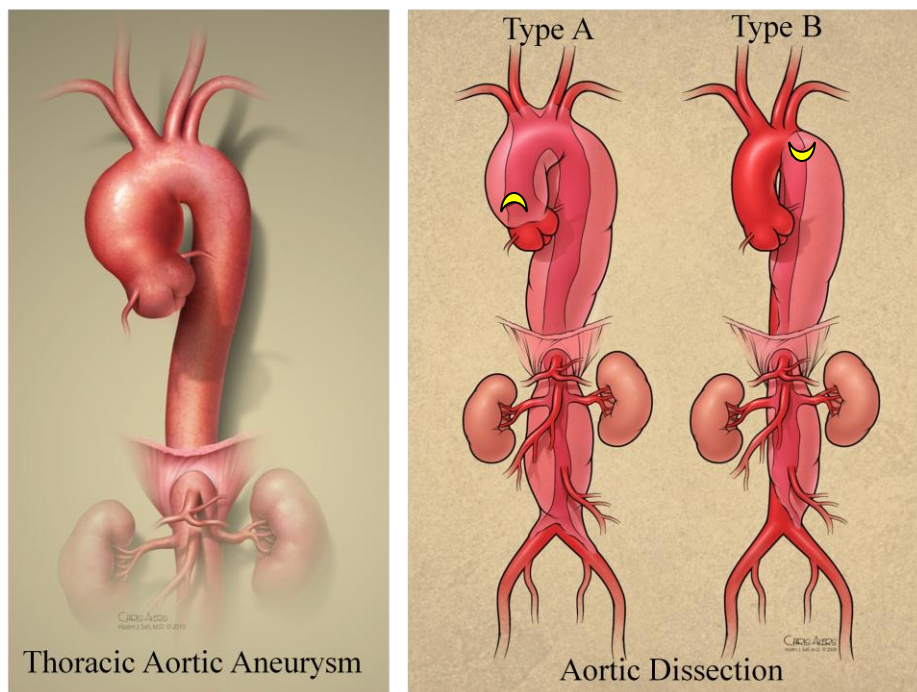


Figure 1.9 Thoracic aortic aneurysms and dissections. Illustration of ascending aortic aneurysm (left) and the Stanford classification of aortic dissection (right). Yellow indicates the site of the tear in the wall: the ascending aorta for a type A dissection vs the descending aorta for a type B dissection.

dissection, or tear in the wall, if the aneurysm is not surgically repaired [44,45].

Dissections are medical emergencies requiring immediate surgery; approximately one third of dissection cases die suddenly and the death rate in survivors of aortic dissections is 1% per hour until surgery is performed [45,46]. Thoracic aortic aneurysms and dissections, collectively termed “TAAD,” are classified by their location within the aorta. The Stanford classification system for aortic dissections classifies any tear originating in the ascending aorta as “Type A” while any tear originating in the descending aorta or arch is “Type B” (**Figure 1.9**) [43,47].

While aneurysms are typically asymptomatic, aortic dissections can cause severe chest pain, in conjunction with sudden changes in blood pressure, dyspnea, sweating, and a feeling of faintness or numbness [44]. Approximately 30 - 40% of patients with acute aortic dissections die before reaching the emergency room [45,46]. For those who do, the clinical presentation is similar to myocardial infarction, making this significantly less common disease difficult to diagnose. Any delay in diagnosis, however, increases the risk of death as the patients’ vascular function declines and the risk of complete aortic rupture increases. Standard diagnostic imaging to detect aortic dissection includes computed tomography (CT) scan and transesophageal echocardiography [45,46]. Surgical repair of the injured artery is the only available recourse for patients with acute dissections, but many patients do not survive the procedure.

Alternatively, if an aneurysm is detected prior to dissections, prophylactic repair can be performed when the aneurysms reaches approximately twice the normal diameter of the aorta [43]. This strategy greatly increases survival, so medical efforts should be focused on identifying patients at risk for TAAD, monitoring the patients, and

proliferation can occur. In other spaces within the wall, apoptotic death of SMCs leads to focal areas of cellular loss. The role of inflammation in the progression of TAAD is not well characterized, but evidence of macrophage accumulation is apparent in a subset of patients, particularly at the end stages of the disease [1,4].

Genetic basis of TAAD

There is a strong genetic component to the pathogenesis of TAAD. First, TAAD is a feature of a number of inherited syndromes, the best characterized of which is Marfan syndrome (MFS). Less than 5% of patients with TAAD have one of these genetic syndromes. An additional 15% of patients indicate a family history of the disease in the absence of syndromic features. These patients are classified as having “familial TAAD” or fTAAD, and their family members in turn are at high risk for the disease [45,51]. The remaining 80% of patients have no known genetic history of the disease, and are classified as “sporadic” or sTAAD. All genes identified to date for either syndromic or familial TAAD are inherited in an autosomal dominant manner. The natural history of the disease in any given patient or family is dependent upon the underlying mutation: some mutations lead to the formation of large stable aneurysms, while others can lead to dissection and rupture with minimal prior enlargement [52]. Thus, identifying mutations can help to dictate the preferred course of treatment for patients with this disease.

MFS is a connective tissue disorder which leads to abnormalities in the skeletal, ocular, pulmonary, and cardiovascular systems [53]. The gene mutated in MFS patients was identified in 1991 as *FBNI*, encoding the extracellular matrix protein fibrillin-1. As

described above, in the aorta fibrillin-1 is the major component of the microfibrils that connect SMCs with the elastin fibers. In addition to its important structural role, fibrillin-1 also plays a signaling role in the aortic wall by sequestering latent growth factors, in particular transforming growth factor β (TGF- β) [1,53]. Mutations in *FBNI* are proposed to induce excessive TGF- β signaling by inhibiting its sequestration in the matrix, and this excessive signaling is believed to underlie the pathogenesis of TAAD in MFS patients [54].

A role for dysregulated TGF- β signaling in TAAD is further supported by multiple mutations within the TGF- β signaling pathway itself that in some cases also cause a syndromic presentation. Mutations in *TGFBR1* and *TGFBR2*, encoding the two cell-surface receptors for the TGF- β ligand, underlie Loeys-Dietz Syndrome (LDS), which involves craniofacial dysmorphism, atrophic scarring, bifid uvula, and arterial tortuosity in addition to TAAD at a very young age [55,56]. Mutations in *SMAD3*, one of the canonical intracellular signaling molecules downstream of TGF- β , cause a presentation of TAAD in conjunction with osteoarthritis [57]. Finally, mutations in *TGFB2*, encoding one of the three TGF- β ligands, cause TAAD in conjunction with mild MFS-like features [58]. Mutations in all four genes can additionally cause fTAAD without significant syndromic features, suggesting that the classification of TAAD lies on a spectrum rather than three distinct and mutually exclusive presentations.

In addition to mutations in genes encoding proteins involved in TGF- β signaling, a second cluster of mutations has been identified leading to TAAD: mutations in genes encoding SMC-specific contractile proteins. The most commonly mutated gene in families with fTAAD is *ACTA2*, encoding the SMC-specific isoform of α -actin [59].

Additionally, mutations in *MYH11* encoding the SMC-specific myosin heavy chain, and in *MLCK* encoding the kinase which regulates myosin contractility, have been identified [60,61]. Furthermore, families with mutations in *MYH11* are also predisposed to a developmental disease known as patent ductus arteriosus (PDA) in which the fetal connection between the aorta and the pulmonary artery fails to close [61].

Surprisingly, studies of a large *ACTA2* family indicated that only 50% of mutation carriers developed TAAD; however, in addition to TAAD the mutation carriers in the family were also at high risk of early-onset vascular occlusive diseases like strokes or coronary artery disease [62]. Further studies of additional families confirmed that *ACTA2* mutations lead to both aneurysmal and occlusive vascular diseases. One particularly severe mutation, R179H, has been identified in a number of children with a syndrome-like presentation of global SMC dysfunction: primary pulmonary hypertension, hypoperistalsis in the gut, bladder dysfunction, and both aortic and cerebrovascular disease [63].

Intriguingly, pathologic examination of the occlusive vascular lesions in these patients reveals an absence of typical atherosclerotic features: the lesions are fibrin, calcium, and lipid poor. Instead, the occlusion appears to occur due solely to hyperplasia of SMCs, as the lesion is exclusively full of proliferating cells that stain positively for SMC markers [2]. These findings suggest that a single mutation can lead to a diverse array of vascular diseases, and that alteration of SMC phenotype towards a more proliferative phenotype may underlie some of the increased risk for vascular occlusive diseases.

TGF- β Signaling and TAAD

As described above, mutations of several components of the TGF- β signaling pathway have been associated with TAAD. The majority of these mutations are predicted to be loss-of-function [64]. However, other studies have reported a paradoxical increase in TGF- β signaling markers in late-stage disease tissue from TAAD patients harboring these mutations [54,58]. Thus, the specific role of TGF- β in driving aneurysm progression remains controversial.

The TGF- β superfamily of growth factors includes three distinct transforming growth factor β ligands. These three ligands each bind to a heterodimer of the two transforming growth factor β receptors (TGFBR1 and TGFBR2), which are receptor tyrosine kinases that phosphorylate each other as well as downstream targets in response to ligand binding. The canonical pathway downstream of the TGF- β receptors involves a family of molecules known as Smads; in response to TGF- β ligand binding to the receptors, Smad2 and Smad3, the receptor-regulated or R-Smads for TGF- β receptors, are activated. These two R-Smads can then bind to the co-Smad, Smad4, and translocate to the nucleus where they activate a program of signal transduction. In addition to the canonical Smad pathway, the TGF- β receptors can also activate non-canonical pathways leading to activation of mitogen-associated protein kinase (MAPK) signaling and other pathways [65].

TGF- β signaling produces a number of short- and long-term effects in SMCs. Many transcriptional targets of TGF- β signaling are extracellular matrix proteins, in particular collagens, which drive a process known as fibrosis. Transcription of extracellular matrix proteins is associated with the proliferative and synthetic phenotype

of SMCs that occurs post vascular injury. However, TGF- β signaling also drives differentiation of SMCs by inducing transcription of contractile genes including *ACTA2* and *MYH11* [66]. Extensive studies of SMCs from patients with mutations in *TGFBR1* or *TGFBR2* indicate that these SMCs are unable to differentiate properly. The cells are characterized by poor expression of contractile markers in conjunction with reduced proliferation and expression of collagen genes [64]. Interestingly, TGF- β signaling can activate both canonical Smad signaling and noncanonical signaling via MAPKs. Smad signaling is intact in *TGFBR2* cells, but non-canonical signaling through p38MAPK and Akt are blunted [64,67]. These studies clearly indicate a loss of function due to mutations in *TGFBR1* or *TGFBR2*, however increased phosphorylated Smads, indicative of increased TGF- β signaling, persist in the tissue.

A similar paradox occurs in patients with *TGFB2* mutations: the cells isolated from these patients show a decrease in *TGFB2* gene expression and TGF- β 2 protein accumulation, but in the diseased tissue both gene expression and protein accumulation are increased [58]. These confusing results suggest that, although these mutations are loss-of-function, at some point in the disease process signaling is turned on to a pathologically high level. However, the exact role of this excessive TGF- β signaling in driving the disease has yet to be established.

Smooth muscle cell dysfunction in TAAD

As genetic mutations in SMC-specific contractile proteins also cause TAAD, an alternative hypothesis regarding the underlying pathogenesis of the disease involves loss of SMC contractility and function. This hypothesis is intriguing, as mutations in the

TGF- β pathway may also lead to a loss of SMC contractility by impairing differentiation of SMCs as described above. Initial studies on SMCs isolated from *ACTA2* and *MYH11* patients support this hypothesis, as these cells completely lack the α -actin filaments that stretch across the entirety of wild-type cells (**Figure 1.11**) [59,68]. If contractile filaments do not form, contractile function in these cells must necessarily be impaired. Although, as described above, there is some debate as to the role of SMC contraction in regulating the mechanical properties of the aorta as a whole, if the SMCs are not able to contract the cells themselves will sense increased, unopposed tension. The cells may attempt to normalize the biomechanical stress by activating signaling pathways, and these signaling pathways, which might include excessive activation of TGF- β , may drive the disease process.

Mutations in *ACTA2* and *MYH11* at least have been correlated with occlusive vascular lesions characterized by hyperplastic SMCs. Our lab has performed a number of studies to confirm that cells harboring mutations in these genes do, in fact, proliferate more rapidly both in culture and *in vivo* [62]. The role of this cellular hyperplasia in driving occlusive disease seems obvious; however, it is unknown whether proliferation of SMCs contributes to aortic aneurysm development.

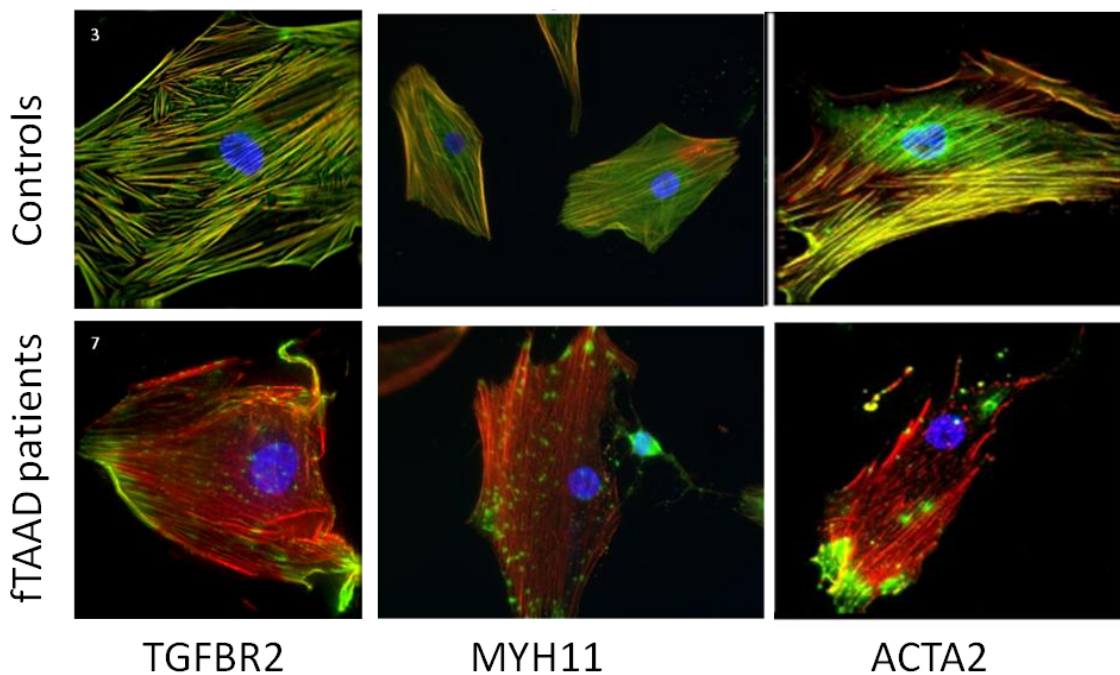


Figure 1.11 Contractile dysfunction in familial TAAD. Immunofluorescent staining of SMCs explanted from controls (top row) shows colocalization of SM-actin staining (green) with phalloidin (red) indicating polymerized SM-actin. SMCs explanted from fTAAD patients with mutations in three different proteins show a loss of polymerized SM-actin. Counterstained with DAPI (blue).

The pathways driving SMC hyperplasia in patients with mutations in *ACTA2* and *MYH11*, however, are less clear. Recent work in our lab has used SMCs completely lacking α -actin from the *Acta2*^{-/-} mouse model to elucidate these pathways. Surprisingly, in these cells the canonical SRF:MRTF axis does not drive hyperplasia. In fact, MRTFs are more nuclearly localized in *Acta2*^{-/-} SMCs than in wild-type cells. Rather, the hyperplasia is driven primarily by increased expression of platelet-derived growth factor receptor β (*Pdgfrb*) downstream of overly active focal adhesions (unpublished data). Follow-up work on a transgenic mouse model harboring a missense mutation in *Acta2* suggests that similar pathways may drive hyperplasia in patient SMCs in conjunction with the SRF:MRTF axis, which is activated by the pools of unpolymerized actin.

Sporadic TAAD

A majority of patients with TAAD do not have any family history of the disease. Well-established risk factors for aneurysm formation in non-familial patients include hypertension, bodybuilding, smoking, and stimulant drug use (e.g. cocaine). Hypertension is the most important risk factor for TAAD, suggesting that increased pressures on the aortic wall may underlie aneurysm pathogenesis [43,45]. Patients at risk for TAAD are thus advised to closely monitor their blood pressures, and doctors are prescribing blood pressure management medications such as beta-blockers to keep pressures low and decrease the acceleration of aortic blood flow [43].

Although sporadic TAAD patients are unlikely to have a causative genetic mutation underlying their disease, genetic factors may contribute to disease risk in these patients. Several recent studies have looked at potential genetic factors in non-familial TAAD, and these studies have confirmed that the pathways and mechanisms identified in familial patients are more widely applicable in understanding the disease. For example, single nucleotide polymorphisms (SNPs) in *FBNI*, the gene responsible for MFS, were highly associated with TAAD in a genome-wide association study (GWAS) [69]. A copy number variant (CNV) screen in sporadic TAAD patients identified a number of genomic deletions and duplication in these patients. Pathway analysis of the genes involved in these CNVs revealed a high proportion of these alterations hit genes involved in SMC contraction and focal adhesions [70]. These broad screens searching for genetic factors contributing to non-familial TAAD thus hit genes and pathways already known to be critically involved in inherited forms of the disease.

Single nucleotide polymorphisms (SNPs) are single amino acid changes in the genetic code that are common in the general population, and can be associated with a very low increase in risk of common diseases, usually a magnitude of 1-2%. While it is useful to look broadly at the genes where SNPs lie, the utility of identifying SNPs as either a diagnostic or a therapeutic tool is low. Mendelian mutations, by contrast, are extremely rare in the population, and correlate almost 100% with disease development. Thus, although studying these mutations allows specific identification of a few at-risk individuals, and certainly, as described above, contributes to overall understanding of the mechanisms of disease, they do not on their own allow us to study unique gene-environment interactions or to predict pathways that influence disease in a much broader spectrum of patients. A third class of genetic contributors to disease, known as rare variants, has both an intermediate allele frequency and an intermediate contribution of increased disease risk. The goal of this dissertation is to study the role of two specific rare variants in the *MYH11* gene in the pathogenesis of TAAD.

Rare variants, MYH11, and TAAD

Although Mendelian mutations in the *MYH11* gene have been associated with TAAD, the mutations identified in those families were uniformly large deletions or frameshift mutations. The exception is a single missense mutation identified in the converter domain: R712Q, which is predicted to dramatically alter the movement of the myosin head [68]. However, sequencing data shows that nonsynonymous missense alterations in *MYH11* are not uncommon in the general population. Furthermore, these alterations were more prevalent in patients with vascular disease than in vascular

disease-free controls. Therefore, we asked whether these single amino acid alterations might be contributing an increased risk of vascular disease in the general population. We chose to study a particular missense alteration, a substitution of a cysteine for an arginine at position 247.

At the same time, results from our initial CNV screen also yielded a surprising finding: a 12-fold enrichment in duplications at the 16p13 locus in the TAAD population compared with the control population. Directly in the middle of the duplicated region lies the *MYH11* gene. Based on our previous results implicating *MYH11* in TAAD, we hypothesized that *MYH11* duplications were the causative risk factor within the 16p13 duplication region. **Therefore, we hypothesized that either a missense mutation in the *MYH11* gene (R247C) or the duplication of the gene would alter SMC phenotype and increase the risk of TAAD.**

Chapter 2: Rare Nonsynonymous Variant in Smooth Muscle Myosin, *Myh11*

R247C, Alters SMC Phenotype

Introduction

For initial analysis of rare variants in *MYH11*, we selected the most recurrent rare missense mutation from our vascular disease cohort, R247C. Sequencing results indicate that this variant is found in patients with TAAD, intracranial aneurysms, early onset strokes, and other vascular diseases (unpublished data). This variant alters an arginine residue within the actin binding domain of the myosin motor head to a cysteine. Additionally, a mutation in the paralogous gene *MYH7*, encoding the cardiac β -myosin heavy chain, was previously identified to cause inherited cardiomyopathy [71,72]. Thus, the R247C variant is a good candidate for investigating the role of rare variants in *MYH11* in vascular disease pathogenesis.

	RLC Phos	Maximal actin-activated ATPase (sec ⁻¹ head ⁻¹ \pm SD) 25°C	In vitro motility (μ m/sec \pm SD) 30°C	Rate of P _i release (+ actin) (sec ⁻¹ \pm SD) 25°C	Rate of MgADP release (+ actin) (sec ⁻¹ \pm SD) 25°C	Duty Ratio (no load)
MYH11 WT	-	~0	0	N.D.	N.D.	
	+	0.87 \pm 0.07	0.38 \pm .06	1.2 \pm 0.3	24 \pm 3	.05
MYH11 R247C	-	~0	0	N.D.	N.D.	
	+	0.31 \pm 0.02	0.32 \pm .05	0.4 \pm 0.1	13 \pm 2	.03

Table 2.1 Enzymatic activity of WT and R247C myosin. Reprinted with permission from Wolters Kluwer Health. [Rare, Nonsynonymous Variant in the Smooth Muscle-Specific Isoform of Myosin Heavy Chain, MYH11, R247C, Alters Force Generation in the Aorta and Phenotype of Smooth Muscle Cells Novelty and Significance. Kuang SQ, Kwartler CS, Byanova KL, Pham J, Gong L, Prakash SK, Huang J, Kamm KE, Stull JT, Sweeney HL, Milewicz DM. *Circulation Research* 2012.]

Dr. H. Lee Sweeney's lab at the University of Pennsylvania performed an initial *in vitro* characterization of the variant by expressing a heavy meromyosin (HMM) construct of *MYH11* with and without the introduced R247C mutation in a baculovirus system. The resulting proteins were purified and put through a number of *in vitro* assays to characterize their function. First, actin-activated ATPase assays were performed using

phalloidin-stabilized actin molecules. Next, transient kinetic assays were performed to assess the rates of ADP release and inorganic phosphate release following the ATPase reaction. Finally, an *in vitro* motility assay was performed to assess the sliding filament velocity of actin moving along the myosin filaments. In each assay, the R247C mutant myosin molecules were significantly slower than the wild-type myosin molecules at performing these actions (**Table 2.1**). These results suggest that the R247C mutation decreases the enzymatic activity of the myosin motor and impedes its force generation, and further suggest that this alteration may contribute to disease pathogenesis.

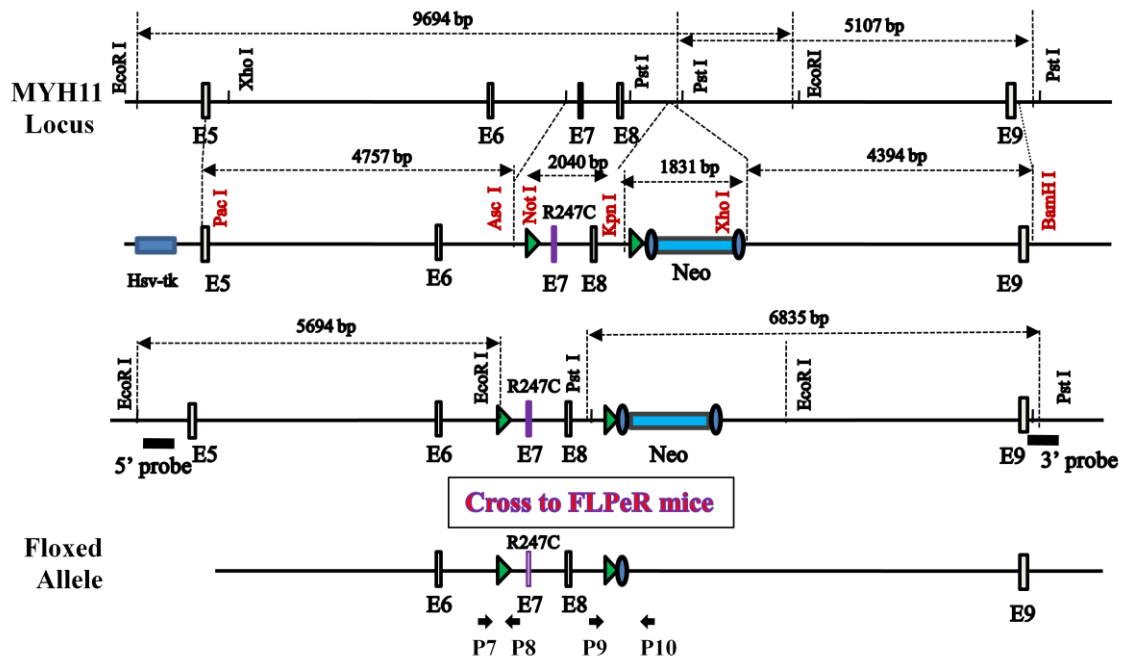


Figure 2.1 Generation of *Myh11*^{R247C/R247C} knockin mice. Schematic showing the design of the targeting strategy for generation of *Myh11*^{R247C/R247C} knockin mice. Reprinted with permission from Wolters Kluwer Health. [Rare, Nonsynonymous Variant in the Smooth Muscle-Specific Isoform of Myosin Heavy Chain, MYH11, R247C, Alters Force Generation in the Aorta and Phenotype of Smooth Muscle Cells Novelty and Significance. Kuang SQ, Kwartler CS, Byanova KL, Pham J, Gong L, Prakash SK, Huang J, Kamm KE, Stull JT, Sweeney HL, Milewicz DM. *Circulation Research* 2012.]

Next, we generated a knock-in mouse model carrying the R247C mutation (**Figure 2.1**). The targeting vector contained a positive neo selection cassette and a

negative tk selection cassette; the selection cassettes were enclosed within two inserted Frt sites for later removal. The mutation was introduced flanked by two loxP sites to allow future generation of a knock-out model. The mutation lies in exon 7 of the coding region, and the targeting vector spanned from intron 6 to intron 9. After construction, the vector was linearized and introduced via electroporation into 129SvEv mouse embryonic stem cells. Positive and negative selection were performed to screen for successfully transfected cells, and Southern blot analysis confirmed appropriate targeting. Finally, the targeted stem cells were injected into C57Bl6 blastocysts to generate founder mice, which were then bred with 129SvEv mice carrying the FLPeR recombinase which removed the Frt-flanked selection cassettes. The final knockin mice were thus generated as mixed 129SvEv and C57Bl6 background.

The Stull lab at University of Texas Southwestern Medical Center performed aortic contractility assays on the newly generated knockin mice. Briefly, aortic rings from the thoracic ascending, thoracic descending, and abdominal aorta were mounted on an isometric force apparatus. After equilibration, the rings were subjected to contractile stimuli, KCl or phenylephrine, and force generation was measured. Aortic rings from the *Myh11*^{R247C/R247C} mice had significantly reduced force generation when compared with wild-type in all three tested tissue locations (**Figure 2.2a**). Tissue was snap-frozen after the initial analysis, and lysates were subjected to urea/glycerol gel electrophoresis to separate phosphorylated myosin light chain from non-phosphorylated. There was no difference in regulatory light chain phosphorylation from the *Myh11*^{R247C/R247C} mice compared with wild-type, indicating that reduced force generation was due to intrinsic

properties of the myosin motor rather than a defect in the signaling leading to contraction (**Figure 2.2b**).

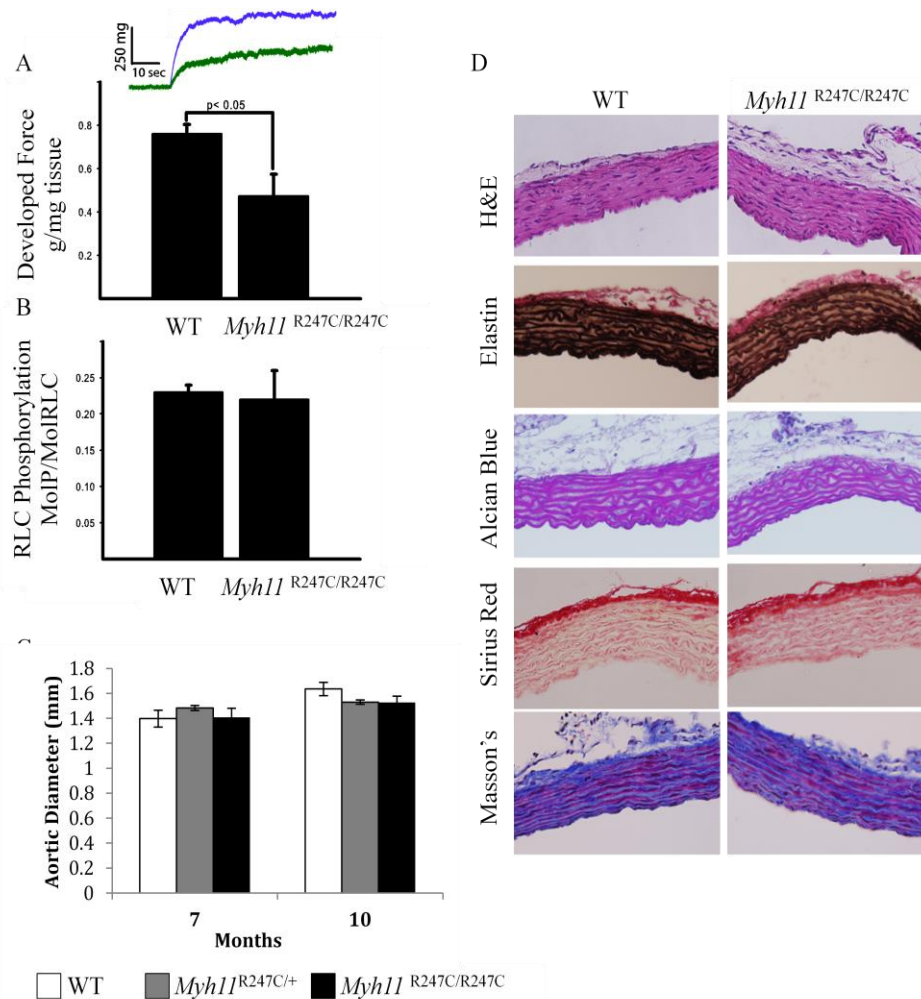


Figure 2.2 Decreased contractility without aortic disease in *Myh11*^{R247C/R247C} mice. A) Decreased force generation by *Myh11*^{R247C/R247C} knockin mice. B) No change in the myosin light chain phosphorylation in *Myh11*^{R247C/R247C} knockin mice. C) *Myh11* genotype has no effect on aortic diameter. D) *Myh11*^{R247C/R247C} knockin mice have no pathologic signs of aortic disease. Reprinted with permission from Wolters Kluwer Health. [Rare, Nonsynonymous Variant in the Smooth Muscle-Specific Isoform of Myosin Heavy Chain, MYH11, R247C, Alters Force Generation in the Aorta and Phenotype of Smooth Muscle Cells Novelty and Significance. Kuang SQ, Kwartler CS, Byanova KL, Pham J, Gong L, Prakash SK, Huang J, Kamm KE, Stull JT, Sweeney HL, Milewicz DM. *Circulation Research* 2012.]

Despite the decrease in aortic contractility, *Myh11*^{R247C/R247C} mice had no signs of spontaneous vascular disease. The blood pressure of the mice was unaffected, and histopathologic examination of the aorta showed no dilatation and no medial degeneration (**Figure 2.2c,d**). Elastin fibers remained intact, and there was no accumulation of proteoglycans. Additionally, the mice had no decrease in survival or reproductive function compared with wild-type. These results show that decreased contractility alone does not lead to aortic disease.

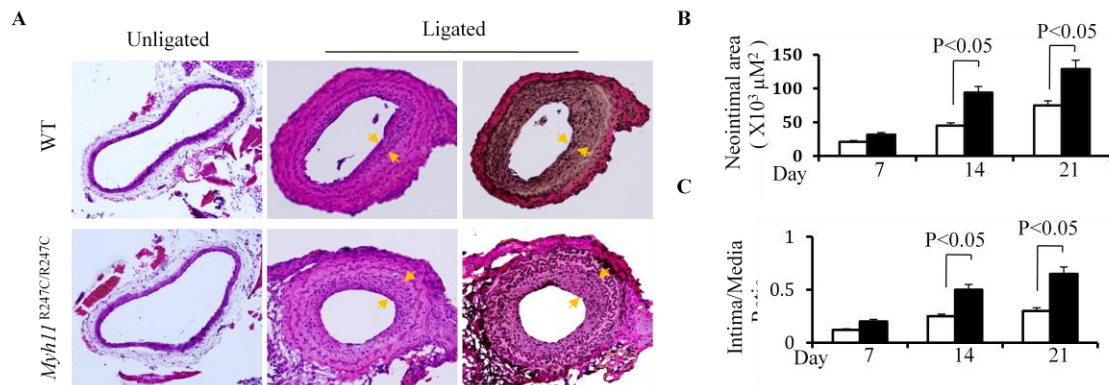


Figure 2.3 Increased vascular injury response in *Myh11*^{R247C/R247C} mice. A/B/C) Increased neointimal proliferation after carotid ligation in *Myh11*^{R247C/R247C} knockin mice. A shows histology from 21 days post injury. B and C show quantitation of this effect over three weeks post surgery. Reprinted with permission from Wolters Kluwer Health. [Rare, Nonsynonymous Variant in the Smooth Muscle-Specific Isoform of Myosin Heavy Chain, MYH11, R247C, Alters Force Generation in the Aorta and Phenotype of Smooth Muscle Cells Novelty and Significance. Kuang SQ, Kwartler CS, Byanova KL, Pham J, Gong L, Prakash SK, Huang J, Kamm KE, Stull JT, Sweeney HL, Milewicz DM. *Circulation Research* 2012.]

Because the R247C alteration is a rare variant, not a Mendelian mutation, these results are not surprising. We hypothesized that a second hit may be needed to induce a disease phenotype in these mice. Because this variant is found in patients with occlusive as well as aneurysmal disease, we initially used an injury model of carotid artery ligation. Briefly, the left common carotid artery is tied off just proximal to the

bifurcation, and the mice are allowed to recover. This is a well-established model of vascular injury, and the vessels undergo extensive remodeling below the injury. The end result of this remodeling is a thickening of the vessel wall as SMCs proliferate and migrate through the internal elastic lamina. The new layer of SMCs is called the “neointima.” The thickness of the neointima left after injury correlates with the proliferative and migratory response of the SMCs to injury, and the *Myh11*^{R247C/R247C} mice had significantly thicker neointimal layers (**Figure 2.3a,b**). These results suggested that the *Myh11* R247C rare variant might predispose to occlusive diseases by increasing the proliferative response of SMCs.

For the first aim of this project, we thus proceeded to further examine the phenotype of SMCs from *Myh11* R247C knockin mice to determine a mechanistic link between the R247C alteration and a possible increase in cellular proliferation.

Materials and Methods

“Vascular SMCs Isolation and Culture

To isolate primary mouse aortic SMCs, aortas were isolated (from the aortic root to the renal arterial bifurcation) from 6-week old WT and *Myh11*^{R247C/R247C} knock-in mice. Whole aortas were collected under sterile conditions and put into biopsy medium (**Table 2.3**). Ascending aorta/arch and descending aortas were separated after the origin of the left subclavian artery. The adventitia was removed, and the remaining medial layer of aorta was chopped into small pieces and put to digestion overnight for 16 h in 5 ml of aortic biopsy medium supplemented with 0.1 mg/ml of collagenase type I, 0.019 mg/ml of elastase type I and 0.0250 mg/ml of soybean trypsin inhibitor. At the end of incubation, the digestion was stopped with 2.5 ml of fetal bovine serum and 2.5 ml of complete SMC medium (**Table 2.3**). Cells and tissue were spun down, resuspended in complete SMC medium and seeded into flasks for further experiments. The identity of these cells as SMCs was verified by staining for smooth muscle α -actin (mouse monoclonal antibody; Sigma-Aldrich, St. Louis, MO) at each passage (95% of cells stained positive for smooth muscle α -actin). SMCs were cultured in complete SMC medium in a 37°C, 5% CO₂-humidified incubator.

Three independent cell lines each were explanted from WT mice, *Myh11*^{R247C/+}, and *Myh11*^{R247C/R247C} mice, using aortas pooled from three to five mice per genotype per explant. The results presented are representative of at least two independent experiments done on each line of SMCs using passage-matched WT and *Myh11*^{R247C/R247C} SMCs. All studies were performed on SMCs at less than passage 5.

Immunoblot Analyses

Aortic tissues or cultured cells were homogenized and lysed in RIPA buffer (**Table 2.3**) supplemented with protease inhibitor cocktail (Sigma-Aldrich, St. Louis, MO) and phosphatase inhibitor cocktail (Sigma-Aldrich, St. Louis, MO). Protein (5µg) for each sample was separated on Tris-HCl gel (Bio-Rad, Hercules, CA) by SDS-PAGE, followed by transfer to polyvinylidene difluoride membranes (Millipore, Bedford, MA). Membranes were immunoblotted with primary antibody and the appropriate horseradish peroxidase-conjugated secondary antibody (Jackson ImmunoResearch Laboratories, West Grove, PA). Immunoblots were visualized by the enhanced chemiluminescence technique (GE Healthcare, Piscataway, NJ). For primary antibodies and dilutions, see **Table 2.2**.

Immunofluorescence in Explanted Aortic SMCs

After cells reached confluence, they were seeded onto coverslips in six-well plates with the density of 13 cells/mm² for 24 h. For MRTF-A staining, Cells were starved in 1% serum media for 24 hours, plus/minus inhibitors and fixed with 4% paraformaldehyde for 10 min. Permeabilization was performed in PBS containing 0.1% Triton X-100 and blocking of nonspecific binding sites was performed in PBS containing 5% donkey serum. Coverslips were then treated with primary antibody (anti-MRTFA (Santa Cruz Biotechnology, Santa Cruz, CA), 1:100) overnight followed by fluorescein isothiocyanate-conjugated secondary antibody (1:100, Jackson ImmunoResearch Laboratories, West Grove, PA) for 1 h. Nuclei were counterstained with DAPI (Vector Laboratories, Burlingame, CA), and then randomly chosen fields on each coverslip were imaged by confocal microscopy (Nikon A1R, Nikon Instruments, Melville, NY). For focal adhesion staining, cells were starved in 1% serum media for 24 hours then treated with or without 10ng/mL TGF-β1 for 48 hours. The same fixation and staining protocol described above was used with primary antibodies anti-vinculin (Sigma-Aldrich, St. Louis, MO) and anti-phospho-FAK (Y397) (Millipore, Bedford, MA). For α-actin staining, cells were starved in 1% serum media for 12 hours, followed by 10ng/mL TGF-β1 for 72 hours. CN03 treatment was added for 24 hours after completion of TGF-β1 incubation. Again, the same fixation and staining protocol were used with primary antibody anti α-SMA (Sigma-Aldrich, St. Louis, MO). For phalloidin staining, coverslips were incubated with Texas Red-labeled phalloidin (1:40 in blocking solution) (Molecular Probes, Eugene, OR) for 30 min.

Analysis of Immunofluorescence Images

All analyses were performed using the Nikon NIS Elements software. Pearson coefficients for colocalization of blue (DAPI stained nuclei) and green (MRTFA) pixels were calculated for at least 15 cells per slide on at least 3 slides for each bar shown on the graph. The same protocol was used to obtain Pearson coefficients for colocalization of green (α -actin) and red (phalloidin) pixels for Figure 6. Individual focal adhesion size was calculated for at least 30 adhesions per cell on at least 10 cells per genotype using the Nikon NIS Elements measurement tool.

Antigen	Company	Species	Uses
SM-actin	Sigma	Mouse	WB, IF
SM-MHC	Biomedical Technologies, Inc	Rabbit	WB
Calponin	Novus Biologicals	Rabbit	WB
MRTF-A	Santa Cruz Biotechnology	Rabbit	IF
Vinculin	Sigma	Mouse-FITC conj.	IF
SM-22 α	Santa Cruz Biotechnology	Rabbit	WB
Phospho-FAK (Y397)	Millipore	Mouse	WB, IF
FAK	Santa Cruz Biotechnology	Rabbit	WB
Phospho-Akt (S473)	Cell Signaling Technology	Rabbit	WB
Akt	Cell Signaling Technology	Rabbit	WB
Phospho-Histone 3 (S10)	Upstate (Millipore)	Rabbit	IHC

Table 2.2 Antibodies used in Chapter 2.

Cell Proliferation Assays

Proliferation of SMCs was quantified using by the incorporation of BrdU. Briefly, SMCs were seeded in 96-well plates (20,000 cells/ well) and grown for 24 hours in SmBm (see SMCs Isolation and Culture section for details) containing 20% FBS. The cells were serum-starved in SmBm containing 1% FBS and plus/minus inhibitors for 30 minutes prior to the addition of BrdU reagent. After 24 hours of incubation, BrdU incorporation was quantified by ELISA according to the manufacturer's instructions (Millipore, Bedford, MA). Inhibitors include NSC23766 (Rac inhibitor) (Tocris Bioscience, Ellisville, MO), PF537228 (FAK inhibitor) (Tocris Bioscience, Ellisville, MO), and CN03 (Rho Activator) (Cytoskeleton, Denver, CO).

Rho and Rac Activation Assays

RhoA and Rac1 activation were quantified using G-LISA assays (Cytoskeleton,

Denver, CO) performed according to the manufacturer's specifications. Briefly, cells were seeded on 6cm dishes (200,000 cells/dish) and grown for 24 h in SmBm containing 20% FBS. The cells were serum-starved in SmBm containing 1% FBS for 24 hours, then treated +/- lypophosphatidic acid (Sigma-Aldrich, St. Louis, MO) for 15 minutes. Cells were lysed in the provided lysis buffer and lysates were snap frozen. Protein, (0.5 µg) was loaded per well of the provided ELISA plate, and activated Rac1 and RhoA were quantified by ELISA assay.

F/G actin Assay

Polymerization of actin was assayed using an F/G actin assay (Cytoskeleton, Denver, CO) performed according to the manufacturer's specifications. Briefly, cells were seeded on 10cm dishes (900,000 cells/dish) and grown for 24 h in SmBm containing 20% FBS. The cells were serum-starved in SmBm containing 1% FBS for 24 hours, then lysed and homogenized in the provided lysis buffer. Samples were pelleted in an ultracentrifuge (Optima TLX Ultracentrifuge, Rotor TLA-110, Beckman Coulter, Brea, CA) at 55,000 rpm for 1 hour at 37°C. Pellets and supernatant fractions were separately processed and processed by SDS-PAGE for subsequent immunoblot analysis.

Media/Buffer	Composition
Aortic biopsy medium	Waymouth's MB 752/1 medium supplemented with 100U/ml penicillin, 100ug/ml streptomycin, 250 ng/ml amphotericin, 2.5 mM L-glutamine, 1 mM MEM non-essential amino acids, 100 mM Hepes buffer, and sodium bicarbonate
Complete SMC medium	SmBm basal media (Lonza/Cambrex) supplemented with 20% FBS, 100 U/ml of penicillin, 100 ug/ml of streptomycin, 250 ng/ml of amphotericin, 0.5 ml of insulin, 1.0 ml of rhEGF, 0.5 ml of rhFGF, 2 mmol/l of l-glutamine, 20 mmol/l of HEPES, 1 mmol/l of sodium pyruvate
1% serum medium	SmBm basal media (Lonza/Cambrex) supplemented with 1% FBS, 100 U/ml of penicillin, 100 ug/ml of streptomycin, 250 ng/ml of amphotericin, 2 mmol/l of l-glutamine, 20 mmol/l of HEPES, 1 mmol/l of sodium pyruvate
RIPA buffer	50 mm of Tris, pH 7.5, 150 mm of NaCl, 1% NP-40, 0.5% sodium deoxycholate and 0.1% SDS) supplemented with protease inhibitor cocktail P8340 (Sigma) and phosphatase inhibitor cocktails 2 and 3 (Sigma)

Table 2.3 Buffer compositions used in Chapter 2.

RNA Extraction and QuaQuantitative Real-time PCR

Total mouse aortic tissue or primary vascular SMC cellular RNA was extracted with Trizol (Invitrogen, Carlsbad, CA) according to the manufacturer's protocol. Reverse transcription reactions were performed using the High Capacity cDNA

Archive Kit (Life Technologies, Carlsbad, CA) according to the manufacturer's protocol. For quantitative real-time PCR analysis of mRNA expression, TaqMan probes were purchased from Applied Biosystems and analyzed using an Applied Biosystems Prism 7900 HT Sequence Detection System (Applied Biosystems, Foster City, CA) according to the manufacturer's protocol. Experiments were performed in triplicate. Gapdh was used as the endogenous control.

Statistical Analysis

All values are expressed as means \pm standard deviation. Statistical differences between WT and mutant mice or cells were analyzed by a Student's t-test.

Morphometric analysis of carotid artery was done by one-way ANOVA.

Differences were considered statistically significant at values of $P < 0.05$. Data for cell culture experiments represent three experiments in triplicates using separate cultures." [73]

Quoted text reprinted with minimal modification with permission from Wolters Kluwer Health [Rare, Nonsynonymous Variant in the Smooth Muscle Specific Isoform of Myosin Heavy Chain, *MYH11*, R247C, Alters Force Generation in the Aorta and Phenotype of Smooth Muscle Cells. Kuang SQ, Kwartler CS, Byanova KL, Pham J, Gong L, Prakash SK, Huang J, Kamm KE, Stull JT, Sweeney HL, Milewicz DM. *Circ Res*. 2012.]

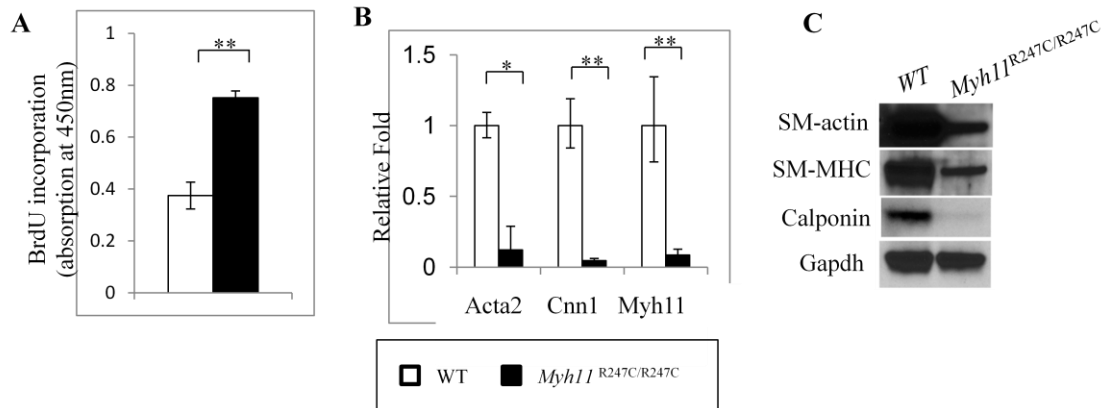


Figure 2.4 *Myh11*^{R247C/R247C} SMCs are dedifferentiated. A) Increased cellular proliferation in *Myh11*^{R247C/R247C} SMCs. B,C) Decreased expression of contractile genes (B) and proteins (C) in *Myh11*^{R247C/R247C} SMCs. Reprinted with permission from Wolters Kluwer Health. [Rare, Nonsynonymous Variant in the Smooth Muscle-Specific Isoform of Myosin Heavy Chain, MYH11, R247C, Alters Force Generation in the Aorta and Phenotype of Smooth Muscle Cells. Novelty and Significance. Kuang SQ, Kwartler CS, Byanova KL, Pham J, Gong L, Prakash SK, Huang J, Kamm KE, Stull JT, Sweeney HL, Milewicz DM. *Circulation Research* 2012.]

Results

Myh11^{R247C/R247C} smooth muscle cells are dedifferentiated

Consistent with the results of the *in vivo* injury model study, *Myh11^{R247C/R247C}* SMCs proliferated significantly more rapidly in culture compared with wild-type cells (**Figure 2.4a**). Because proliferation and expression of contractile markers are often negatively correlated, we next looked at both gene expression and protein accumulation of commonly used contractile markers: *Acta2* (SM-actin), *Cnn1* (calponin), and *Myh11* (SM-MHC). All three genes were expressed at significantly lower levels in *Myh11^{R247C/R247C}* SMCs than in wild-type cells, and Western blot analysis showed concomitantly reduced protein levels (**Figure 2.4b,c**). Treatment with TGF- β 1, which drives increased contractile gene expression in wild-type SMCs, was unable to rescue the decreased expression seen in *Myh11^{R247C/R247C}* SMCs (data not shown). These initial results suggest that the *Myh11^{R247C/R247C}* SMCs are canonically dedifferentiated.

We next assessed whether the SRF:MRTF axis were responsible for the observed dedifferentiated phenotype. Immunofluorescence revealed a significant shift in the localization of MRTF-A from predominantly nuclear in wild-type cells to predominantly cytoplasmic in *Myh11^{R247C/R247C}* SMCs (**Figure 2.5c**). MRTF localization is dependent on actin filament formation, so we asked whether there was an increased unpolymerized actin fraction in the knockin cells. Immunofluorescent analysis shows thick filaments of smooth muscle α -actin spanning the cell body in wild-type SMCs, but a combination of thinner, shorter filaments and unpolymerized α -actin in *Myh11^{R247C/R247C}* SMCs (**Figure 2.5a**). These results were confirmed using an ultracentrifugation based assay that separates polymerized from unpolymerized actin: a comparison of α -actin content in the

supernatant compared with the pellet shows a significantly altered ratio of polymerized to unpolymerized actin in the *Myh11*^{R247C/R247C} SMCs (**Figure 2.5b**). Thus, unpolymerized actin pulls MRTF out of the nucleus, leading to decreased contractile gene expression and increased cellular proliferation in *Myh11*^{R247C/R247C} SMCs. However, the link between a mutation in *Myh11* and decreased actin filament formation remained to be determined.

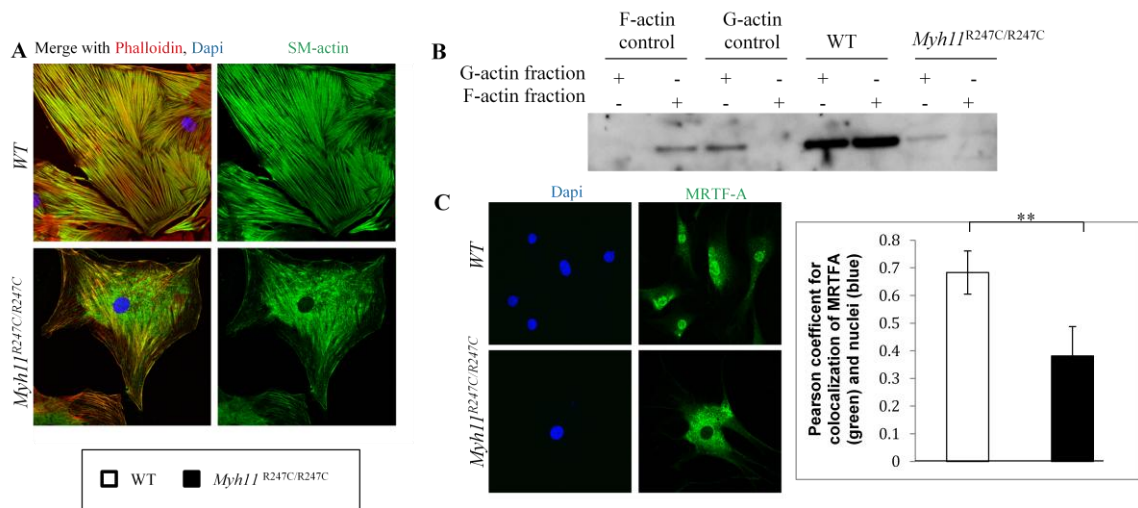


Figure 2.5 The SRF;MRTF axis drives dedifferentiation in *Myh11*^{R247C/R247C} SMCs. A) Immunofluorescences shows decreased numbers of SM-actin filaments (green) in *Myh11*^{R247C/R247C} SMCs. B) Ultracentrifugation assay shows decreased F-actin fraction in *Myh11*^{R247C/R247C} SMCs. C) Decreased nuclear localization of MRTF in *Myh11*^{R247C/R247C} SMCs. Reprinted with permission from Wolters Kluwer Health. [Rare, Nonsynonymous Variant in the Smooth Muscle-Specific Isoform of Myosin Heavy Chain, MYH11, R247C, Alters Force Generation in the Aorta and Phenotype of Smooth Muscle Cells Novelty and Significance. Kuang SQ, Kwartler CS, Byanova KL, Pham J, Gong L, Prakash SK, Huang J, Kamm KE, Stull JT, Sweeney HL, Milewicz DM. *Circulation Research* 2012.]

*Altered focal adhesions in *Myh11*^{R247C/R247C} SMCs*

As described in Chapter 1, focal adhesions are the force sensors of the cell, located at the plasma membrane. Intracellular force generation, via myosin contractility, drives maturation of focal adhesions. Impairment of myosin contractility using

blebbistatin prevented focal adhesion maturation in fibroblasts, resulting in smaller adhesions and a change in the composition of the complexes from enrichment of RhoA activators in mature adhesions to enrichment of Rac1 activators in less mature adhesions [74]. Because the R247C rare variant causes a decrease in myosin force generation, we asked whether the focal adhesions in *Myh11*^{R247C/R247C} SMCs might similarly be less mature. Vinculin is a commonly used marker for focal adhesions, as its protein content within the adhesion does not change with maturation [75]. Immunofluorescence for vinculin showed significantly smaller focal adhesions in *Myh11*^{R247C/R247C} SMCs. Consistent with the gene expression results, focal adhesions in *Myh11*^{R247C/R247C} SMCs did not increase in size after TGF- β 1 treatment while focal adhesions in wild-type SMCs became larger, increasing the difference in size between the two cell types (**Figure 2.6a**).

Secondly, we assessed cellular levels of Rac1 and RhoA activation as a proxy for the change in composition of the focal adhesions. Rac1 activation was significantly increased in *Myh11*^{R247C/R247C} SMCs compared with wild-type cells at baseline (**Figure 2.6b**). RhoA activation was slightly decreased at baseline, but the effect became significant after a 5-minute stimulation with the known RhoA activator lysophosphatidic acid (LPA) (**Figure 2.6c**). These results are consistent with less mature focal adhesions in *Myh11*^{R247C/R247C} SMCs.

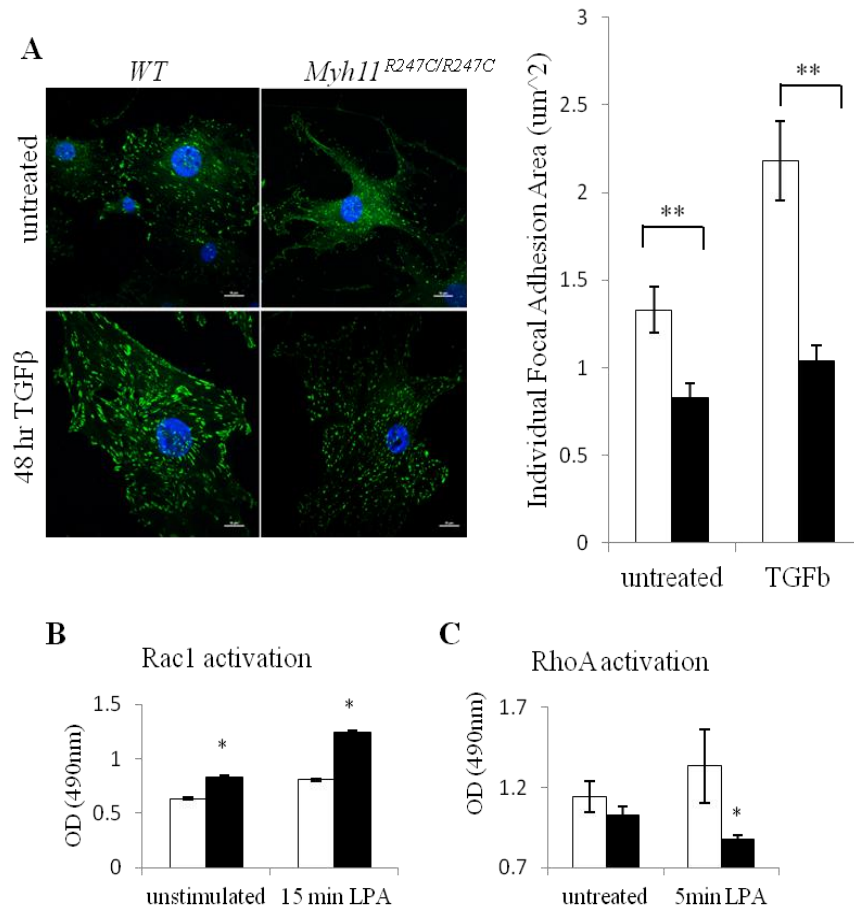


Figure 2.6 Altered focal adhesions in *Myh11*^{R247C/R247C} SMCs. A) Immunofluorescences for vinculin (green) shows smaller focal adhesions in *Myh11*^{R247C/R247C} SMCs with and without TGF-β stimulation. B,C) Increased Rac1 (B) and decreased RhoA (C) activation in *Myh11*^{R247C/R247C} SMCs . Reprinted with permission from Wolters Kluwer Health. [Rare, Nonsynonymous Variant in the Smooth Muscle-Specific Isoform of Myosin Heavy Chain, MYH11, R247C, Alters Force Generation in the Aorta and Phenotype of Smooth Muscle Cells Novelty and Significance. Kuang SQ, Kwartler CS, Byanova KL, Pham J, Gong L, Prakash SK, Huang J, Kamm KE, Stull JT, Sweeney HL, Milewicz DM. *Circulation Research* 2012.]

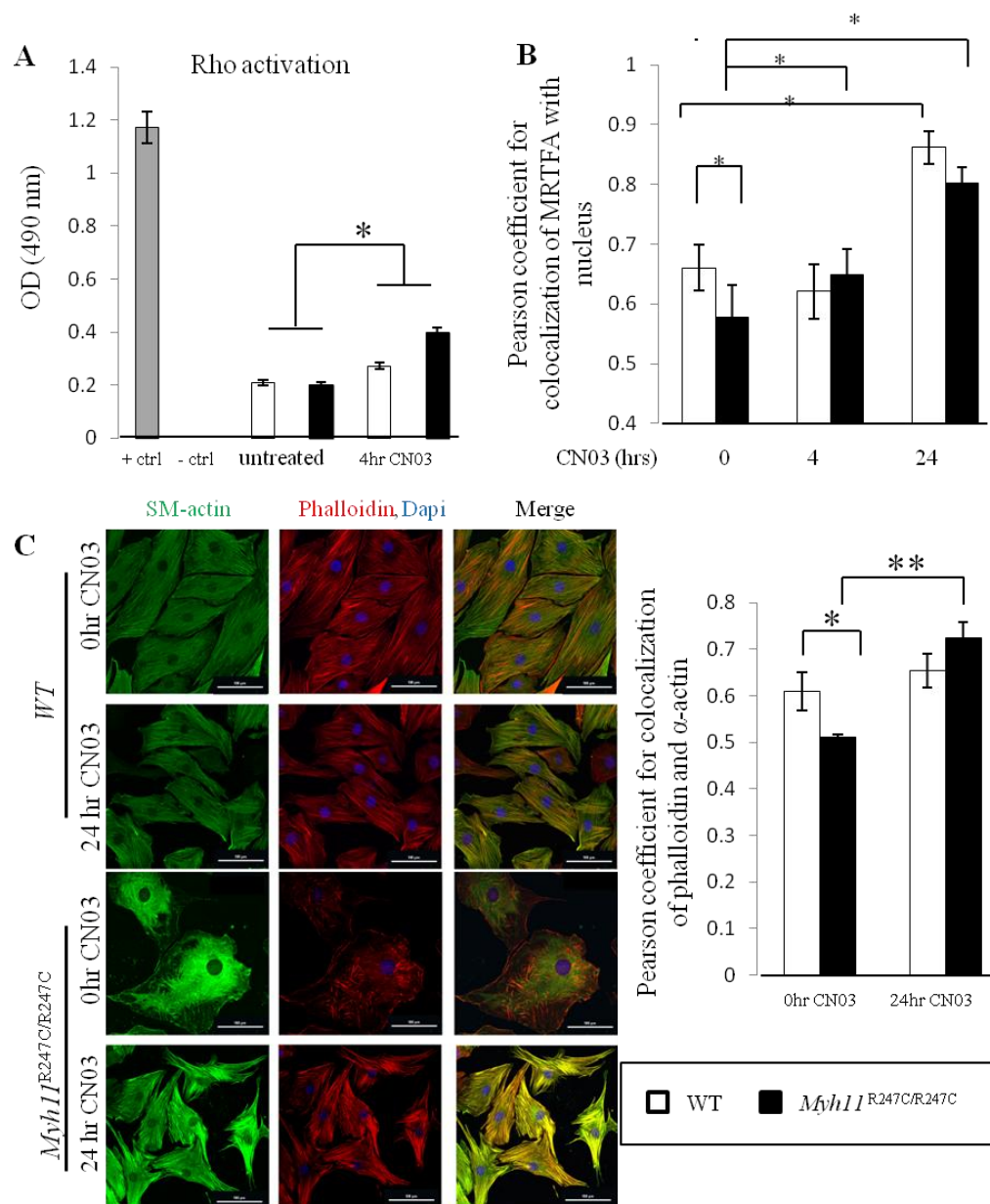


Figure 2.7 CN03 treatment drives actin polymerization in *Myh11*^{R247C/R247C} SMCs. A) Treatment with CN03 increases activation of RhoA . B) Treatment with CN03 for 4 or 24 hours increases nuclear localization of MRTFA in *Myh11*^{R247C/R247C} SMCs (C) Treatment with CN03 for 24 hours drives actin polymerization in *Myh11*^{R247C/R247C} SMCs . Reprinted with permission from Wolters Kluwer Health. [Rare, Nonsynonymous Variant in the Smooth Muscle-Specific Isoform of Myosin Heavy Chain, MYH11, R247C, Alters Force Generation in the Aorta and Phenotype of Smooth Muscle CellsNovelty and Significance. Kuang SQ, Kwartler CS, Byanova KL, Pham J, Gong L, Prakash SK, Huang J, Kamm KE, Stull JT, Sweeney HL, Milewicz DM. *Circulation Research* 2012.]

Pharmacologic activation of RhoA rescues the dedifferentiated phenotype of $Myh11^{R247C/R247C}$ SMCs

RhoA activation in SMCs drives polymerization of actin [42]; thus, we asked whether activating RhoA in $Myh11^{R247C/R247C}$ SMCs could rescue the dedifferentiated phenotype. We used a pharmacological compound called “CN03” derived from a bacterial endotoxin. CN03 works by deaminating glutamine residue 63, causing RhoA to become constitutively active (**Figure 2.7a**). Treatment of $Myh11^{R247C/R247C}$ SMCs with CN03 successfully increased actin polymerization (**Figure 2.7c**). Additionally, MRTF-A localization became more nuclear following CN03 treatment, and expression of contractile genes and proteins were significantly increased **Figure 2.7b, Figure 2.8a,b**). Thus, the lack of maturation of the focal adhesions, and the resulting decrease in RhoA activation, drives the dedifferentiated phenotype in $Myh11^{R247C/R247C}$ SMCs.

However, treatment with CN03 only partially prevented the increased cellular proliferation of $Myh11^{R247C/R247C}$ SMCs (**Figure 2.8c**). This result implies that the SRF:MRTF axis alone is incompletely responsible for driving proliferation in dedifferentiated SMCs, and suggests that alternatively dedifferentiation merely sensitizes SMCs to proliferative stimuli. The next question was which proliferative stimuli were driving the increased cellular proliferation of $Myh11^{R247C/R247C}$ SMCs.

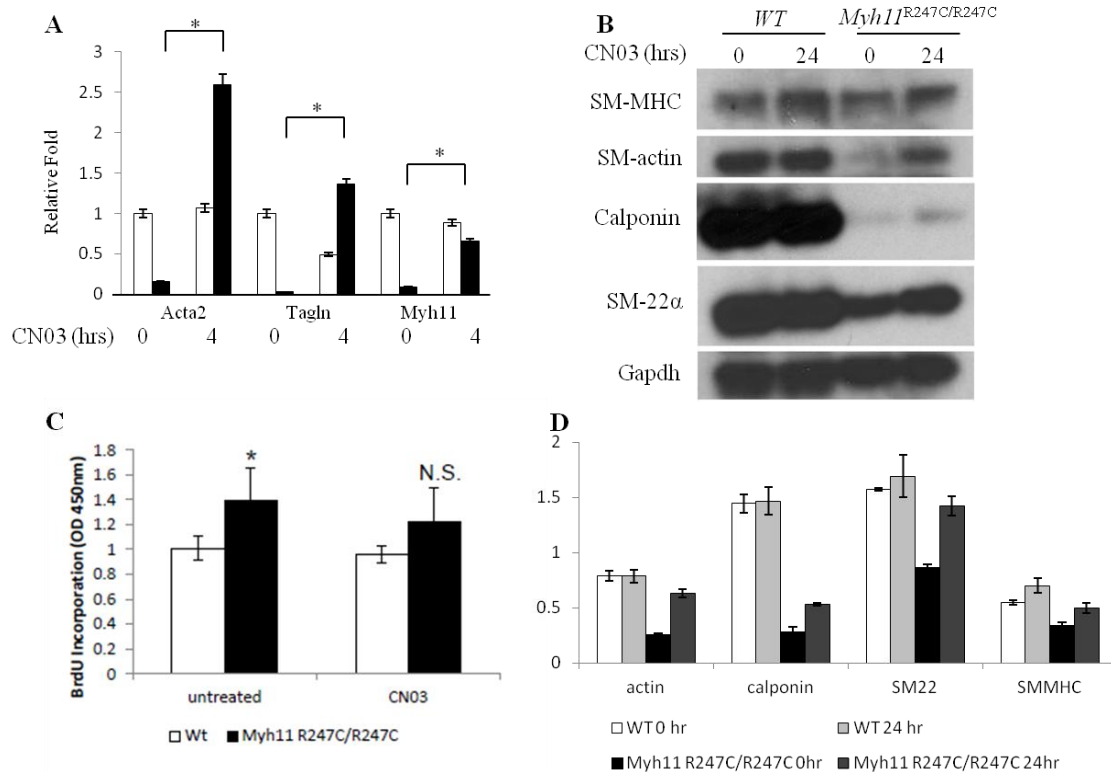


Figure 2.8 CN03 treatment drives SMC differentiation in *Myh11*^{R247C/R247C} SMCs. A, B) Treatment with CN03 increases expression of contractile gene mRNA (A) after 4 hours and proteins (B) after 24 hours in *Myh11*^{R247C/R247C} SMCs. C) Treatment with CN03 for 24 hours partially blocks proliferation in *Myh11*^{R247C/R247C} SMCs. D) Densitometry quantification of B. Reprinted with permission from Wolters Kluwer Health. [Rare, Nonsynonymous Variant in the Smooth Muscle-Specific Isoform of Myosin Heavy Chain, MYH11, R247C, Alters Force Generation in the Aorta and Phenotype of Smooth Muscle Cells Novelty and Significance. Kuang SQ, Kwartler CS, Byanova KL, Pham J, Gong L, Prakash SK, Huang J, Kamm KE, Stull JT, Sweeney HL, Milewicz DM. *Circulation Research* 2012.]

*Focal adhesion kinase drives proliferation in *Myh11*^{R247C/R247C} SMCs*

Focal adhesion kinase is a signaling protein localized to focal adhesions, which drives activation of multiple downstream pathways including a number of proliferative pathways like MAPK [76]. Focal adhesion kinase is also known to be more active in less mature focal adhesions. Therefore, we assessed whether focal adhesion kinase was more active in *Myh11*^{R247C/R247C} SMCs, and whether this increased activation led to the

observed proliferative phenotype. Both immunofluorescence and Western blot analyses indicate an increase in activated focal adhesion kinase in *Myh11*^{R247C/R247C} SMCs, as assessed by phosphorylation of tyrosine 397 (**Figure 2.9a,b**). Similarly, downstream activation of Akt was concomitantly increased in *Myh11*^{R247C/R247C} SMCs as well.

Treatment of *Myh11*^{R247C/R247C} SMCs with an inhibitor of focal adhesion kinase, PF-573228, did not have any effect on actin polymerization, MRTF-A localization, or contractile gene expression (data not shown). However, PF-228 did partially and significantly blunt cellular proliferation in *Myh11*^{R247C/R247C} SMCs (**Figure 2.9c**). This result suggests that focal adhesion kinase is one proliferative stimulus that contributes to

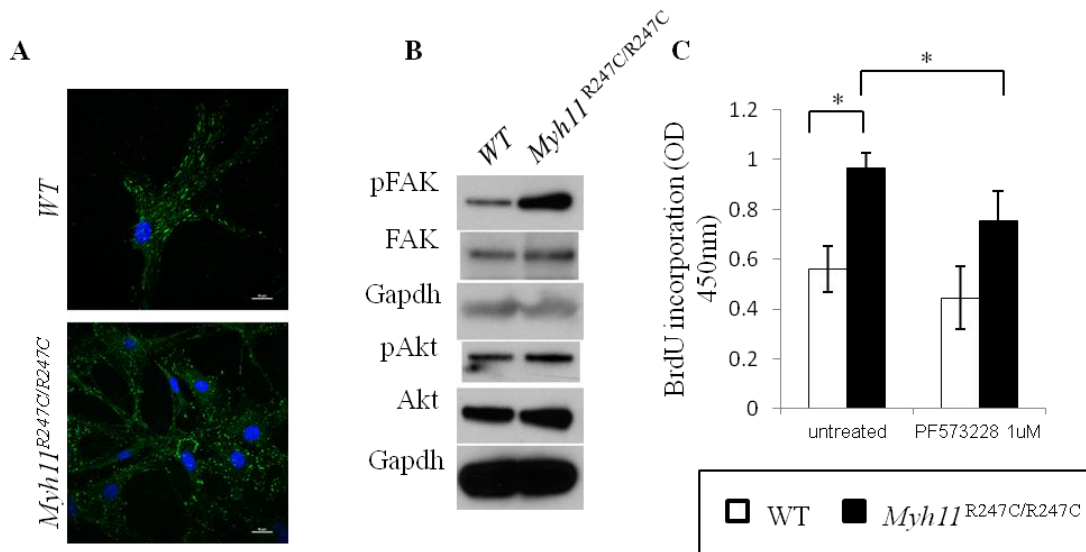


Figure 2.9 Focal adhesion kinase activation *Myh11*^{R247C/R247C} SMCs. A, B) Activation of FAK in *Myh11*^{R247C/R247C} SMCs shown by immunofluorescence (A) and Western blot (B). C) Treatment with an inhibitor of FAK, PF537228 for 24 hours partially blocks proliferation in *Myh11*^{R247C/R247C} SMCs. Reprinted with permission from Wolters Kluwer Health. [Rare, Nonsynonymous Variant in the Smooth Muscle-Specific Isoform of Myosin Heavy Chain, MYH11, R247C, Alters Force Generation in the Aorta and Phenotype of Smooth Muscle Cells Novelty and Significance. Kuang SQ, Kwartler CS, Byanova KL, Pham J, Gong L, Prakash SK, Huang J, Kamm KE, Stull JT, Sweeney HL, Milewicz DM. *Circulation Research* 2012.]

the phenotype seen in *Myh11*^{R247C/R247C} SMCs.

SMCs in Myh11^{R247C/R247C} *aortas are not dedifferentiated*

Although the phenotype and mechanism have been established in SMCs in culture, the question remains whether there is any alteration in SMC phenotype *in vivo* in *Myh11*^{R247C/R247C} tissues. Ascending aortic tissue from *Myh11*^{R247C/R247C} and wild-type mice was harvested, but there was no difference in expression levels of contractile genes or proteins *in vivo* (**Figure 2.10a,b**). Similarly, staining for phospho-histone 3 (PH3), a marker of proliferating cells [77], shows no increase in proliferating SMC nuclei in the *Myh11*^{R247C/R247C} aortas (**Figure 2.10c,d**). Finally, analysis of Rac1 and RhoA activation reveals no difference between *Myh11*^{R247C/R247C} and wild-type aortas (**Figure 2.10e,f**). Thus, this phenotype occurs in *Myh11*^{R247C/R247C} SMCs after explanting, but is not prevalent within the aortic tissue. These results suggest that this phenotype may be injury-induced, as explanting SMCs induces an injury-like response and carotid injury induced a proliferative phenotype in *Myh11*^{R247C/R247C} mice.

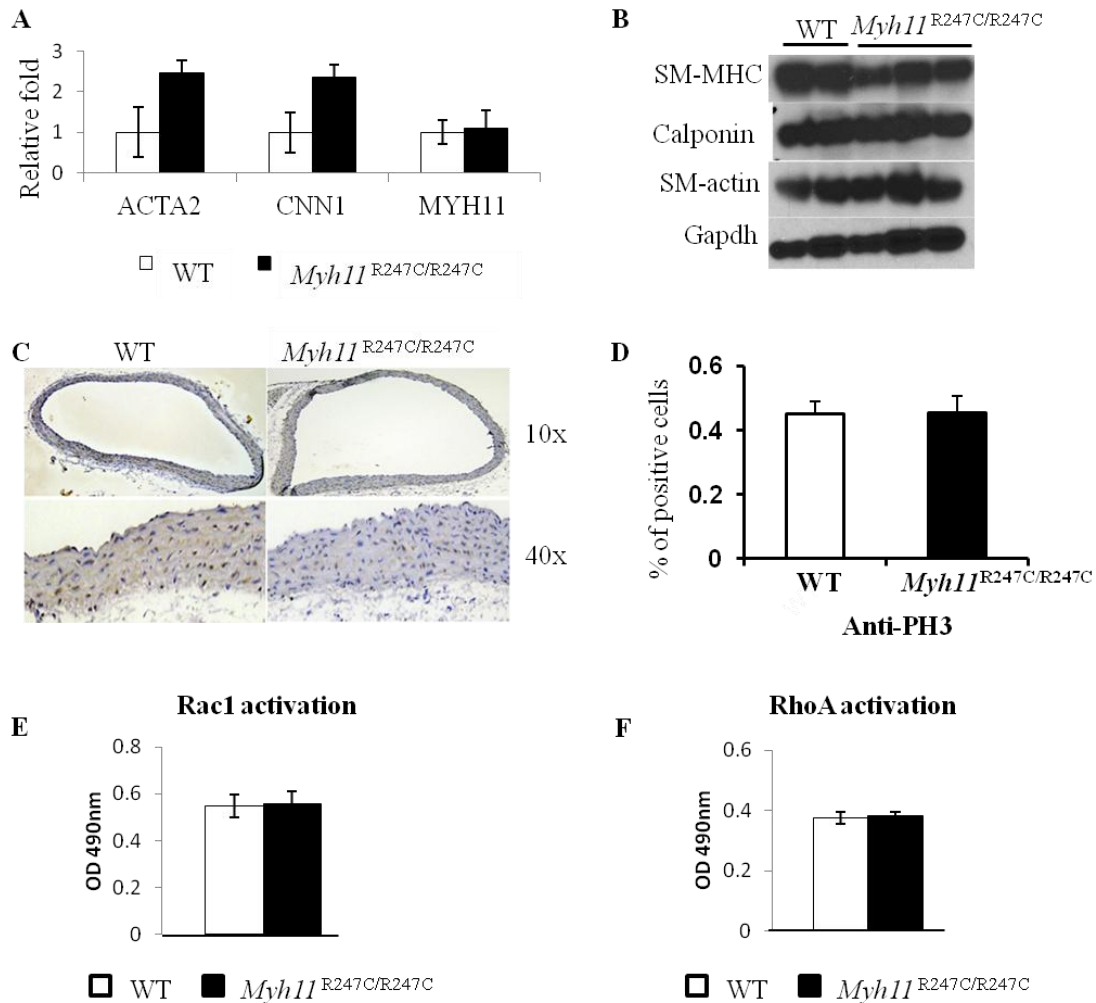


Figure 2.10 *Myh11*^{R247C/R247C} SMCs within the aortic wall are not dedifferentiated. A, B) Levels of contractile genes (A) and proteins (B) are similar between *Myh11*^{R247C/R247C} and wild-type aortas. C, D) No change in phospho-histone 3 staining in *Myh11*^{R247C/R247C} aortas, (D) shows quantitation of positive cells. E, F) No change in Rac1 (E) or RhoA (F) activation in *Myh11*^{R247C/R247C} aortas. Reprinted with permission from Wolters Kluwer Health. [Rare, Nonsynonymous Variant in the Smooth Muscle-Specific Isoform of Myosin Heavy Chain, MYH11, R247C, Alters Force Generation in the Aorta and Phenotype of Smooth Muscle Cells Novelty and Significance. Kuang SQ, Kwartler CS, Byanova KL, Pham J, Gong L, Prakash SK, Huang J, Kamm KE, Stull JT, Sweeney HL, Milewicz DM. *Circulation Research* 2012.]

Discussion

The R247C alteration introduced into the mouse *Myh11* gene causes a decrease in aortic contractility but does not lead to aortic disease. However, carotid injury did lead

to an increased vascular proliferative response, suggesting that a second hit can induce disease in *Myh11*^{R247C/R247C} mice. SMCs explanted from *Myh11*^{R247C/R247C} mice are dedifferentiated, with reduced expression of contractile genes and increased proliferation. The canonical SRF: MRTF axis drives the observed dedifferentiation in *Myh11*^{R247C/R247C} SMCs: pools of unpolymerized actin sequester the transcriptional coactivator MRTFs in the cytoplasm, preventing the transcription of SMC contractile genes.

In conjunction with the dedifferentiated phenotype of *Myh11*^{R247C/R247C} SMCs, focal adhesions in these cells are less mature. Focal adhesions (FAs) are dynamic protein complexes at the cell membrane that promote adhesion of the cells to the extracellular matrix and also drive signaling in response to changes in force generation [78]. Increasing intracellular tension, driving by acto-myosin contractility, promotes focal adhesion maturation. As FAs mature, they both increase in size and change in composition: nascent FAs form, then as actin stress fibers begin to polymerize at the site of the complexes additional proteins, including paxillin, are recruited [79]. Further force generation, in form of myosin motor function, is required for complete maturation of FAs. A recent paper looked at the composition of FAs in fibroblasts with or without treatment with the myosin motor poison blebbistatin. In the absence of myosin motor function, FAs contained Rac1 activating molecules like β -pix, while mature FAs in cells with uncompromised myosin motors were alternatively enriched for RhoA activators like testin [74]. RhoA has previously been shown to regulate actin polymerization, and downstream of polymerization also regulates SMC differentiation [42]. Modulation of RhoA signaling dramatically impacts contractile gene expression: knockdown of RhoA reduces SMC differentiation, while constitutive activation of RhoA increases expression

of marker genes [80]. Thus, FA maturation drives a positive feedback loop by increasing activation of RhoA, driving further differentiation of SMCs, maintains the intracellular force, and leading to further FA maturation.

The R247C variant in *Myh11* causes decreased capacity for force generation by the mutant smooth muscle myosin motor. FAs in *Myh11*^{R247C/R247C} SMCs are therefore unable to fully mature due to decreased intracellular force generation. In fact, pharmacologic activation of RhoA completely rescued the dedifferentiated phenotype of *Myh11*^{R247C/R247C} SMCs, suggesting that the loss of FA maturation, and concomitant decrease in RhoA activation, is the causative factor driving dedifferentiation. Importantly, SMCs also express two non-muscle myosin heavy chain molecules (*Myh9* and *Myh10*), but these fully functional, less specialized myosin molecules were unable to compensate for the mutant smooth muscle myosin to drive normal FA maturation. Thus, this part of my dissertation proves that smooth muscle-specific myosin function is necessary to drive FA maturation in SMCs, and that loss of that motor function can disrupt SMC differentiation by preventing FA maturation.

However, in the intact, uninjured aorta, *Myh11*^{R247C/R247C} SMCs show no difference in contractile protein expression, proliferation, or RhoA activation. FAs in the tissue are called dense plaques, which promote interactions of the complex extracellular matrix with the contractile fibers of the SMCs through integrin receptors. The dense plaques are constantly exposed to biomechanical stress and strain due to pulsatile blood flow, in contrast to FAs in static culture. Loss of integrin linked kinase (ILK), a kinase localized to focal adhesions that binds to both integrins and components of the actin cytoskeleton, led to a similar cellular phenotype *in vitro* as the R247C mutation: loss of

RhoA activity and dedifferentiation of SMCs [81]. However, unlike our model, the ILK knockout mice had a similar phenotype *in vivo*. Interestingly, the ILK knockout mice have a similar phenotype to patients with *MYH11* mutations: TAAD with patent ductus arteriosus [61]. Therefore, ILK may be a potential source of RhoA activation *in vivo* in the *Myh11*^{R247C/R247C} aortas, or alternatively the continuous external biomechanical forces on the aorta may compensate for the partial loss of intracellular myosin force generation to allow maturation of the dense plaques within *Myh11*^{R247C/R247C} aortic SMCs. Patients with *MYH11* mutations have more severe defects in myosin function as the mutations identified are predicted to disrupt myosin filament formation. It may be that complete loss of myosin force generation, like the aberrant signaling responses to external force cues in ILK knockout mice, is sufficient to provoke a phenotype *in vivo*.

Surprisingly, *Myh11*^{R247C/R247C} mice do not have a phenotype in other smooth muscle tissues like the bladder, uterus, or intestines. Mice with complete *Myh11* knockout die shortly after birth due to bladder and intestinal dysfunction [82], however the *Myh11*^{R247C/R247C} mice show no defects in weight gain and no alterations in reproductive capacity. However, physiologically, SMCs in all tissues have a large contractile reserve as myosin light chain kinase is rarely fully activated [83,84]. This contractile reserve may protect smooth muscle tissues from the partial defect in myosin function seen in *Myh11*^{R247C/R247C} mice.

In conclusion, the R247C rare variant does disrupt smooth muscle myosin motor function and aortic contractility, and under circumstances of vascular injury can alter SMC phenotype due to loss of FA maturation (**see model Figure 2.11**). Taken together, these data support the hypothesis that the R247C rare variant may contribute to vascular

disease when accompanied by additional environmental or genetic risk factors. This hypothesis will be further examined in Chapter 3.

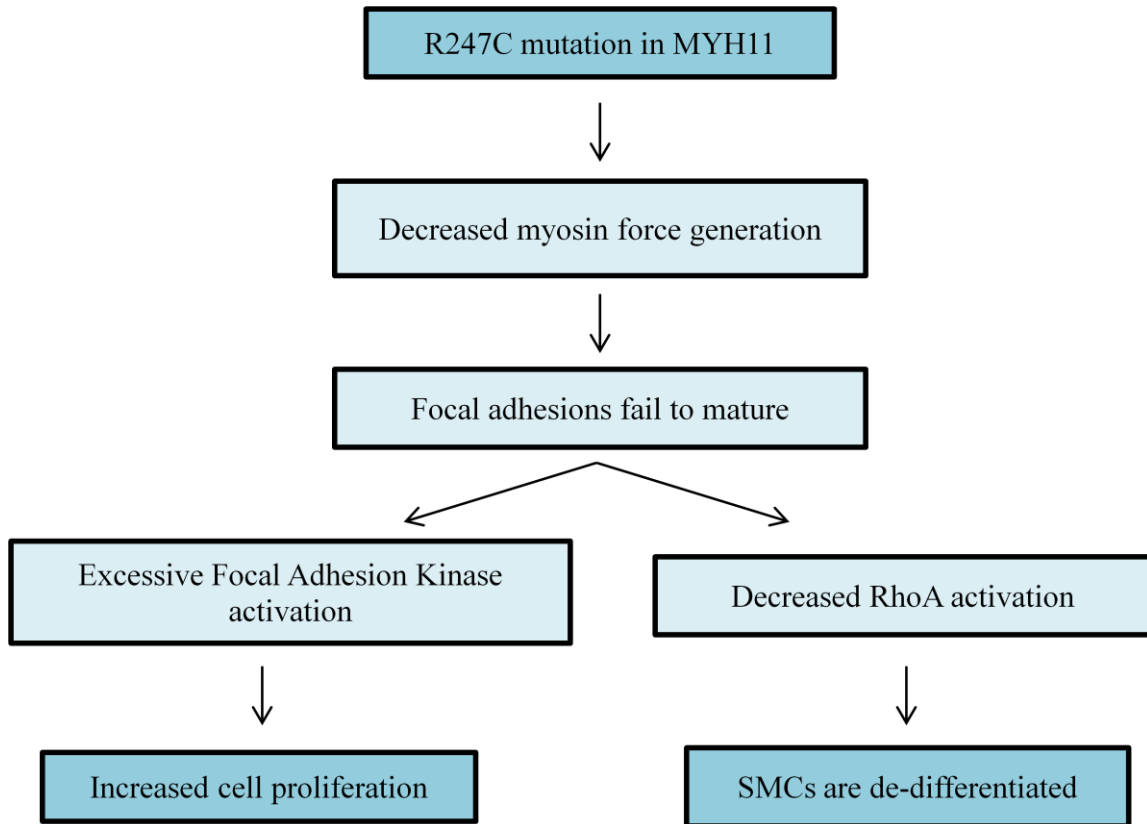


Figure 2.11. Proposed model of phenotypic alteration in *Myh11*^{R247C/R247C} SMCs. Diagram shows a summary of findings forming a complete pathway linking the R247C rare variant to SMC phenotypic changes.

Chapter 3: *Myh11* R247C allele modifies the aneurysm phenotype of *Acta2*^{-/-} mice

Introduction

As discussed in Chapter 2, the *Myh11*^{R247C/R247C} knockin mouse model does not show evidence of vascular disease, but at the same time, the aortas of these mice demonstrate decreased contraction. Therefore, we sought to determine if we could elicit aortic disease in the *Myh11*^{R247C/R247C} knockin mouse by introducing a “second genetic hit”. To test this hypothesis, we introduced the R247C rare variant in mice with knockout of *Acta2*, encoding the smooth muscle α -actin. Previous studies have extensively characterized the *Acta2*^{-/-} mouse model. The initial studies done on this mouse indicated normal vascular development and no overt signs of disease except for difficulty recovering the blood pressure after a hypotensive stimulus [85]. However, further characterization of *Acta2*^{-/-} mice in our lab revealed a previously unappreciated phenotype of aortic dilatation with minimal medial degeneration. In fact, histologic examination of *Acta2*^{-/-} ascending aortas showed an increased number of elastic lamellae within the aortic wall, indicating that there is a developmental effect of this mutation (**Figure 3.1a,b**). The mechanism driving the increased elastin deposition during development is not known, however at 4 weeks of age, SMC density and positive staining for PH3 are also increased in the wall of *Acta2*^{-/-} aortas (unpublished data). These results suggest a potential role for cellular hyperplasia in driving the developmental phenotype of extra elastin layers.

Dilatation of the aorta in *Acta2*^{-/-} mice becomes significant at 12 weeks of age, observable both by echocardiography and also by histology (**Figure 3.1c**). At 6 months of age, these aortas show preliminary signs of medial degeneration, with focal fragmentation of elastin filaments localized near the intimal layer of the aortic wall

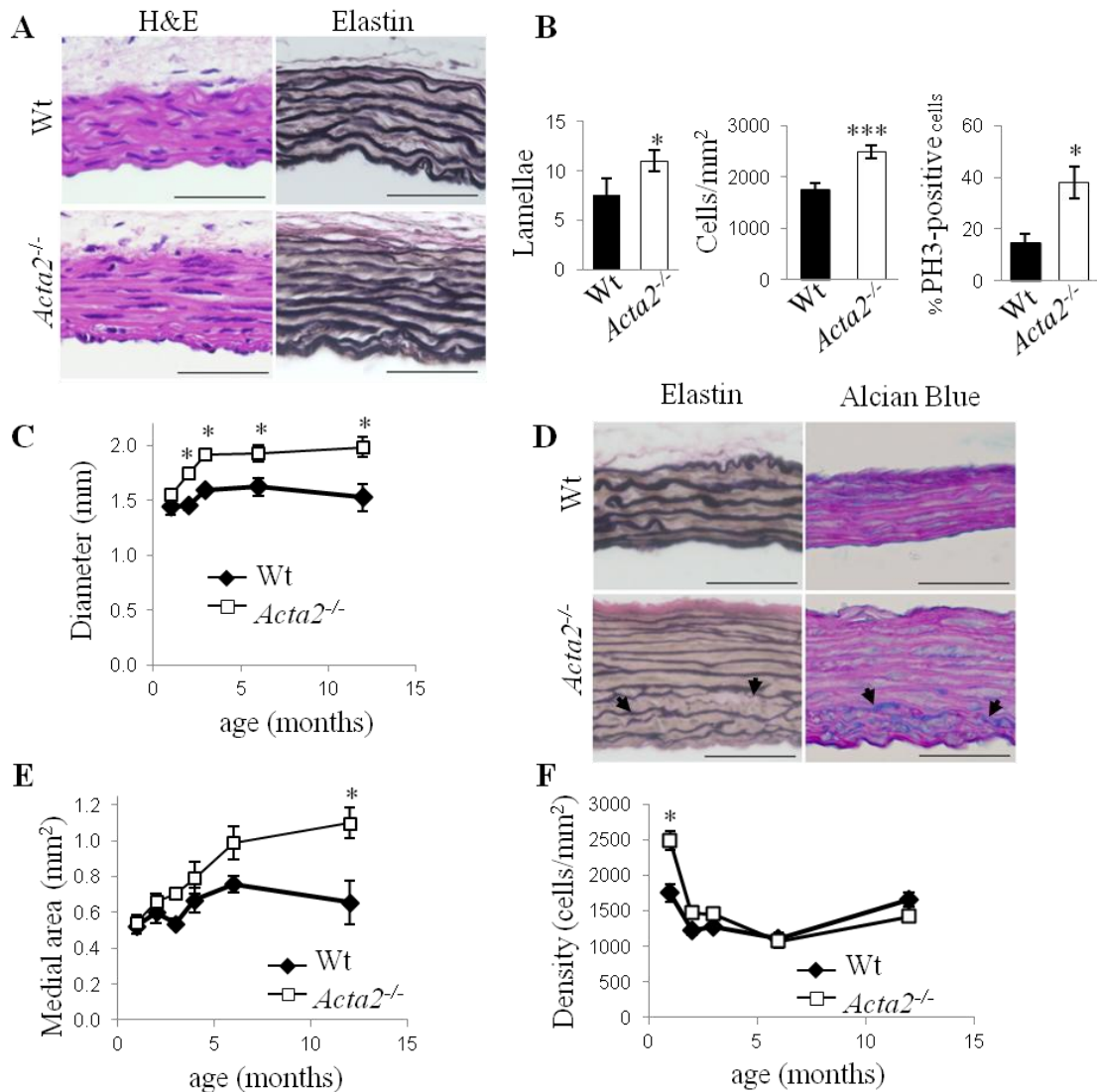


Figure 3.1. Aneurysm formation in *Acta2*^{-/-} mice. A B) Pathology (A) and quantitation (B) at 4 weeks of age shows increased numbers of elastic lamellae and increased cell density in *Acta2*^{-/-} mice. C) Increased aortic diameter, measured by histology, in *Acta2*^{-/-} mice becomes significant at 2 months of age. D) Pathology at 6 months of age shows minimal medial degeneration in *Acta2*^{-/-} mice. Arrows represent sites of elastin fragmentation (elastin) or proteoglycan accumulation (Alcian blue). E) Increased medial area in *Acta2*^{-/-} aortas becomes significant at 12 months of age. F) Cell density is significantly greater in *Acta2*^{-/-} aortas at 1 month of age, but normalizes by 2 months of age. From Jiumei Cao et. al unpublished data, reprinted with permission.

(Figure 3.1d). Minimal proteoglycan accumulation accompanies the changes in elastin.

At earlier timepoints, medial degeneration is not evident. Additionally, the thickness of the medial layer increases over time and becomes significant relative to wild-type by one

year of age (**Figure 3.1e**). However, despite the early indication of proliferative pathology, the SMC density in the aortic wall decreases over time, and equalizes with the wild-type cell density by 12 weeks (unpublished data) (**Figure 3.1f**). This result implies that cellular hypertrophy, rather than proliferation, underlies the medial thickening that occurs as part of the disease process.

Studies performed in other mouse models of genetically triggered aneurysms indicate an important role for angiotensin signaling in aneurysm formation. Specifically, aneurysm formation in a Marfan mouse model (*Fbn1*^{C1093G/+}) is reversed by treatment with the angiotensin type 1 receptor (Agtr1) blocker, losartan [54]. Proteoglycan accumulation and elastin fiber fragmentation were also significantly blunted by losartan treatment. As a result of these studies, our lab initiated a treatment trial of the *Acta2*^{-/-} mice with losartan. Similar to the Marfan mouse model, aortic dilatation in *Acta2*^{-/-} mice is ameliorated by losartan according to our preliminary data (unpublished data). Taken together, the data accumulated so far indicates that increased angiotensin receptor type I-driven signaling may underlie significant portions of the aneurysmal pathology.

The role of decreased contractility in driving aneurysm formation remains to be fully elucidated. The genetic lesions identified thus far are all expected to disrupt the elastin-contractile unit, and thus would affect the response of SMCs to biomechanical forces. However, the *Myh11*^{R247C/R247C} mouse model has decreased aortic contractility but does not develop aortic disease, suggesting that additional signals are necessary to induce pathologic changes. Those signals have yet to be identified, but may include increased activation of angiotensin receptor signaling. Nonetheless, the relationship between loss of contractility and aortic disease remains incompletely characterized.

The goal of this study is first to determine whether the R247C rare variant in *Myh11* can act as a modifier gene for aortic disease either by increasing or accelerating the presentation of the disease in an established model of aneurysm formation (*Acta2*^{-/-} mice) or by inducing disease in conjunction with a second, non-disease causing variant (*Acta2*^{+/-} mice). Secondly, we hope to use this system to evaluate the potential role of contractile dysfunction and signaling changes in driving aneurysm formation.

Materials and Methods

Mouse breeding scheme

Acta2^{-/-} male mice on a pure C57Bl/6 background were crossed with *Myh11*^{R247C/R247C} female mice on a mixed C57Bl/6 and 129sV background. The resulting pups were all *Acta2*^{+/-} *Myh11*^{R247C/+}. These F1 pups were bred to each other to result in all 9 possible *Acta2 Myh11* genotypes. All mice used for the study were 75% C57Bl/6 and 25% 129sV background from the same generation of crosses (F2). For n numbers of mice enrolled in each arm of the study, see **Table 3.1**.

Study	+/+ +/+	+/+ R/+	+/+ R/R	+/- +/+	+/- R/+	+/- R/R	-/- +/+	-/- R/+	-/- R/R
Echo 4 weeks	5	8	6	5	6	4	6	7	7
Echo 8 weeks	6	6	7	5	7	6	7	6	8
Echo 12 weeks	6	7	8	7	7	10	9	6	9
Echo 24 weeks	7	6	6	7	7	9	9	6	8
Histology 12 weeks	2	4	4	5	2	5	4	5	7
Histology 24 weeks	2	3	4	7	5	3	5	8	5

Table 3.1 n numbers of mice per genotype for each aspect of the study.

Echocardiography scanning and analysis

We used 6-8 mice per genotype. Aortic diameter was assessed *in vivo* in live mice using echocardiographic imaging. Mice were anesthetized with inhaled isoflurane (1.5-4%), hooked up to a heart rate monitor, and then Nair was used to remove the fur on the thorax. Scanning was performed with a 40 MHz 704 scanhead on a Vevo 770 echocardiography machine (VisualSonics), and at least four images were stored for each mouse. Each image contains 100 frames over the course of multiple heart beat cycles. Images were transferred off the Vevo 770 machine and analyzed using Sante Dicom Editor software (Santesoft LTD, Athens, Greece). Aortic diameter was measured at peak tension, at which point the aorta has reaches its maximum diameter. At least three measurements were made per session, which were then averaged to obtain the final reported measurement. Aortic diameters were normalized to mouse weight, taken at the same time as the echocardiographic measurements, to compensate for the mixed gender groups used in the study.

Histology processing and analysis

Mice were anesthetized using freshly prepared 2.5% avertin, then the chest cavity was opened to expose the heart. A 26 gauge needle was inserted into the left ventricle, and the mouse was fully perfused with 5mL Dulbecco's phosphate buffered saline, followed by 5mL of 10% neutral buffered formalin. Following perfusion fixation, the ascending aorta was exposed and dissected out of the mouse. Cuts were made proximal to the aortic root at the heart and between the two carotid branches at the aortic arch. The

right carotid artery was kept to orient the vessel. Tissue was left to fix in 10% neutral buffered formalin, then subjected to a series of dehydrating washes in 50%, 70%, 95%, and 100% ethanol, followed by incubation in histoclear before being embedded in paraffin.

Paraffin blocks were sectioned into 5µm sections, which were stained with hematoxylin and eosin or with MOVAT pentachrome according to standard protocols. Analysis was performed using ImageJ software. The color threshold tool was used to designate and count pixels within the aortic wall that were black (elastin), blue (proteoglycans), or red (muscle cells). Elastin breaks were quantitated by visual inspection.

qPCR and Western blot analysis

After removal of the ascending aorta (see protocol above), tissue was snap frozen, then homogenized using a Fisherbrand handheld tissue homogenizer in either Trizol (RNA) or RIPA buffer (protein, see Chapter 2 for buffer composition). RNA and protein were isolated and quantitative RT-PCR and Western blotting were performed according to standard protocols (see Chapter 2 for detailed descriptions).

Contractility assays

Four week old mice were anesthetized with 2.5% avertin and the ascending aortas were dissected out, measured and weighed, and mounted on wire triangles. The mounted tissue was hooked up to an isometric force apparatus, then equilibrated and stretched to 1.8g. Tissue was allowed to recover for 45 minutes following initial

stretching. Physiological buffer was used during all recovery periods (118.5mM NaCl, 4.75mM KCl, 1.2mM MgSO₄, 1.2mM KH₂PO₄, 24.9mM NaHCO₃, 1.6mM CaCl₂, 10.0mM D-glucose, pre-gassed with 95% O₂/5% CO₂ at 37°C). Rings were stimulated four times with KCl (90mM) for 5 minutes each, separated by 5-minute recovery periods in physiological buffer. Tissue was allowed to equilibrate for 45 minutes following the last stimulation with KCl, then were stimulated once with 10mM phenylephrine for 5 minutes. Finally, tissues were snap frozen with clamps pre-cooled in liquid nitrogen and stored at -80°C for possible future protein analysis.

Statistical analysis

Kruskal-Wallis, a nonparametric statistical test suitable for comparing multiple groups, was used for all multigroup comparisons. General p values reported indicate significant differences between the means of all 9 groups (the KW statistic). Dunn's post-tests were performed to assess significant differences between *Acta2*^{+/-} *Myh11*^{+/+} and *Acta2*^{+/-} *Myh11*^{R247C/R247C} groups as well as between *Acta2*^{-/-} *Myh11*^{+/+} and *Acta2*^{-/-} *Myh11*^{R247C/R247C}. No other pairs of groups were specifically compared.

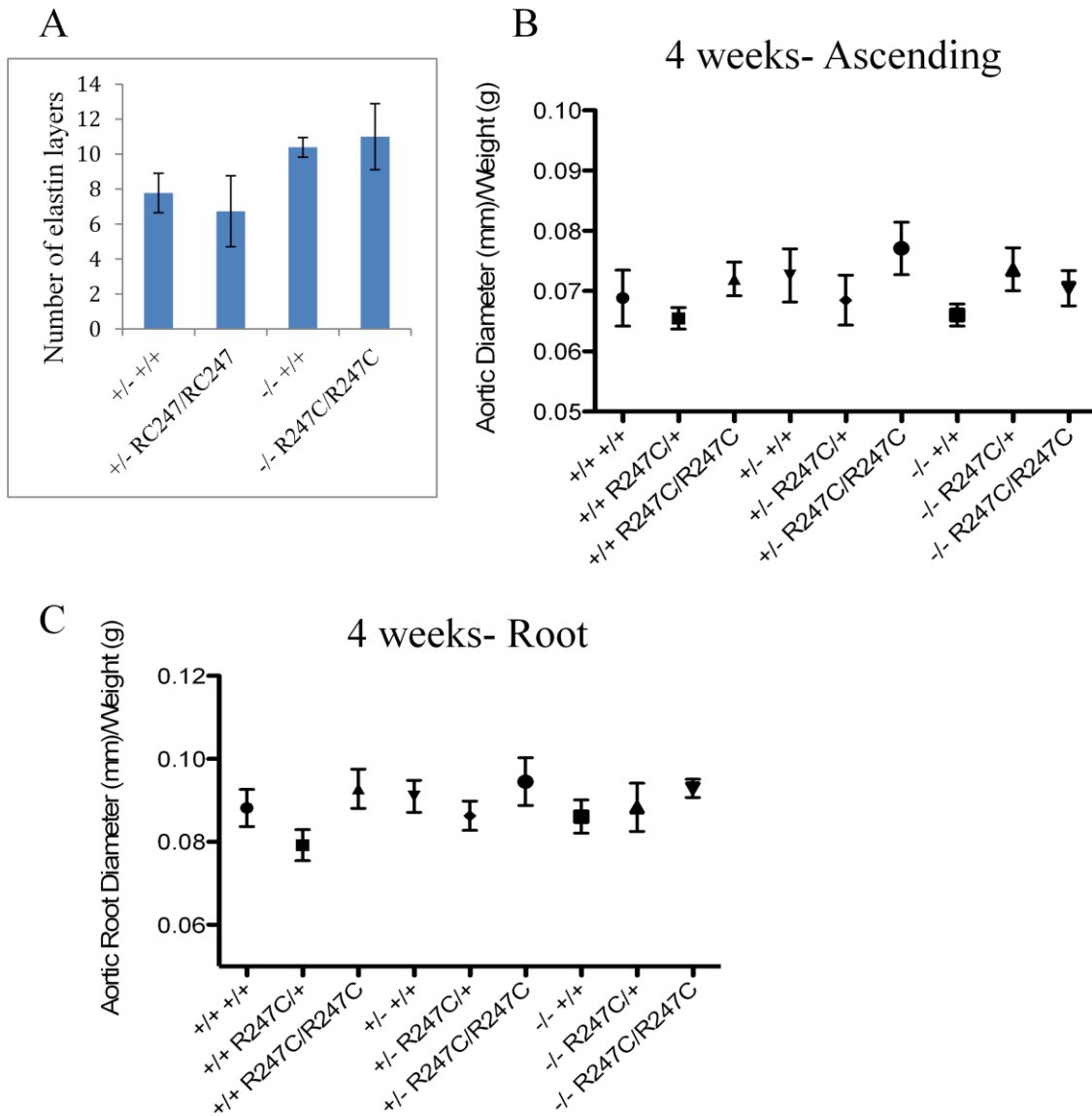


Figure 3.2. No aortic dilation in *Acta2*^{-/-} *Myh11*^{R247C/R247C} mice at 4 weeks of age. A) The R247C allele does not affect the number of elastin layers layed down during development in *Acta2*^{-/-} mice. B,C) No significant difference in the aortic diameter at the ascending (B) or root (C) level in any genotype of mice at 4 weeks of age.

Results

Introduction of the Myh11 R247C mutation does not affect the developmental phenotype of Acta2^{-/-} mice

As described above, *Acta2^{-/-}* mice have a developmental phenotype leading to increased numbers of elastic lamellae in the aorta observable at all timepoints. The homozygous addition of the R247C allele affected the number of elastic lamellae laid down (**Figure 3.2a**). Additionally, at 4 weeks of age, there is no difference in the mean diameter of the ascending aortas of any of the 9 genotypes ($p=0.33$), nor is any dilatation observable at the aortic root ($p=0.31$) (**Figure 3.2b,c**).

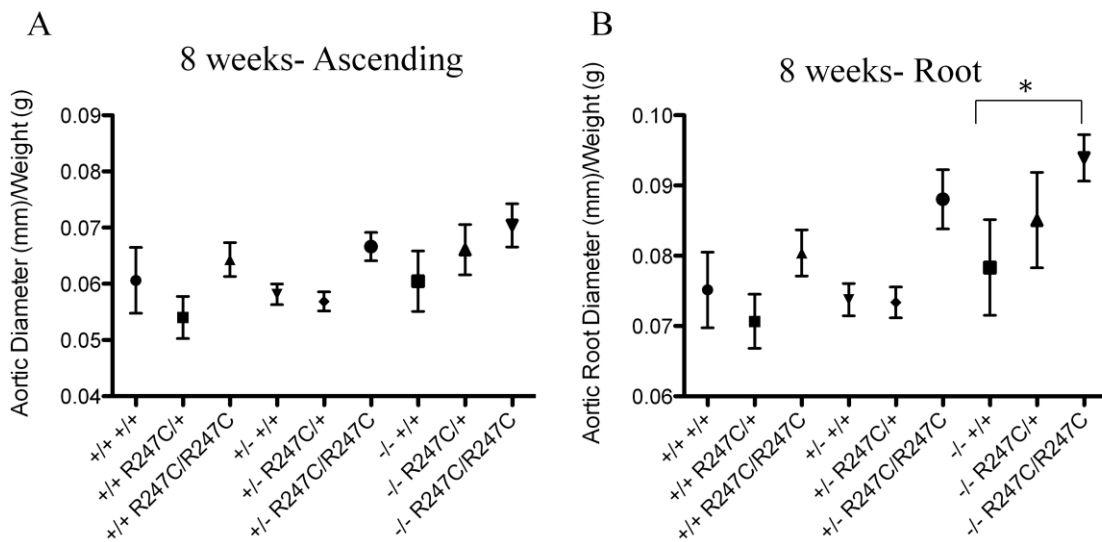


Figure 3.3. *Myh11* R247C allele modifies *Acta2^{-/-}* aortic phenotype at 8 weeks of age. A, B) By 8 weeks of age, *Acta2^{-/-} Myh11^{R247C/R247C}* mice show a trend towards increased aortic diameter in the ascending aorta (A) and a significantly increased aortic diameter at the aortic root (B).

*Aortic dilatation becomes significant by 8 weeks of age in *Acta2^{-/-} Myh11^{R247C/R247C}* mice*

By 8 weeks of age, echocardiographic analysis shows a trend towards increasing ascending aortic diameter with the addition of the R247C allele ($p=0.07$) (**Figure 3.3a**).

Neither of the post-tests between pairs of genotypes showed a significant increase in aortic diameter, however there is a trend towards increased aortic diameter with homozygous addition of the *Myh11* R247C gene on the *Acta2*^{+/-} background. Similarly, there is a dose dependent effect of the R247C allele on ascending aortic diameter on the *Acta2*^{-/-} background. At the level of the aortic root, there is a significant dilatation

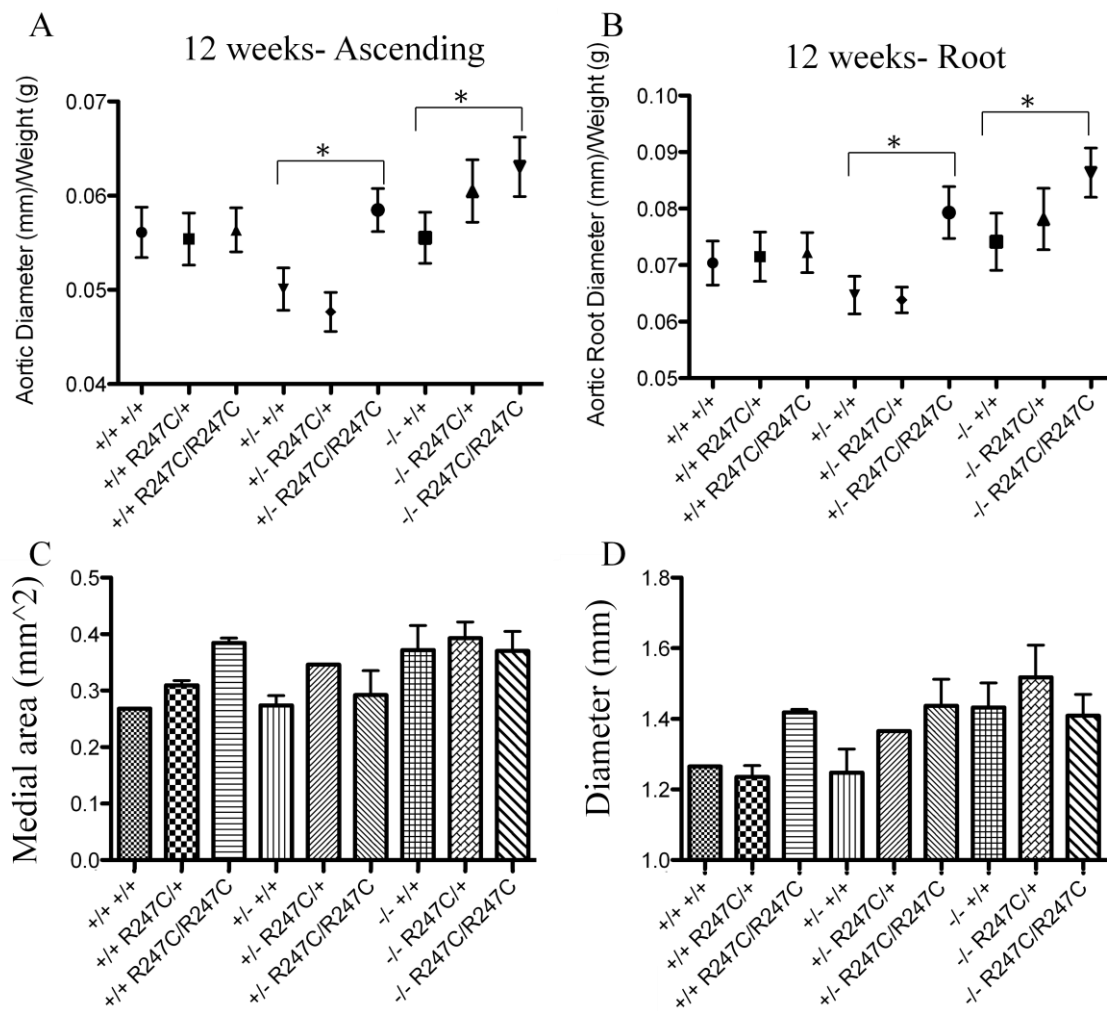


Figure 3.4. *Myh11* R247C allele increases *Acta2*^{-/-} aortic diameter at 12 weeks of age. A, B) By 12 weeks of age, *Acta2*^{-/-} *Myh11*^{R247C/R247C} mice show a significantly increased aortic diameter at the level of both the ascending aorta (A) and the aortic root (B) by echocardiography. C) No significant difference in medial area at 12 weeks of age. D) Histology measurements confirm increased diameter in *Acta2*^{+/-} *Myh11*^{R247C/R247C} mice.

present ($p=0.01$), and similarly the $Acta2^{+/-} Myh11^{R247C/R247C}$ aortas are enlarged compared with $Acta2^{+/-} Myh11^{+/+}$ aortas (not significant) while there is a gene dose effect with the addition of the R247C allele to the $Acta2^{-/-}$ mice ($p<0.05$) (**Figure 3.3b**).

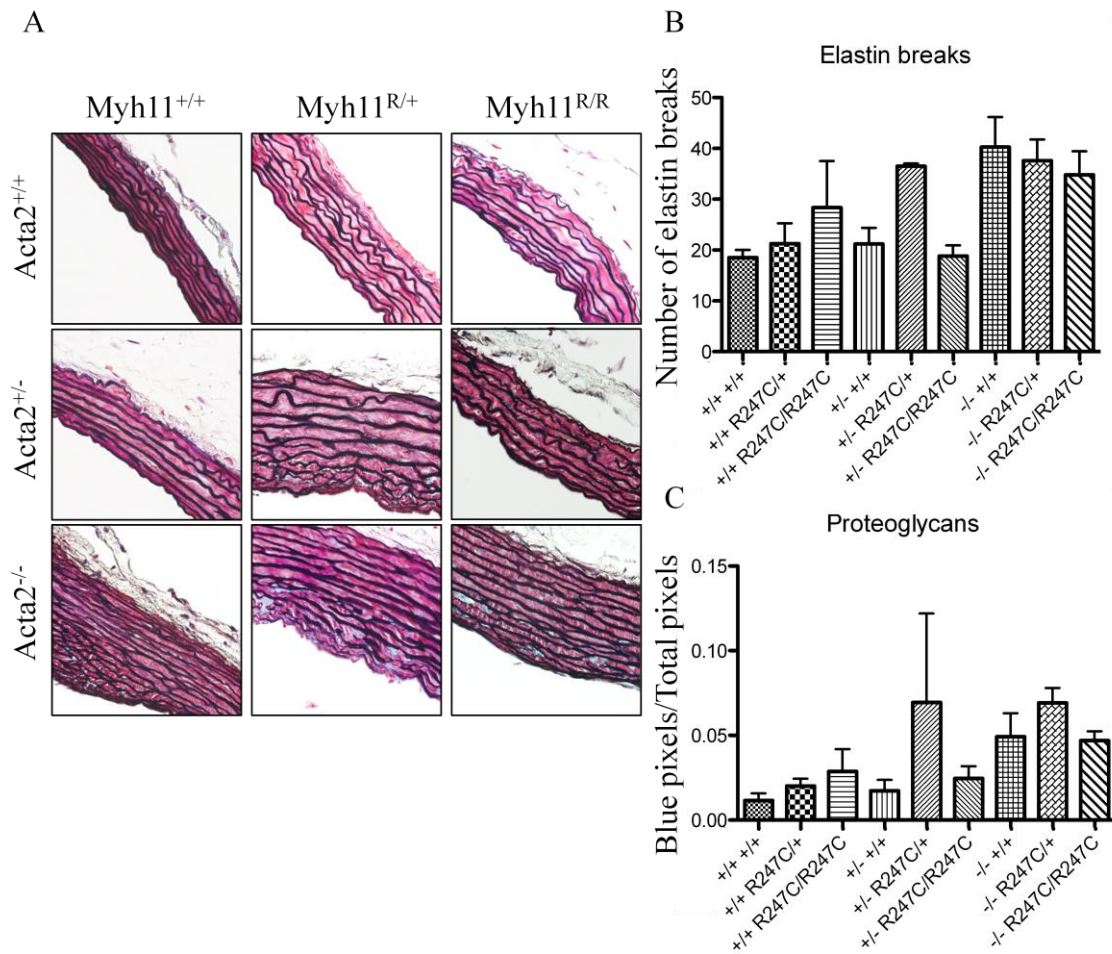


Figure 3.5. *Myh11* R247C allele does not affect medial degeneration in *Acta2*^{-/-} aortas at 12 weeks of age. A) Representative aortic sections stained with MOVAT pentachrome from each of the 9 genotypes at 12 weeks of age. B, C) Analysis of elastin fragmentation (B) and proteoglycan deposition (C) shows that the R247C allele does not impact medial degeneration at 12 weeks of age.

By 12 weeks of age, aortic dilatation becomes significant and medial degeneration begins

By 12 weeks of age, the changes in aortic diameter across all genotypes becomes significant at the level of both the ascending aorta (p=0.01) and the aortic root (p=0.01) (**Figure 3.4a,b**). Again, the trend suggests that the homozygous R247C allele combined with loss of one Acta2 allele (*Acta2*^{+/-}) elicits aneurysm formation. In contrast, there is a dose-dependent effect on the *Acta2*^{-/-} background. These results therefore confirm that over time the modifying effect of the R247C allele on aortic phenotype remains similar, but becomes more statistically significant.

Histologic analysis of the 12 week aortas shows very limited effects of introduction of the R247C allele on medial thickening, proteoglycan deposition, or elastin fragmentation (**Figure 3.4c, Figure 3.5a,b,c**). The *Acta2*^{-/-} aortas, regardless of the R247C gene dose, have increased medial area, increased percent area of proteoglycans, and increased numbers of elastin breaks compared to wild-type or *Myh11*^{R247C/R247C}. However, there are no significant differences between groups containing different numbers of R247C alleles on the same *Acta2* background.

At 6 months of age, both aortic dilatation and medial degeneration are significantly greater in Acta2^{-/-}Myh11^{R247C/R247C} aortas

As at 8 and 12 weeks of age, at 6 months of age there is a significant dose dependent effect of the R247C allele on the aortic root and ascending aortic diameters of *Acta2*^{-/-} mice (**Figure 3.6a,b**). By 6 months, we begin to see a similar dose dependent effect in the *Acta2*^{+/-} background, suggesting that perhaps as the mice age a heterozygous R247C allele might also induce disease on this background. Again both ascending (p=0.02) and root (p=0.02) diameters are significantly different between groups.

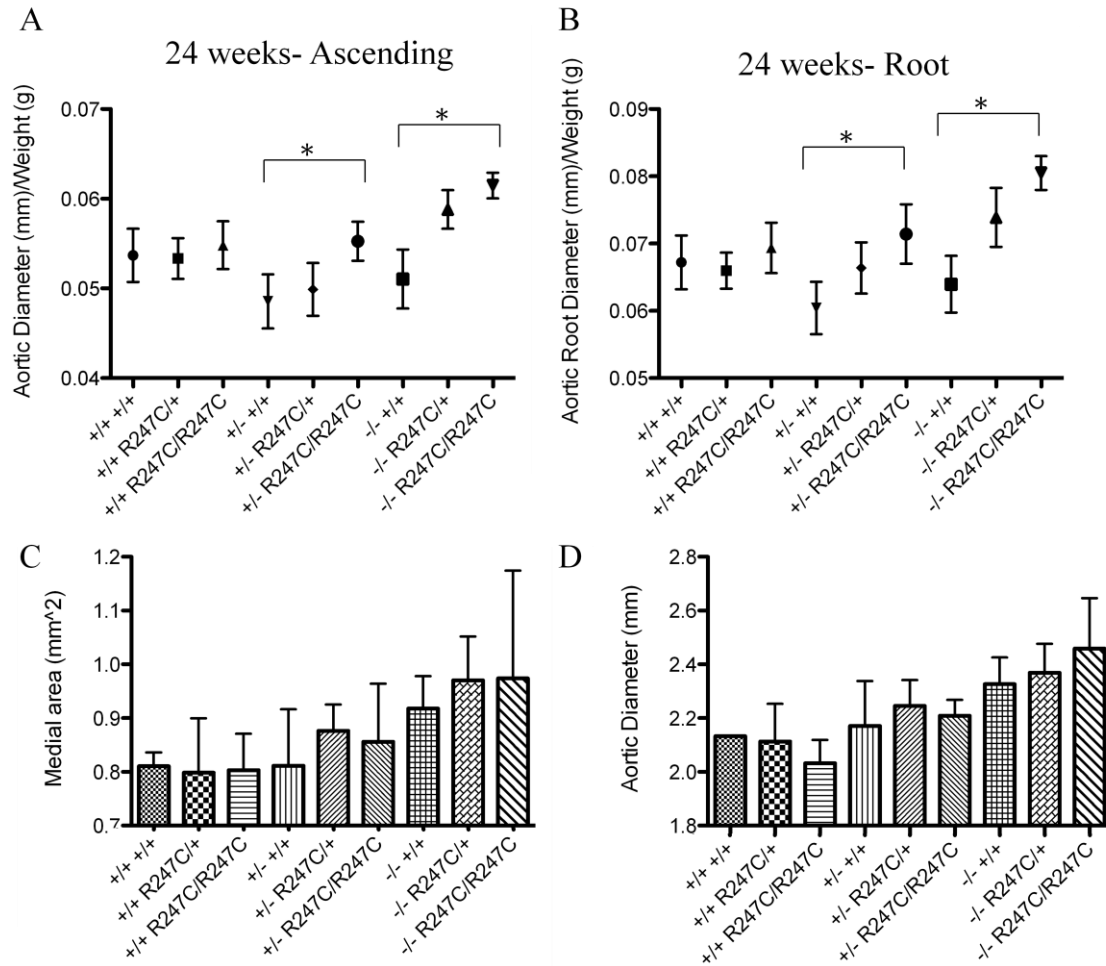


Figure 3.6. *Myh11* R247C allele increases *Acta2*^{-/-} aortic diameter at 24 weeks of age. A, B) At 24 weeks of age, *Acta2*^{-/-} *Myh11*^{R247C/R247C} mice show a significantly increased aortic diameter at the level of both the ascending aorta (A) and the aortic root (B) by echocardiography. C, D) Medial area (C) and histologic measurements of aortic diameter (D) reflect the same trend as echocardiographic findings.

In contrast to earlier analyses, however, proteoglycan deposition is increased in a dose-dependent manner with the addition of the R247C allele on the *Acta2*^{-/-} background (Figure 3.7a,c). Similarly, the *Acta2*^{+/-} *Myh11*^{R247C/R247C} aortas have increased proteoglycan deposition compared with *Acta2*^{+/-} mice with zero or one copies of the R247C allele. However, elastin breaks are not increased in *Acta2*^{+/-} *Myh11*^{R247C/R247C} aortas, or in *Acta2*^{-/-} *Myh11*^{R247C/+} aortas, suggesting either that the R247C allele may preferentially increase proteoglycan deposition over elastin fragmentation, or that

proteoglycan deposition generally precedes elastin fragmentation in the disease process (Figure 3.7b). There is a trend towards increased medial area as the aortic diameter increases, but the results are not significant (Figure 3.6c).

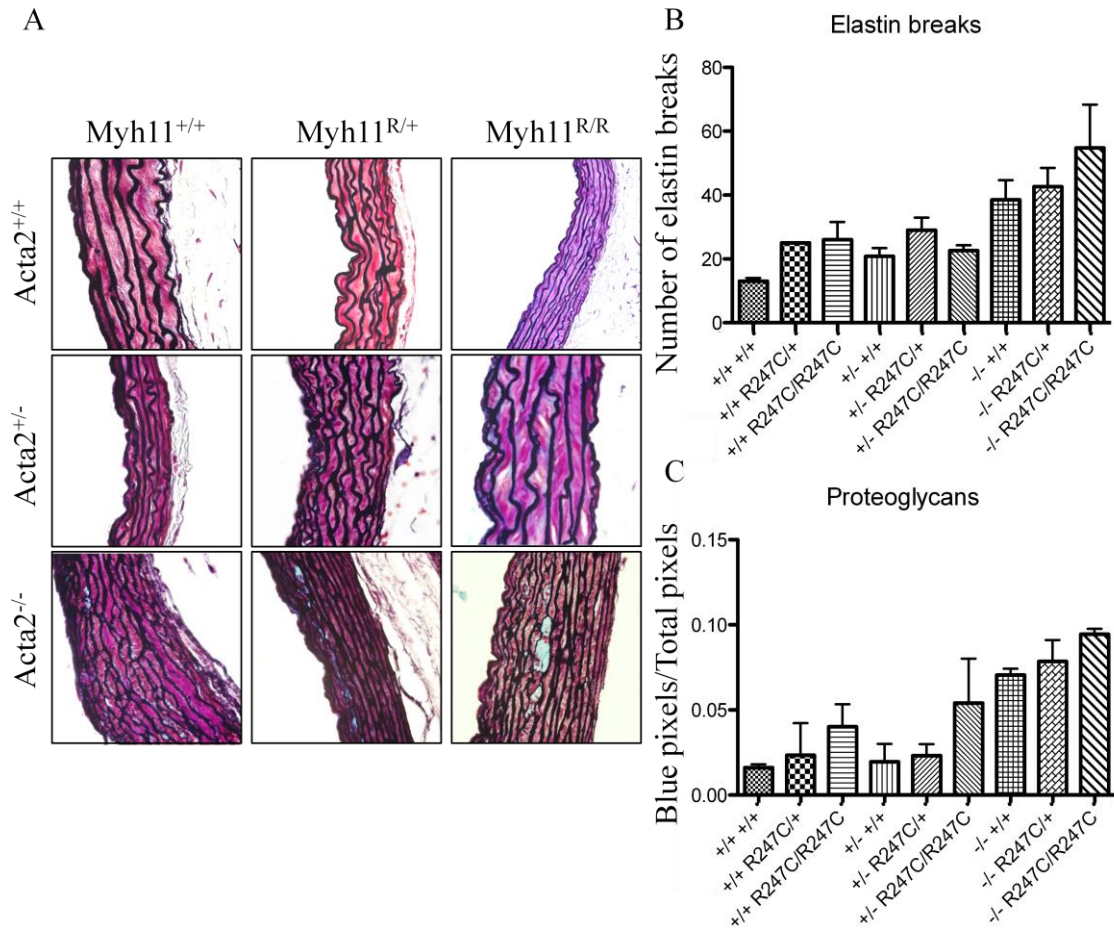


Figure 3.7. Myh11 R247C allele increases proteoglycan deposition in Acta2^{-/-} aortas at 24 weeks of age. A) Representative aortic sections stained with MOVAT pentachrome from each of the 9 genotypes at 24 weeks of age. B, C) Analysis of elastin fragmentation (B) and proteoglycan deposition (C) shows that the R247C allele increases medial degeneration in Acta2^{-/-} aortas but only impacts proteoglycan deposition in Acta2^{-/-} aortas.

Addition of the R247C allele does not further decrease contractility in the Acta2^{+/-} or Acta2^{-/-} aortas

We hypothesized that the R247C allele would further decrease contractility in

Acta2^{+/-} and *Acta2*^{-/-} aortas, and that a threshold level of decreased contractility could be established beyond which aortic disease results. Contractility assays were performed to determine the role of decreased contractility in the modifying effect of the *Myh11* R247C alteration. Surprisingly the presence of the R247C allele had no effect on the contractility of either *Acta2*^{+/-} or *Acta2*^{-/-} aortas in response to either KCl or phenylephrine (**Figure 3.8**). These results contradict our hypothesis, and suggest that an alternative mechanism distinct from decreased contractility underlies the enhanced aortic aneurysm and pathology apparent with the addition of the R247C allele.

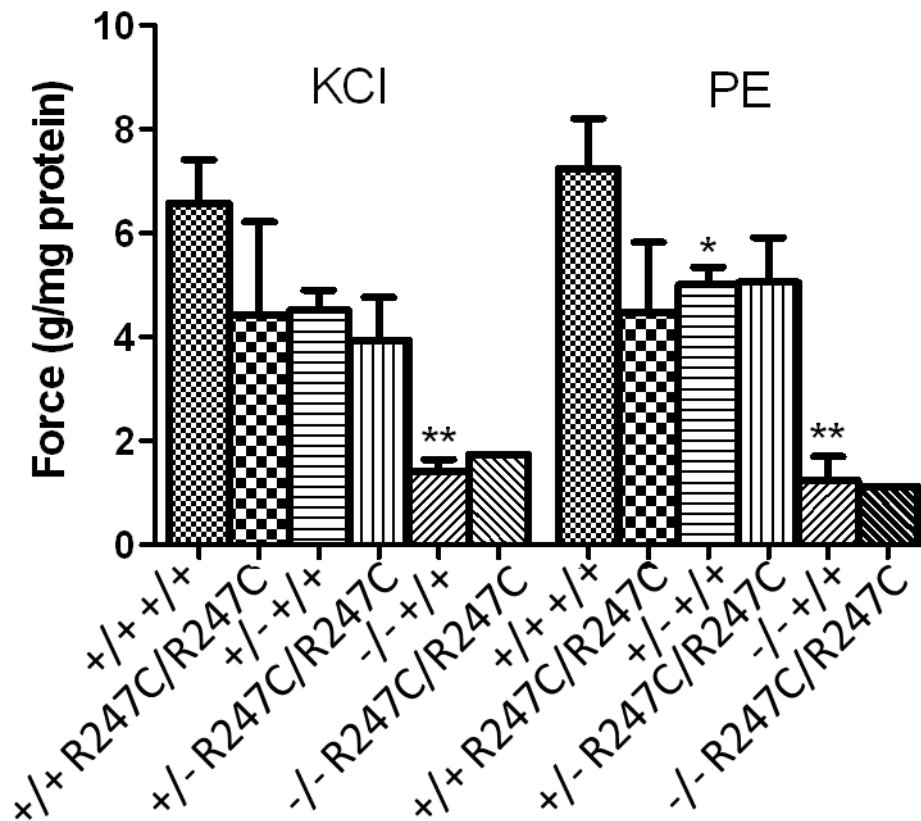


Figure 3.8 *Myh11* R247C allele does not affect contractility of *Acta2*^{-/-} aortas. The addition of the R247C allele does not impact aortic contractility in response to either KCl or phenylephrine (PE) in *Acta2*^{+/-} or *Acta2*^{-/-} mice.

Discussion

The addition of the R247C allele worsens the aortic disease phenotype in *Acta2*^{-/-} mice and induces aortic disease in *Acta2*^{+/-} mice. By 8 weeks of age, aortic diameter is increased in mice of either *Acta2* genotype carrying homozygous R247C alleles compared with *Myh11*^{+/+} littermates. As the mice age, the aortic diameter progressively increases. Therefore, the R247C allele both accelerates the onset of aortic disease and increases its severity.

The data presented speak to two distinct clinically relevant patient populations whose disease has previously been unexplained. First, the *Acta2*^{+/-} *Myh11*^{R247C/R247C} mice are analogous to young patients who present with TAAD with no family history, no environmental risk factors for disease, and no identifiable *de novo* mutation in the previously characterized disease-causing genes [86]. Here, heterozygous loss of *Acta2* and the *Myh11* R247C missense mutation, which independently do not cause any pathology, lead to disease when they co-occur. These results suggest that patients could inherit multiple rare genetic variants that cumulatively cause disease, while each parent carries a subset of variants that are insufficient to provoke a phenotype.

Furthermore, clinical histories of families with TAAD reveal significant variability in the age of onset, and even in the severity of the clinical presentation, between family members who carry identical disease causing mutations [87]. The earlier onset and increased severity of disease in *Acta2*^{-/-} *Myh11*^{R247C/R247C} mice suggests that rare variants that differ between affected family members may drive the clinical variability, promoting more severe disease in a subset of family members.

Initially, we hypothesized that the modifying effect of the R247C allele would be due to decreased aortic contractility, and therefore we expected to see a synergistic loss of contractility at early timepoints in the genotypes that later developed more disease. However, the presence of the R247C allele had no effect on the contractility of *Acta2*^{+/-} or *Acta2*^{-/-} aortas, suggesting that the mechanism underlying increased disease in mice carrying that allele is not additive contractile dysfunction. Since loss of force generation in the myosin motor is the most direct phenotypic outcome of the R247C mutation, this result was surprising. However, the cellular data presented in Chapter 2 suggest that downstream signaling effects of this loss of myosin motor function have a profound effect on SMC phenotype. Plausibly, although aortic contractility itself is not affected by the combination of the *Myh11* R247C allele and the loss of *Acta2*, distinct downstream signaling driven by each genetic change combines to provoke a more severe disease.

Despite evidence of significant aortic enlargement at 8 weeks of age, the expected R247C-induced increase in medial degeneration does not become significant until 6 months of age. Proteoglycan deposition is increased in *Acta2*^{-/-} *Myh11*^{R247C/R247C} mice compared with *Acta2*^{-/-} *Myh11*^{+/+} mice and is also significantly increased in *Acta2*^{+/-} *Myh11*^{R247C/R247C} mice than in *Acta2*^{+/-} *Myh11*^{+/+} mice. However, elastin fragmentation is only affected by the R247C allele on the *Acta2*^{-/-} background. These results taken together suggest a disease progression in this particular mouse model whereby aortic dilatation is the initial observable effect, followed by proteoglycan deposition, and eventually by elastin fragmentation. Previous data shows that increased matrix metalloproteinase (MMP) activity drives elastin fragmentation in multiple aneurysm models, and unpublished data from our lab indicates that signaling by glycogen synthase

kinase 3 β (GSK3 β) drives expression of proteoglycans in SMCs [50]. However the mechanistic links between aortic dilatation and GSK3 β signaling or between GSK3 β signaling and MMP activity are incompletely established. Future work on this mouse model will examine the activity of MMPs and will establish patterns of signaling changes including potential increases in GSK3 β activation or in angiotensin receptor type 1-driven signaling.

In summary, the data show that *Myh11* R247C is a modifier allele for aortic disease: it can cause disease in conjunction with another benign genetic variant (heterozygous loss of *Acta2*), and it can accelerate disease progression in a genetic model of aneurysm formation (homozygous loss of *Acta2*).

Chapter 4: 16p13 Duplications Lead to Increased Contractile Protein Turnover

Introduction

To identify novel genetic variants associated with sporadic TAAD, DNA samples isolated from spit or blood samples from approximately 800 Caucasian TAAD patients without a family history of disease were subjected to a copy-number variant (CNV) screen, along with 4500 control DNA samples. Initial screening was performed on an Illumina whole genome SNP array, and statistically interesting results were pulled out using two separate CNV algorithms. Data were confirmed using specific quantitative PCR based assays, and further replicated using an additional patient cohort. This analysis identified a recurrent CNV, duplications at the 16p13.1 chromosomal locus, that is associated with thoracic aortic disease [88]. Low copy repeats are prevalent in this region of the genome, making it a hotspot for nonhomologous recombination and therefore a common site of CNVs. Previous studies had implicated both deletions and duplications in this locus in the pathogenesis of multiple different neuropsychiatric disorders, including schizophrenia and autism [89-91]. However, the genetic data from these earlier studies indicated a 2- to 3-fold enrichment of these CNVs in these neuropsychiatric patients compared with unaffected controls. Our data showed a reproducible 11-fold enrichment of 16p13.1 duplications in patients with TAAD, and in fact this specific CNV was present in 1% of all patients with TAAD compared to less than 0.1% of the general population. Therefore, 16p13.1 duplications are the most common genetic risk factor for TAAD identified to date.

Patients carrying the 16p13.1 duplications were more likely to have a younger age of disease presentation. Uniformly, these patients had hypertension and presented with dissections without signs of prior aortic enlargement. Due to the high density of low

copy repeats in the 16p13.1 region, unrelated patients had distinct break points marking the ends of their duplicated regions. However, a common region containing nine genes was duplicated in every patient identified with 16p13.1 duplication. Directly in the center of the commonly duplicated region lies *MYH11*. Due to our previous knowledge of a link between *MYH11* and vascular disease, we hypothesized that *MYH11* is the gene that causes increased risk of TAAD in people with 16p13.1 duplications.

Little is known about how gene duplications lead to human disease. In particular, the molecular mechanisms linking three copies of *MYH11* with a predisposition for aortic dissection are not immediately apparent. Because the additional copy of the *MYH11* gene should increase the expression and production of myosin heavy chain, we focused on possible pathways that would link this overexpression to the disease. As described in Chapter 1, the *MYH11* gene encodes four distinct transcripts leading to four isoforms of the smooth muscle myosin heavy chain protein, of which two are expressed in the aorta [92]. Transgenic mouse models overexpressing each of those two isoforms were previously generated and characterized. Despite evidence of successful transgene expression from the use of a tagged myosin protein, neither transgenic expression of SM1 nor SM2 altered the ratio between the two isoforms in aortic tissue (**Figure 4.1a**). However, both transgenic models did result in profound effects on the contractility of the aorta: the SM1 model had increased aortic contractility while the SM2 model had decreased aortic contractility (**Figure 4.1b,c**) [33]. These results suggest that the overexpression of myosin leads to selective degradation that normalizes the total amount and isoform ratio of myosin in the cell. Simultaneously, the changes in contractility support the hypothesis that overexpression of myosin affects

smooth muscle cell phenotype in a similar manner to other causes of genetically triggered aortic disease.

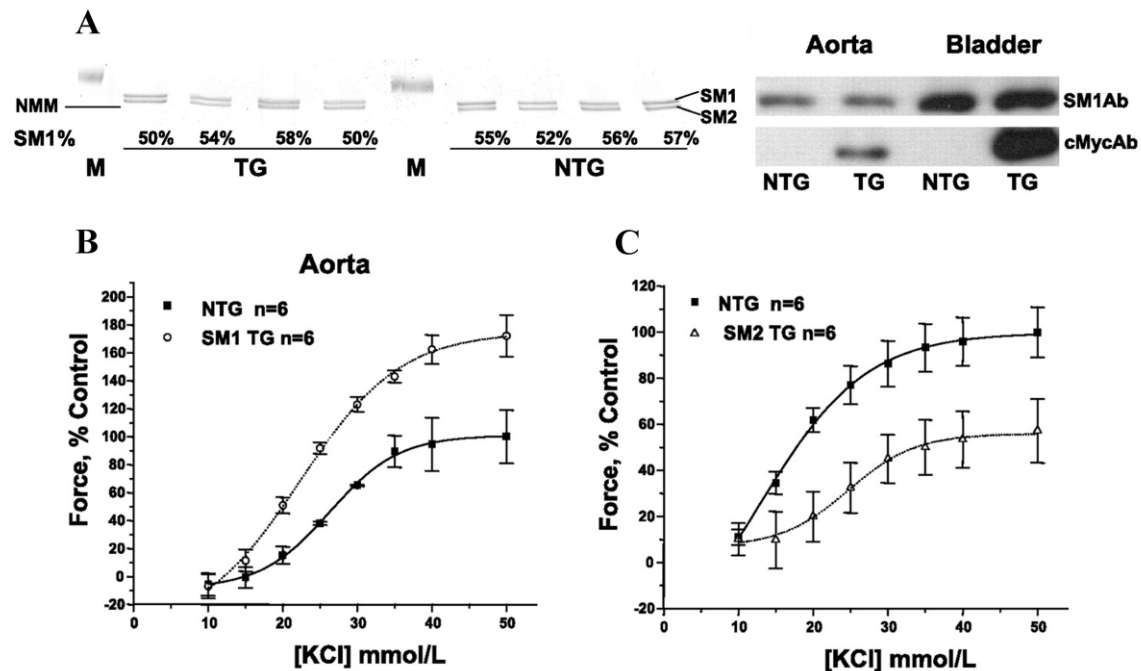


Figure 4.1 Transgenic overexpression of myosin isoforms alters aortic contractility. A) Transgenic overexpression of either SM1 or SM2 does not affect the ratio of SM1:SM2 or the total level of myosin protein. B) SM1 transgenic mice have increased aortic contractility. C) SM2 transgenic mice have decreased aortic contractility. Reprinted with permission from Expression and function of COOH-terminal myosin heavy chain isoforms in mouse smooth muscle. Martin AF, Bhatti S, Pyne-Geithman GJ, Farjah M, Manaves V, Walker L, Franks R, Strauch AR, Paul RJ. *Am J Cell Physiol.* 2007.

Myosin heavy chain molecules require a specific molecular chaperone to ensure proper protein folding; folding of myosin is critical as monomers of myosin interact with each other to form first dimers, then filaments. Increased expression of myosin would therefore reduce access of individual molecules to the required chaperone protein, potentially resulting in a pool misfolded monomers that could have outsized effects on filament formation. The myosin-specific chaperone, first described in the nematode worm *Caenorhabditis elegans* (*C. elegans*), is known as Unc45 [93]. Mammalian organisms have two Unc45 genes, encoding two distinct isoforms of the chaperone

called Unc45a and Unc45b [94]. Unc45b is specifically expressed in striated muscle and acts as the chaperone for cardiac and skeletal muscle myosins. Unc45a is ubiquitously expressed, and is the canonical chaperone for nonmuscle and smooth muscle myosins. Early work performed on this chaperone in the *C. elegans* model indicated that the ratio of expression of myosin to Unc45 is tightly regulated. Worms engineered to either underexpress or overexpress Unc45 both showed accelerated degradation of myosin protein via the ubiquitin-proteasome system (**Figure 4.2a,b,c**) [95].

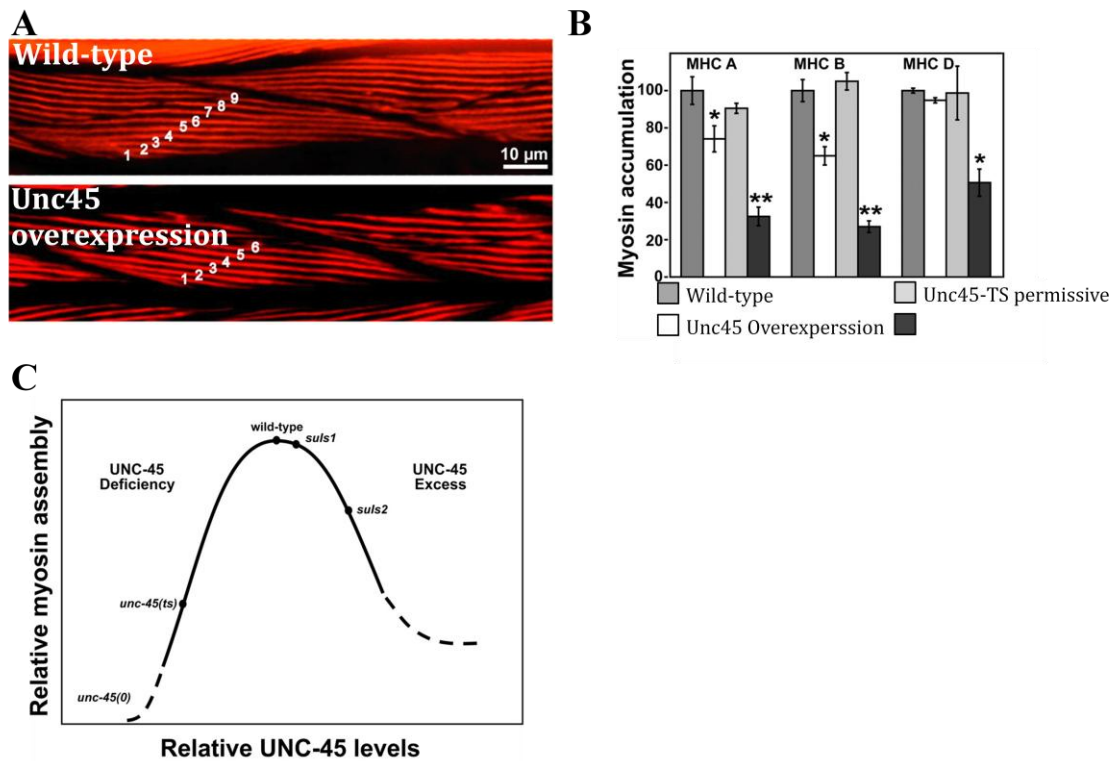


Figure 4.2 Unc45 overexpression drives myosin degradation in *C. elegans*. A) Reduced numbers of myosin filaments in *C. elegans* muscle cells with Unc45 overexpression. B) Loss (dark grey bars) or overexpression (white bars) of Unc45 reduces accumulation of all isoforms of myosin heavy chain in *C. elegans*. C) Model showing the requirement of Unc45 for stable assembly of myosin filaments. Reprinted with permission from The UNC-45 chaperone mediates sarcomere assembly through myosin degradation in *Caenorhabditis elegans*. Landsverk ML, Li S, Hutagalung AH, Najafov A, Hoppe T, Barral JM, Epstein HF. *J. Cell Biol.* 2007.

Therefore, studies on Unc45 suggest a potential mechanism by which overexpression of *MYH11* in 16p13.1 duplication patients could cause disease: paradoxically, too much myosin expressed could drive degradation of myosin protein and leave the SMCs unable to properly contract.

Materials and Methods

Protocols for vascular SMC explant from aortic tissue, cell culture, RNA isolation from cells or tissue and quantitative PCR, protein isolation from cells or tissue and Western blotting, and immunofluorescent cellular staining are described in detail in Chapter 2. For additional antibodies used in this chapter see **Table 4.1**.

Antigen	Company	Species	Uses
LC3	Novus Biologicals	Rabbit	WB
p62	Sigma	Rabbit	WB
Phospho-AMPK	Cell Signaling Technology	Rabbit	WB
AMPK	Cell Signaling Technology	Rabbit	WB
Phospho-ACC	Cell Signaling Technology	Rabbit	WB
ACC	Cell Signaling Technology	Rabbit	WB
Phospho-p70S6K	Cell Signaling Technology	Rabbit	WB
p70S6K	Cell Signaling Technology	Rabbit	WB
Phospho-S6	Cell Signaling Technology	Rabbit	WB
Phospho-PERK	Cell Signaling Technology	Rabbit	WB
PERK	Cell Signaling Technology	Rabbit	WB
Phospho-EIF2 α	Cell Signaling Technology	Rabbit	WB
EIF2 α	Cell Signaling Technology	Rabbit	WB
Grp94	Enzo Life Sciences	Rabbit	WB
Grp78	Enzo Life Sciences	Rabbit	WB

Erp72	Enzo Life Sciences	Rabbit	WB
MLC ₂₀	ECM Biosciences	Mouse	IF
MLC ₂₀	Cell Signaling Technology	Rabbit	WB
Phospho-MLC ₂₀ (Ser19)	Cell Signaling Technology	Rabbit	WB

Table 4.1 Antibodies used in Chapter 4.

Radiolabeled pulse-chase assay

Confluent cells were seeded into 35mm dishes (100,000 cells per dish) and allowed to attach overnight. Media was changed to 1% serum containing medium for 24 hours before being switched to pulse media (1% serum containing media plus 0.1uCi/mL ¹⁴C labeled phenylalanine). At specified timepoints throughout the pulse period, media was removed, and cells were lysed in 1mL 10% trichloroacetic acid and stored at 4°C until the end of the experiment. At the end of the pulse period (48 hours), the media were changed on remaining plates to chase media (1% serum containing media plus 2mM excess unlabeled phenylalanine). At specified timepoints during the chase period, a 500uL aliquot of media was removed and combined with 500uL of 20% trichloroacetic acid. These aliquots were also stored at 4°C until the end of the experiment. At the end of the experiment, all lysates were combined with scintillation fluid and analyzed on a 1900TR liquid scintillation analyzer (Packard Instruments). Protein synthesis rates were calculated using the incorporation of ¹⁴C into cellular protein over the pulse period, while protein degradation rates were calculated using the rate of ¹⁴C release into the media over the chase period as measured by dpm [163].

Infection with RFP-GFP-LC3 lentivirus

The RFP-GFP-LC3 lentivirus and a control lentivirus were both generously given to us by Joseph Hill, M.D., Ph.D., and his lab at University of Texas Southwestern Medical Center. Cells were seeded as for other immunofluorescence protocols, and after being allowed to incubate overnight, cells were treated with 1% serum containing media supplemented with 1 μ L/mL polybrene and viral titers at a multiplicity of infection of 5, determined through initial dose-dependent experiments to find the optimal multiplicity of infection. After 72 hours of incubation with the virus, cells were fixed in 4% paraformaldehyde as described previously, and coverslips were mounted in Vectashield mounting media with a DAPI counterstain.

Collagen contraction assays

Cells were separated into 250,000 cell aliquots and seeded within a matrix of type I collagen from rat tail (BD Biosciences). The collagen mixture was prepared according to the manufacturer's specifications at a final concentration of 1mg/mL collagen. Gels were allowed to polymerize at room temperature for at least one hour, then were immediately treated with 1% serum containing media with or without the addition of 1mg/mL 4-phenylbutyric acid. Gels were allowed to incubate for 5 days to accumulate tension, and then were released from attachment to the cell culture plastic to induce contraction. Gels were photographed 10 minutes after release, and measurements were performed using ImageJ software [164].

Calcium imaging

Cells were seeded onto 10mm coverslips at a density of 5,000 cells per coverslip and allowed to attach overnight. Cells were then incubated in 1% serum media with or without the addition of 1mg/mL 4-phenylbutyric acid for 24 hours. Coverslips were pre-treated with 4uM Fura-2AM (Teflabs) for 30 minutes at 37°C, then transferred to calcium free ECS buffer (140 mM NaCl, 5 mM KCl, 1mM MgCl₂, 10 mM HEPES, 10 Glucose (pH 7.4)) for the remainder of the experiment. Coverslips were mounted for viewing on a Nikon TE200 microscope, and imaging was performed with Incytim2 software. Measurements were taken at 340nm and 380nm, and the intensity ratio was used to determine calcium levels. This provides an internal control so that the success of dye-loading does not affect the concentration readouts. Baseline measurements were taken for one minute, then 1uM thapsigargin was added to the buffer. Measurements of cytoplasmic calcium continued out to six minutes to allow partial recovery from the thapsigargin [165].

Results

Increased protein turnover in systems of myosin overexpression

Initial characterization was performed using frozen aortic tissue samples from patients with 16p13 duplications. Compared with control tissue samples, 16p13 duplication patient tissue showed a significant increase in expression of *MYH11*. Surprisingly, there was a similar increase in expression of other contractile proteins (*ACTA2* and *CNN1*) (**Figure 4.3a**). However, there was no concomitant increase in the accumulation of SM-MHC protein level, or of actin or calponin protein levels (**Figure**

4.3b). These results suggested that there may be translational control or increased degradation of the proteins..

A specific chaperone called *Unc45a* helps to fold the smooth muscle and nonmuscle myosin heavy chain isoforms. In 16p13 duplication patient tissue, both mRNA expression and protein accumulation of *Unc45a* was significantly decreased compared with control tissue (**Figure 4.3c,d**). However, ectopic expression of *Unc45b*, typically seen only in cardiac and skeletal muscled cells, was observed in the tissue (**Figure 4.3d**).

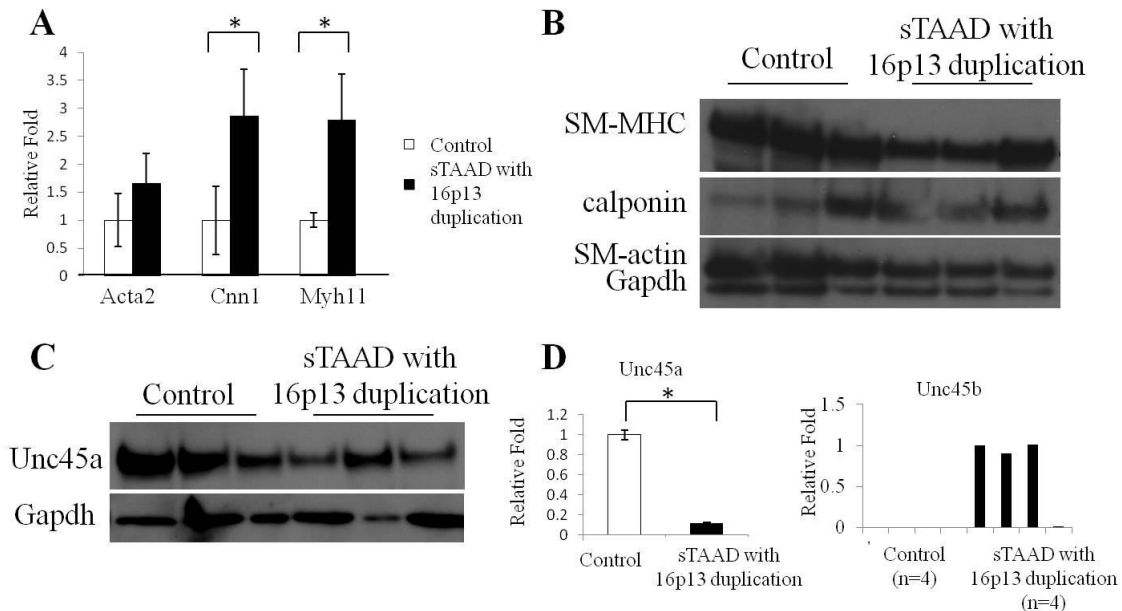


Figure 4.3 Changes in contractile gene expression and *Unc45* isoform expression in tissue from 16p13 duplication patients. A) Increased expression of contractile genes in frozen tissue from patients with 16p13 duplication. B) No change in contractile protein levels in aortic tissue with 16p13 duplication. C,D) Reduced expression of *Unc45a* and ectopic expression of *Unc45b* in patients with 16p13 duplication.

The mouse SM1 cell model of myosin overexpression shows the same phenotype as the 16p13 duplication tissue: increased contractile gene expression, with no change in contractile protein levels compared with wild-type cells, accompanied by decreased *Unc45a* mRNA expression and ectopic expression of *Unc45b* (**Figure 4.4a,b,c,d**). These results suggest that the SM1 cells are a good model to study the cellular changes associated with overexpression of *Myh11*.

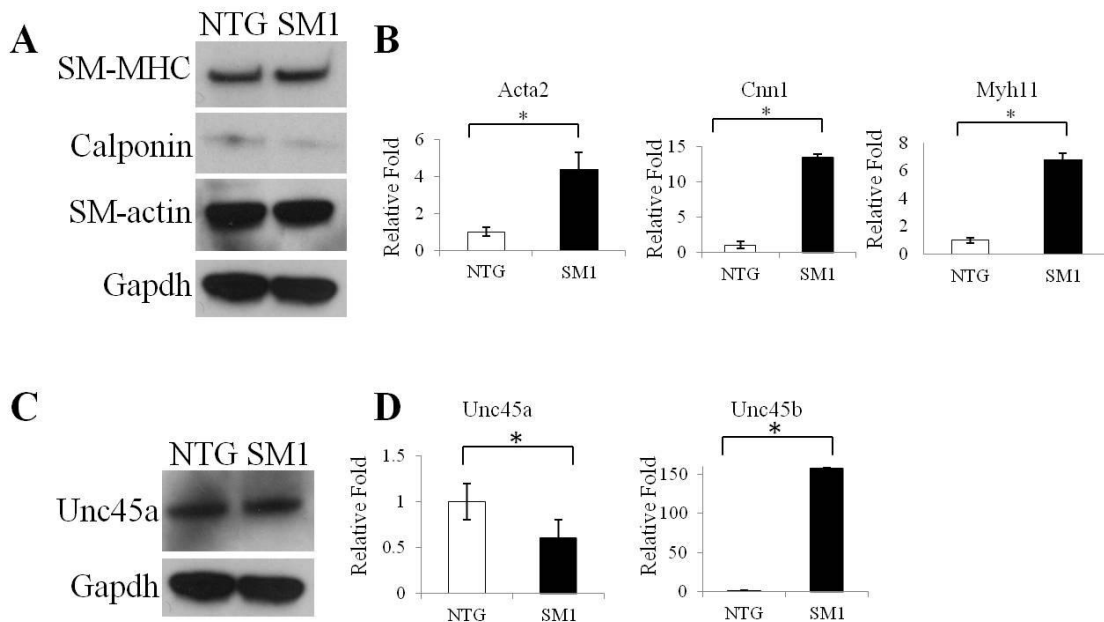


Figure 4.4 SM1 transgenic cells recapitulate phenotype of patient tissue. A) No change in contractile protein levels in cultured SM1 SMCs. B) Increased expression of contractile genes in culture SM1 SMCs. C,D) Reduced expression of *Unc45a* and ectopic expression of *Unc45b* in SM1 SMCs.

Because increased expression at the mRNA but not the protein level suggested a possible phenotype of increased protein turnover, we blocked elongation using cycloheximide and followed protein degradation over time. Cycloheximide is a protein translation inhibitor that is well tolerated by SMCs and does not cause cell death [96,97]. In wild-type (abbreviated here as NTG for nontransgenic) cells, the contractile proteins remain highly stable up to 36 hours after protein translation is inhibited (**Figure 4.5a**). These results are consistent with previous reports about the half-life of contractile proteins in all muscle cells [98,99]. However, in SM1 SMCs, contractile protein levels begin to decay by 24 hours. Because cycloheximide does disrupt the translation system, we used a second pulse-chase assay to more globally assess total protein synthesis and degradation. Phenylalanine labeled with ^{14}C was introduced into the culture media, and the cells incorporate it into new cellular proteins. Protein synthesis can be assessed by looking at accumulation of ^{14}C in the cellular protein lysates, while degradation can be assessed by the release of ^{14}C into the media during the chase period [163]. Both protein synthesis and degradation were significantly increased in SM1 cells compared with NTG cells (**Figure 4.5b,c**). This result is consistent with a phenotype of increased protein turnover.

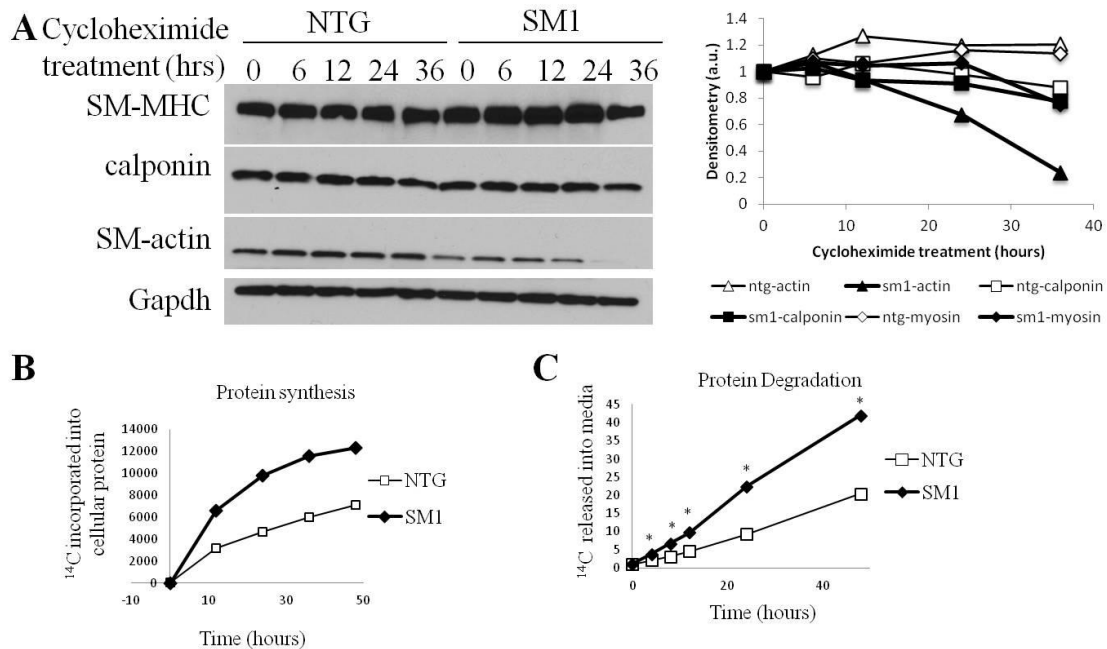


Figure 4.5 Increased protein turnover in SM1 SMCs. A) Treatment with cycloheximide shows accelerated degradation of contractile proteins in SM1 cells, quantified to the right. B,C) Radioactive pulse-chase assay shows increased global protein synthesis (B) and degradation (C) in SM1 SMCs.

Protein turnover in SM1 cells is driven by autophagy and not proteasomal degradation

SM1 and NTG SMCs were treated with a proteasome inhibitor, bortezomib, to assess whether the ubiquitin-proteasome system were responsible for the observed increase in protein degradation. However, treatment with bortezomib does not lead to increased accumulation of contractile proteins in SM1 SMCs; rather, the levels of SM-MHC protein are decreased after 24 hours of bortezomib treatment (**Figure 4.6a**). To confirm that the decreased protein levels were due to changes in protein degradation rather than changes in mRNA expression, we assessed gene expression of contractile genes during bortezomib treatment. In NTG cells, by 4 hours after the initiation of bortezomib treatment expression of *Acta2*, *Cnn1*, and *Myh11* all decrease significantly

(Figure 4.6b). Despite this decrease in expression, there is no change in protein level of SM-MHC, SM-actin, or calponin, suggesting that the proteasome may be responsible for regulating contractile protein turnover in NTG cells. By contrast, in SM1 cells, expression of contractile genes actually increases at early time points of bortezomib treatment, and does not decrease up to 24 hours of treatment. Taken together with the decrease in protein levels, these results suggest that the ubiquitin-proteasome system is not responsible for degrading contractile proteins in SM1 cells.

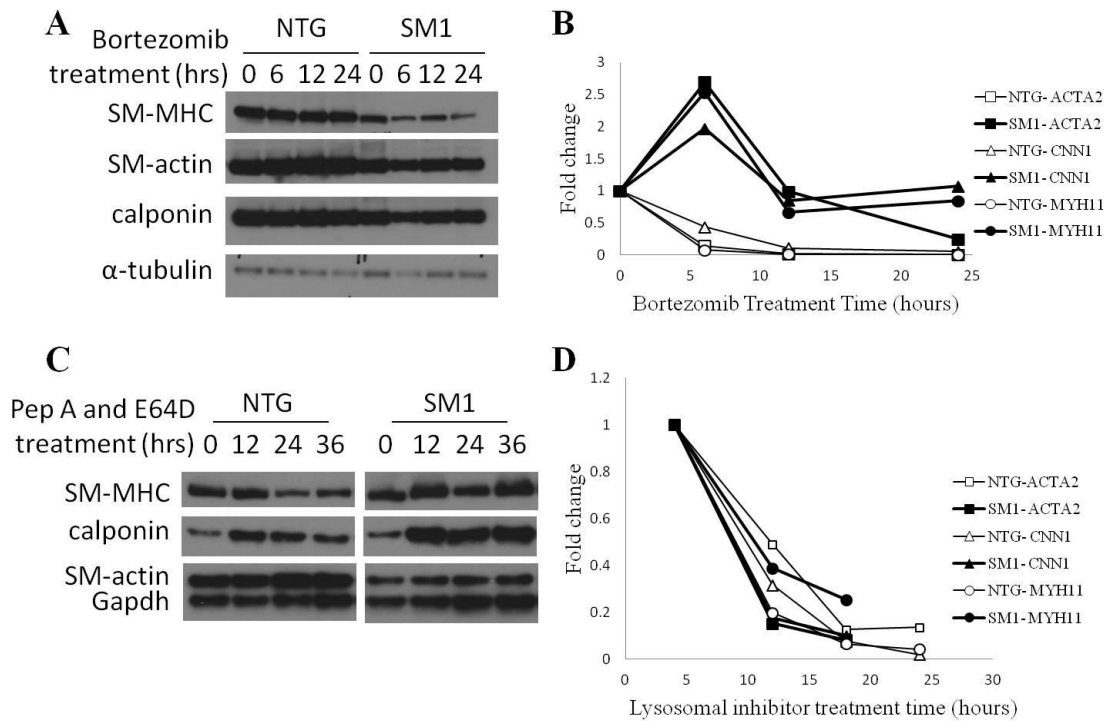


Figure 4.6 Autophagy, not the proteasome, drives protein degradation in SM1 SMCs. A) Treatment with the proteasome inhibitor bortezomib does not induce contractile protein accumulation in SM1 SMCs. B) Bortezomib decreases contractile gene expression by qPCR in NTG cells, but not in SM1 cells. C) Treatment with lysosomal inhibitors pepstatin A and e64d causes accumulation of contractile proteins in SM1 but not NTG cells. D) Lysosomal inhibitor treatment decreases contractile gene expression (assessed by qPCR) in both NTG and SM1 cells.

Next we examined whether the other protein degradation pathway, autophagy, was responsible for the degradation of contractile proteins in SM1 cells by using a combination of the lysosomal inhibitors pepstatin A and E64d to block autophagy. Unlike the results with bortezomib, lysosomal inhibitors lead to an accumulation of contractile proteins in SM1 SMCs over 36 hours of treatment, but not in NTG SMCs, supporting that autophagy is involved in the degradation of these proteins (**Figure 4.6c**). Message levels for all three contractile genes significantly decrease by 12 hours after initiation of lysosomal inhibitor treatment in both genotypes (**Figure 4.6d**).

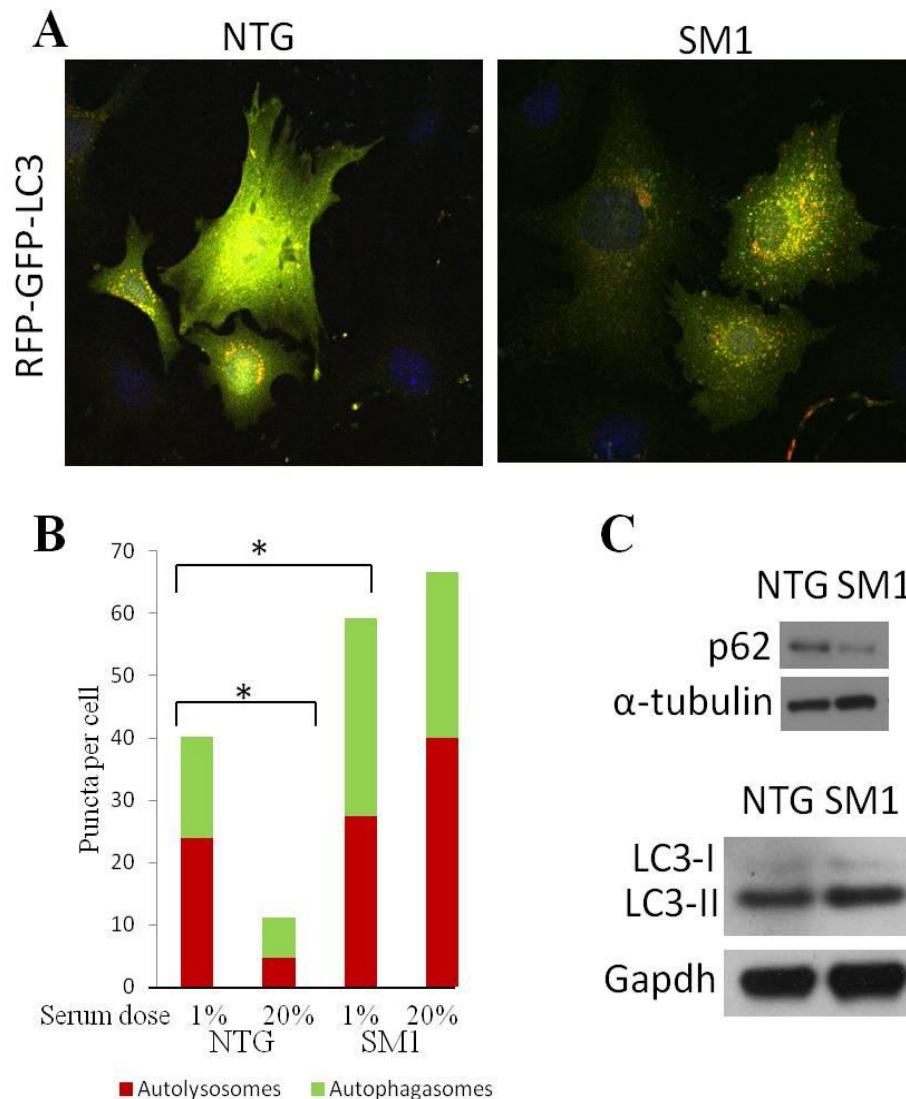


Figure 4.7 Increased autophagy markers in SM1 cells. A) Immunofluorescence with an RFP-GFP-LC3 lentivirus shows increased autophagic flux in SM1 cells by increases in both autophagosomes (yellow dots) and autolysosomes (red dots). B) Quantitation of immunofluorescent images confirms increased autophagy in SM1 cells. C) Western blotting shows decreased accumulation of p62 and increased processing of LC3 in SM1 cells.

To further assess if autophagy is increased in SM1 cells, we looked by immunoblot analysis at markers of autophagic activity. LC3 is a key protein involved in the autophagic pathway; as autophagy progresses, LC3 undergoes proteolysis, then lipidation and associates with the autophagosomal membrane [100]. Despite being

larger, lipidated LC3, or LC3 II, therefore migrates faster on a Western blot than LC3 I due to increased hydrophobicity. The LC3 II to LC3 I ratio is significantly increased in SM1 compared with NTG cells (**Figure 4.7c**). Likewise, p62 is a protein known to be degraded by autophagy, and decreased levels of p62, as seen in SM1 compared with NTG cells, are the result of increased autophagy (**Figure 4.7c**) [101]. Finally, we used an RFP-GFP-LC3 expressing lentivirus to assess autophagic flux in the cells. At early stages of autophagy, LC3 is tagged with both RFP and GFP. During initial autophagosome formation, LC3 staining becomes punctate and the dots appear yellow. As the autophagosome fuses with the lysosome to form an autolysosome, the pH of the compartment decreases and GFP is destabilized, leaving only RFP expression, changing the LC3 fluorescence to red. Based on quantitation of puncta in fixed cells, SM1 cells have significantly more autophagosomes and autolysosomes than NTG cells, suggesting an increase in autophagic flux (**Figure 4.7a,b**).

mTOR signaling and autophagy in SM1 cells

The most commonly studied cellular pathway leading to increased autophagy is a decrease in mammalian target of rapamycin (mTOR) signaling [102]. The current data in the field indicate that AMP-associated protein kinase (AMPK) and mTOR are the primary regulators of autophagy initiation, with AMPK as an activator of the process and mTOR as an inhibitor [103]. The two kinases similarly have been shown to inhibit each other [104]. Thus, under normal conditions when nutrient levels are high, AMPK is not activated, and mTOR remains active to drive protein synthesis. Under conditions of starvation or cellular stress, AMPK becomes activated, mTOR gets turned off, protein

synthesis decreases and autophagy goes up in an effort to conserve energy. There is a moderate increase in SM1 cells in phosphorylation of ACC, the downstream target of AMPK (**Figure 4.8a**). However, SM1 cells also have increased global levels of protein synthesis, and signaling downstream of mTOR, indicated by the phosphorylation of p70S6 kinase and of the ribosomal protein S6, was dramatically increased in SM1 cells than in NTG cells (**Figure 4.8b**). Therefore, an alternative cellular pathway must be

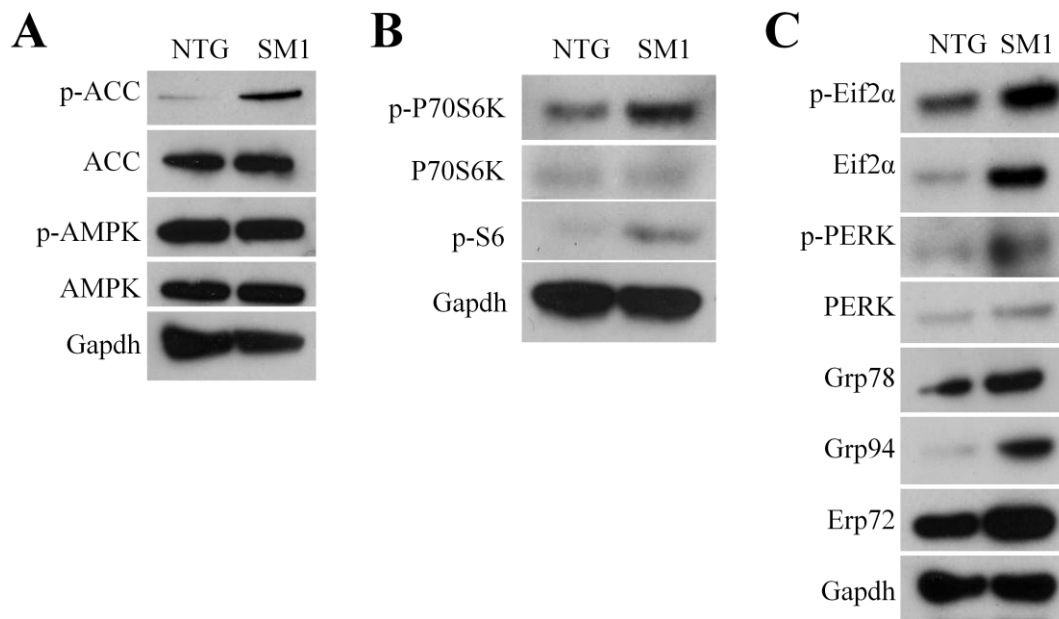


Figure 4.8 Altered signaling pathways in SM1 cells. A) Increased AMPK-related signaling in SM1 cells. B) Increased mTOR-driven signaling in SM1 cells. C) Increased accumulation of ER stress markers in SM1 cells.

driving autophagy in the SM1 cells.

ER stress in SM1 cells

Another cellular process that has been linked with autophagy is the induction of endoplasmic reticulum (ER) stress pathways [105-106]. Nascently translated proteins are processed in either the cytoplasm or the ER for proper protein folding and post-translational modifications. However, if the system is slowed down for any reason, the

ER sends out signals to drive transcription and translation of supporting proteins, shut down any nonessential protein synthesis, and induce autophagy. Because of the increase in global protein synthesis, as well as the imbalance in expression of SM-MHC and its Unc45 chaperone, we hypothesized that ER stress might be increased in the SM1 cells, and could potentially be driving autophagy. Phosphorylation of PERK and its downstream target eIF2 α indicates activation of one of the three major signaling pathways initiated by ER stress [107]. Grp78, Grp94, and Erp72 are all chaperone proteins that are upregulated to help relieve ER stress [108]. All markers assessed were upregulated in SM1 cells compared with NTG cells (**Figure 4.8c**).

Increased contraction in SM1 cells

Intriguingly, the SM1 transgenic mice have increased aortic contractility *in vivo*. Although the contractile proteins are clearly turned over more rapidly, it is unclear what effect the increased turnover has on filament formation and stability. To assess filament architecture, we first used immunofluorescence to visualize the filaments in paraformaldehyde fixed cells. Staining for either the myosin regulatory light chain or α -actin reveals thin, stretched out filaments across the cell body of NTG SMCs (**Figure 4.9a**). However, the filament structure in SM1 cells appears less organized and the staining appears brighter. For further insight, we performed an ultracentrifugation based assay to separate polymerized from unpolymerized actin. There was no difference in the ratio of polymerized to unpolymerized actin between SM1 and NTG cells (**Figure 4.9b**). These results suggest that while filaments could potentially be less stable in SM1 cells,

the actual number of filaments present in the cell at any given time is comparable to the NTG SMCs.

To further probe the question of contractility, we use a collagen gel contraction assay. After incubation in 1% serum media for four days, the gels were released and allowed to contract. Gels populated with SM1 cells contracted significantly more than gels populated with NTG cells (**Figure 4.9d**).

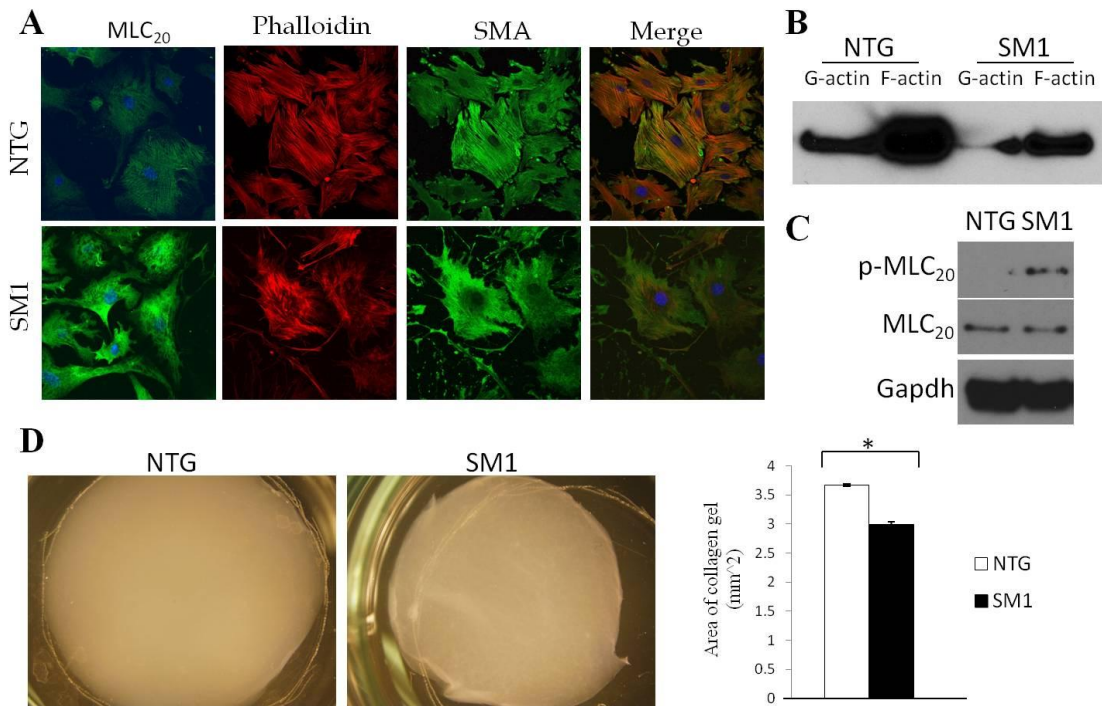


Figure 4.9 Increased contractility of SM1 SMCs. A) Immunofluorescence showing contractile filament formation in SM1 cells. B) Ultracentrifugation assay shows similar ratios of F/G actin in NTG and SM1 cells. C) Western blotting confirms increased phosphorylation of myosin regulatory light chain in SM1 cells. D) Collagen gel contraction assays show increased contraction of SM1 SMCs.

Since increased contraction does not seem to be due to increased numbers of contractile filaments, we next asked whether signaling driving smooth muscle contraction was increased. As described in Chapter 1, phosphorylation of the myosin light chain is the primary determinant of SMC contractility [14]. SM1 cells have significantly more phosphorylated myosin light chain at residue serine 19, indicating that alterations in signaling pathways may be driving the observed increase in contractility (**Figure 4.9c**).

Calcium signaling changes in SM1 cells

Increases in intracellular calcium ion concentration lead to increased activity of the myosin light chain kinase, and thus increased phosphorylation of the myosin light chain. Additionally, one of the known effects of ER stress is the release of calcium ions from stores within the ER [109]. Therefore, we sought to determine if baseline cytosolic calcium concentrations were increased in SM1 cells and, if so, would the cells respond aberrantly to thapsigargin, a drug that inhibits calcium reuptake into the ER. After fura2-am loading, cells were placed in calcium free buffer and imaged over time and after addition of thapsigargin. SM1 cells did have a higher baseline intracellular calcium concentration than NTG cells, and thapsigargin treatment also induced a faster response, but the amplitude of the response was reduced (**Figure 4.10a,b,c,d**). These changes are consistent with increased release of calcium from ER stores at baseline.

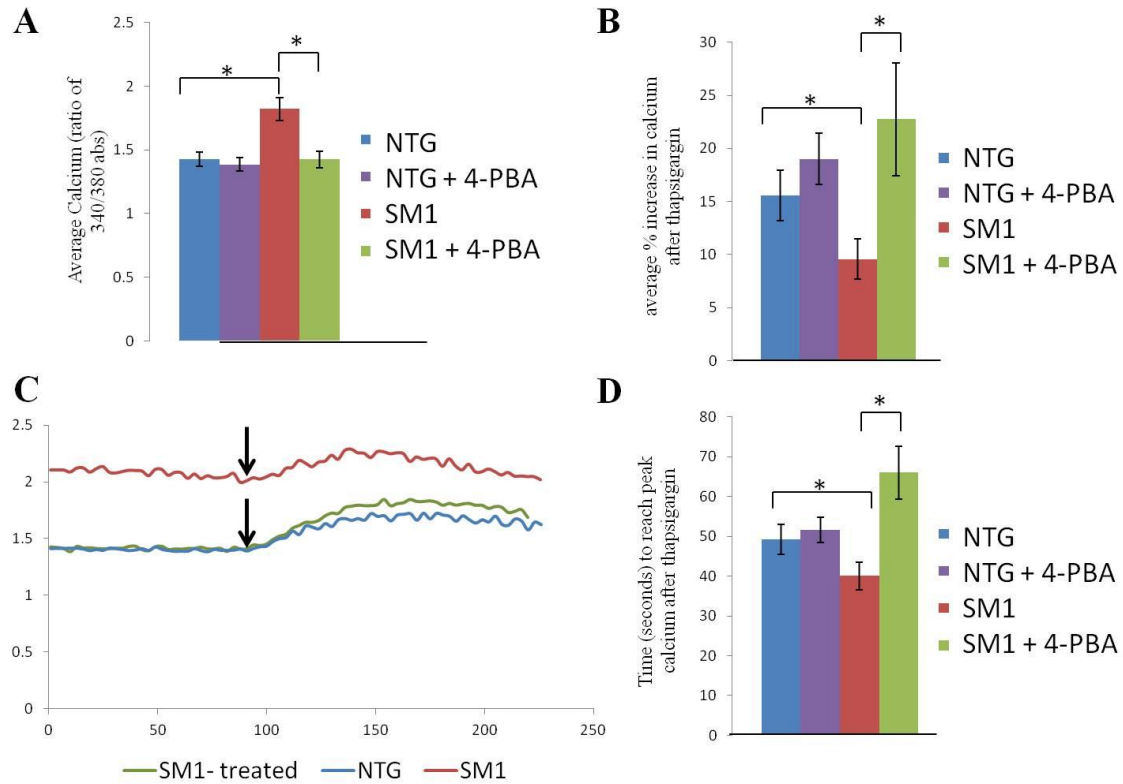


Figure 4.10 Changes in calcium in SM1 SMCs. A) Average baseline cytosolic calcium levels are increased in SM1 cells (red bar). Treatment with 4-pba (green bar) rescues the increased calcium. B) Average percent increase in cytosolic calcium after thapsigargin treatment is lowest in untreated SM1 cells (red bar), but 4-pba treatment rescues the effect (green bar). C) Representative calcium trace showing the differential response of untreated SM1 cells compared with NTG cells and SM1 cells treated with 4-PBA. Black arrows indicate the time of thapsigargin addition. D) SM1 cells reach the peak calcium concentration after thapsigargin administration faster than NTG cells, but this change is rescued by treatment with 4-PBA.

4-phenylbutyric acid reduces autophagy and normalizes calcium signaling in SM1 cells

A small molecule chaperone compound, 4-phenylbutyric acid (4-PBA), has been shown to relieve ER stress-related phenotypes in a number of systems [110-112]. In SM1 cells, treatment with 4-PBA reduces the number of autophagosomes, suggesting that autophagy in SM1 cells is, in fact, downstream of ER stress (**Figure 4.11a**).

Western blotting shows decreased LC3 processing in SM1 cells after treatment with 4-

PBA, further supporting the hypothesis that ER stress leads to autophagy in these cells (Figure 4.11b). Treatment of SM1 cells with 4-PBA also normalizes the intracellular calcium ion concentrations and response to thapsigargin, yet the compound had no effect on calcium in NTG cells (Figure 4.10a,b,c,d).

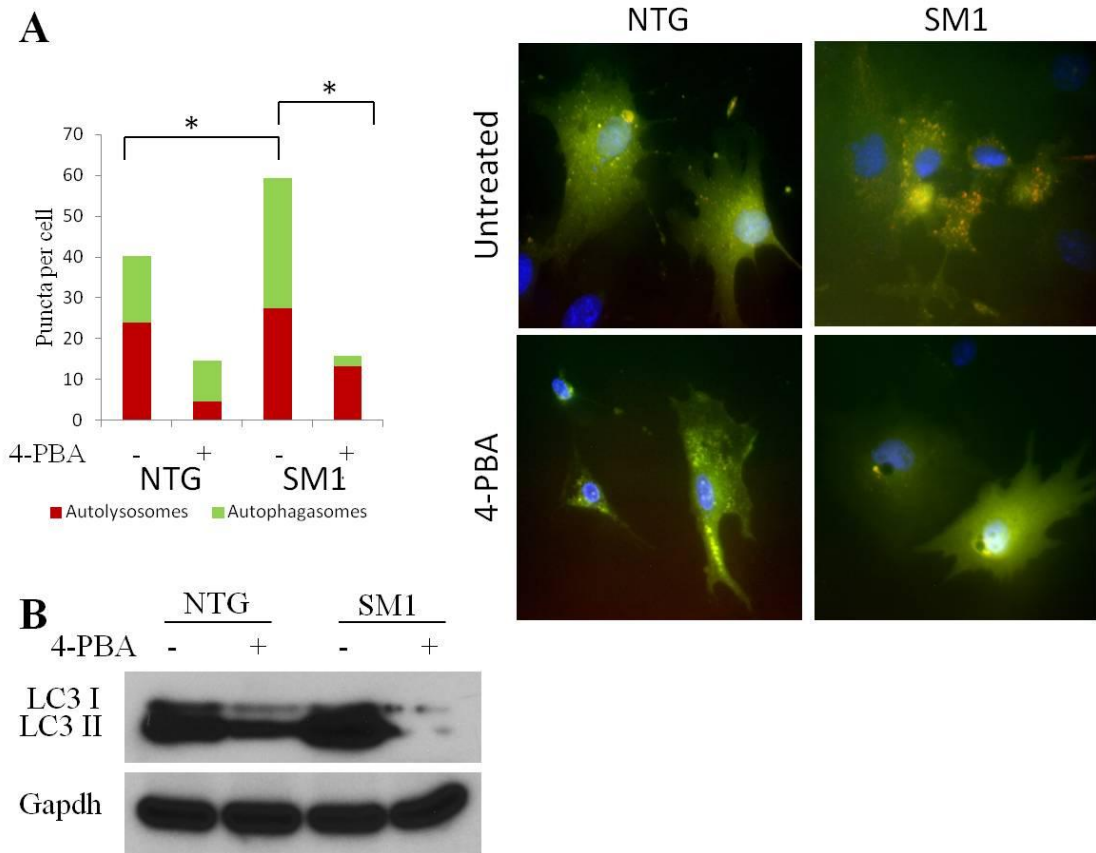


Figure 4.11 Treatment with 4-PBA reduces autophagy in SM1 cells. A) Treatment with 4-PBA decreases the number of autophagosomes and autolysosomes present in SM1 cells infected with RFP-GFP-LC3 lentivirus. B) Western blotting confirms a decrease in LC3 processing with treatment of 4-PBA, particularly in SM1 cells.

Discussion

SMCs overexpressing myosin heavy chain have a unique phenotype characterized by increased protein turnover of contractile proteins in conjunction with increased cellular contractility. In frozen aortic tissue from patients with 16p13.1 duplications, as well as in SM1 transgenic mouse SMCs, contractile genes, including *MYH11* but also *ACTA2* and *CNN1*, are expressed at higher levels than in wild-type tissue or cells. However, in both cases, there is no corresponding increase in protein levels of these contractile proteins. In the SM1 SMCs, analysis using cycloheximide or radiolabeled amino acids confirms a global increase protein turnover, with both protein synthesis and protein degradation occurring more rapidly in SM1 than in NTG cells.

Surprisingly, the increased protein degradation seen in SM1 cells is not driven by the ubiquitin-proteasome system. Although previous work in *C. elegans* indicated that any alteration in the ratio of Unc45 to myosin heavy chain expression led to ubiquitination and degradation of myosin heavy chain [95], treatment with a proteasome inhibitor did not induce accumulation of contractile proteins in SM1 cells. Instead, autophagy is responsible for the protein turnover. Autophagy is a process of nonspecific, bulk protein degradation that occurs as a protective measure in times of cellular stress. Autophagy literally translates as “self eating” in Greek; the process involves turning over proteins and cellular organelles to release nutrients and amino acids for reuse in more essential cellular processes [113]. All cells have a low but constant level of autophagic degradation, but autophagy is induced during various types of cellular stress including nutrient deprivation or organelle damage. Briefly, signaling events that initiate autophagy lead to the formation of a double-membrane vesicle known as an

autophagosome engulfing the product to be turned over. Once formed, the autophagosome fuses with a lysosome, and the acidic pH along with the variety of proteolytic enzymes inside the compartment digest the cargo. The breakdown products are released back into the cytosol [114,115]. Unregulated autophagy has previously been associated with a number of human diseases including cancer and neurodegenerative diseases [116-119].

The most well-characterized mechanism driving autophagy induction is inhibition of mTOR: in fact, activated mTOR signaling inhibits autophagy induction via a direct interaction between mTOR and Atg1, one of the initiators of the autophagy cascade [102,103]. AMPK also directly interacts with Atg1, and opposes the activity to mTOR to initiate autophagy when reserves of ATP are depleted [103]. However, in SM1 cells mTOR-driven signaling is actually increased, not decreased, so an alternative mechanism must be driving autophagy. Specifically, the results presented suggest that ER stress activation leads to autophagy. Until recently, mTOR activation and autophagy were thought to mutually antagonize each other. Signals of nutrient deprivation induce autophagy and downregulate mTOR, while signals of satiety downregulate autophagy and induce protein synthesis via mTOR activation. Accumulated data now suggest that mTOR activity and autophagy can coexist, and in fact may mutually reinforce each other [120,121]. Certain free amino acids (specifically leucine and other branched chain amino acids) are a potent activator of mTOR signaling via the small G protein Rag, and autophagy generates free amino acids in localized areas of the cell by chewing up cellular proteins [122-124]. A recent study proposed that a protein complex called Ragulator after the Rag G-proteins couples autophagy to localized mTOR activation in a

feedback loop [123]. This model explains why the activated mTOR does not in turn inhibit autophagy: the discrete localization within these complexes prevents mTOR from interacting with and inhibiting Atg1 [125,126]. Similar pathways may be occurring in SM1 cells, allowing mTOR to be active and driving further protein synthesis that causes more ER stress, leading to more autophagy and more mTOR activation.

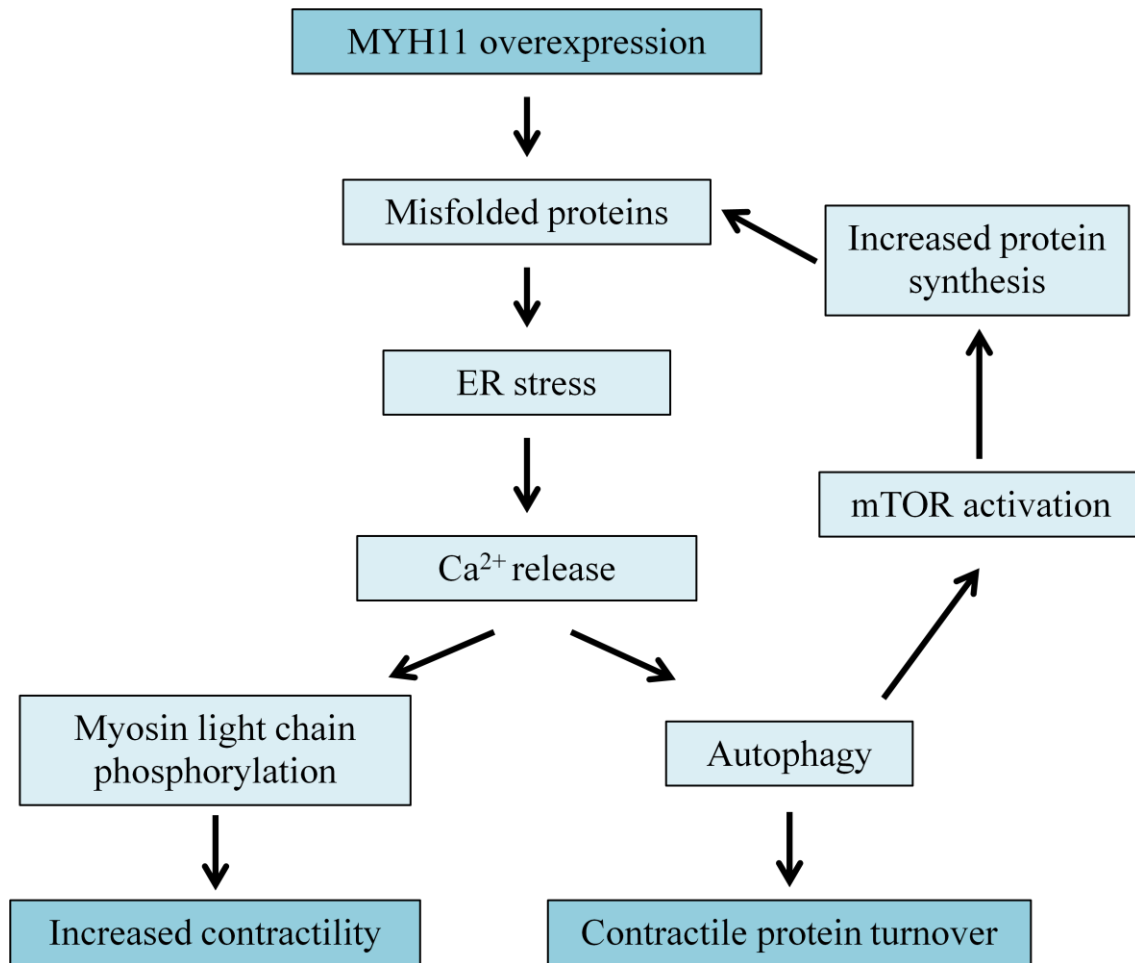


Figure 4.12 Model of cellular pathways in SM1 cells. Illustration shows interactions between pathways and phenotypes identified in SM1 cells.

Here, the discussion of ER stress refers more specifically to the unfolded protein response, a pathway activated by the accumulation of unfolded proteins in the

endoplasmic reticulum as the protein folding machinery becomes overwhelmed. Three transmembrane proteins lying on the ER membrane transduce the stress signal resulting from accumulation of unfolded proteins: Atf6, Ire1, and PERK, which in turn activate a number of signaling cascades leading to the redirection of cellular energy towards resolving ER stress [107]. Specific downstream effects of these ER stress pathways include increased transcription of chaperone proteins, increased protein degradation, and typically reduced protein synthesis [106]. A causative link between ER stress and autophagy induction has been established, but the exact molecular mechanisms have yet to be elucidated [105,127]. One possible mechanism involves the release of calcium ions from the ER triggered by ER stress: increased calcium concentration in the cytosol has been associated with induction of autophagy [109,128,129]. Increased cytosolic calcium also directly affects contraction by the SMC through activation of the myosin light chain kinase. In fact, SM1 cells are more contractile due to increased phosphorylation of the myosin light chain; they also have increased cytosolic calcium concentrations which are reversed by treatment with an ER stress reliever. This is the first study which has linked ER stress-induced calcium changes with alterations in muscle cell contractile function **(see model, Figure 4.12)**.

Previously described genetic triggers of TAAD are all predicted to decrease SMC contractile function. The results showing increased contractility in the aortas and cultured SMCs of SM1 transgenic mice are therefore confusing. All patients with 16p13.1 duplications have hypertension, so one possible explanation is that the duplications are actually a genetic cause of hypertension due to increased SMC contractility, and that the propensity towards high blood pressure drives the increased

risk of aortic dissection. Alternatively, the SM1 model is imperfect as it only overexpresses the SM1A isoform of myosin. Previous studies indicate that the SM1 myosin has a greater force generation capacity than SM2 myosin [31,32]. However, there does not appear to be any change in the ratio of SM1:SM2 myosin in the aortic tissue of SM1 transgenic mice [33]. The excessive activation of multiple metabolic processes in SM1 cells could instead drive increased production of reactive oxygen species; increased reactive oxygen species are associated with aortic disease [130,131]. Finally, and perhaps most plausibly the increased metabolic stress in SMCs overexpressing myosin could leave the cells unable to respond to secondary stresses such as increased biomechanical forces. A “second hit”, like hypertension, would therefore dramatically affect the phenotype of myosin-overexpressing SMCs, most likely leading to cell death and driving aortic pathology.

Although the use of the SM1 cell model has allowed for significant findings about the role of increased myosin expression in regulating SMC phenotype, many questions remain. A second model either linking SM1 transgene-induced phenotypic changes to aortic disease in a live animal model or showing the same pathways activated in SMCs derived from 16p13.1 duplication patients is necessary to confirm the findings described in this study. However, these data support our hypothesis that rare variants in the *MYH11* gene affect SMC phenotype and contractility. Furthermore, if these results are supported by future studies in additional models, these data suggest that small molecule chemical chaperones, previously approved for treatment of urea cycle disorders, may be useful to prevent disease in patients with 16p13.1 duplications

[111,132]. As this is the single more common genetic alteration seen in TAAD patients, a specific therapy to prevent aortic dissection would benefit a large patient population.

Chapter 5: Discussion

The focus of my work was broadly to determine how rare variants in *MYH11* contribute to the pathogenesis of vascular diseases in humans. Two rare variants associated with TAAD were selected for study: the most commonly identified nonsynonymous missense variant, R247C, and duplications of the 16p13.1 locus spanning the *MYH11* gene. We hypothesized, based on genetic data linking these variants with vascular disease, that each would alter the SMC phenotype and increase risk of disease.

Based on genetic data gathered from patients, as well as the cellular and *in vivo* data presented here, rare variants in *MYH11* have the potential to predispose to multiple distinct vascular pathologies, including vascular occlusive disease, aneurysm formation, and aortic dissection.

SMC proliferation drives genetically triggered vascular occlusive disease

Vascular occlusive diseases like ischemic stroke and coronary artery disease are typically associated with the formation of atherosclerotic plaques. Atherosclerosis occurs due to accumulation of plasma-derived lipids in the vessel wall, followed by recruitment of inflammatory cells including monocytes. Monocytes engulf the oxidized lipid plaques within the wall to become foam cells. As the disease progresses, the plaque can become complicated by cellular necrosis and thrombus formation, which in turn directly cause cessation of blood flow [133]. However, another essential part of the disease process is the production of cytokines and accumulation of reactive oxygen species in the wall that alter the behavior of the smooth muscle cells in the medial layer and the fibroblasts in the adventitia. In particular, SMCs undergo phenotypic switching to become

proliferative and migratory, and they begin producing collagens and other extracellular matrix proteins that contribute to fibrosis within the atherosclerotic plaque. In rare cases, pathologists have noted the presence of plaque-like occlusions in arteries that lack lipid accumulation. These lesions are called fibromuscular lesions, as they are populated predominantly with muscle cells and their fibrotic output [134].

Due to the lethal nature of its complications, genetic contributors to atherosclerosis have been heavily researched. The first genetic factors, and to date the majority of genes, identified to increase risk of coronary artery disease and other atherosclerosis-related vascular complications affect circulating lipid levels [135]. Genes involved in endothelial integrity, oxidative stress, and thrombus formation have also been implicated in increasing risk for atherosclerosis [136]. Notably, a role for genes controlling SMC proliferation has not been extensively studied.

As mutations in *ACTA2* were initially identified as a major cause of inherited TAAD, the clinical histories of families carrying these mutations suggested a surprising link between TAAD and early-onset vascular occlusive diseases such as ischemic stroke. Several individuals with *ACTA2* mutations also have a bilateral stroke syndrome called Moyamoya disease. Moyamoya disease afflicts young patients with repeated strokes in the terminal portion of the carotid artery at the base of the brain; patients are identified by the characteristic formation of small collateral vessels around the occluded artery apparent on contrast imaging [137,138]. Pathologic examination of the lesions in Moyamoya patients reveals intimal occlusion by proliferating smooth muscle cells with little lipid deposition and some inflammatory cell infiltration [139,140]. Moyamoya disease runs in families and afflicts young patients, but although genetic mapping studies

have identified multiple loci, causative genetic mutations have remained elusive [141-143]. Although Moyamoya disease occurs among patients with some known genetic syndromes, *ACTA2* thus became the first gene associated with nonsyndromic inheritance of Moyamoya disease [2].

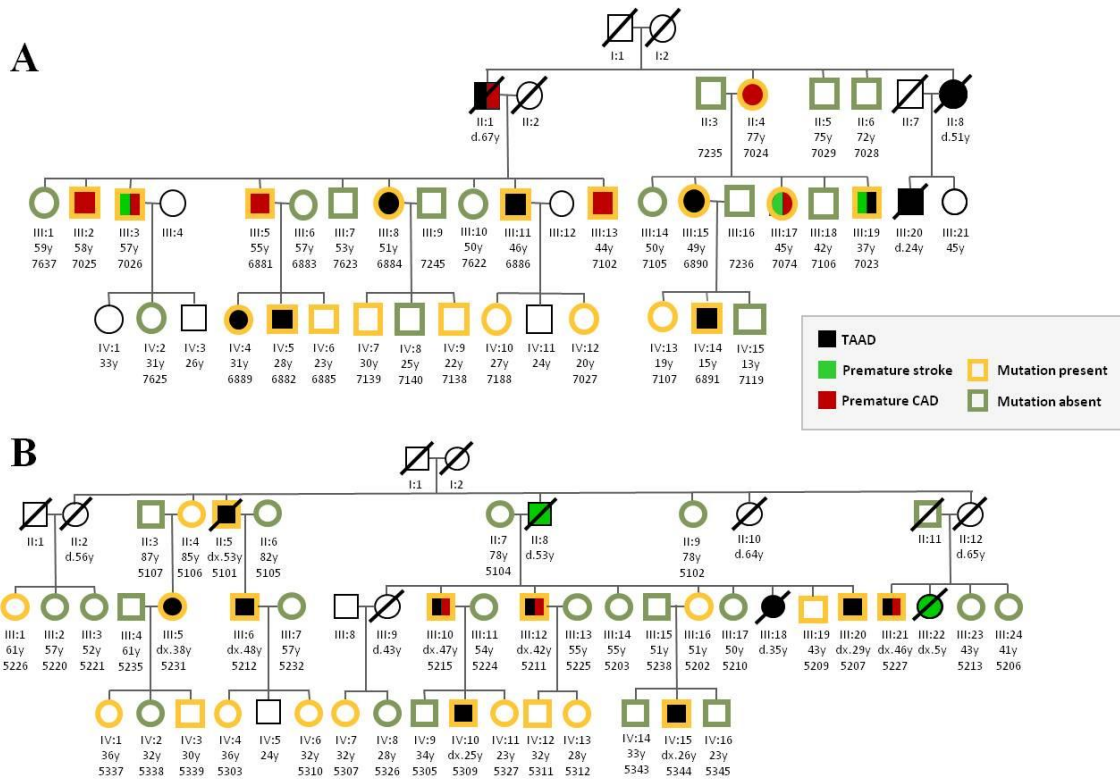


Figure 5.1 Co-occurrence of vascular occlusive disease with TAAD in *ACTA2* and *MYH11* families. A) Pedigree of a family with *ACTA2* mutation showing 50% penetrance of TAAD with affected relatives developing premature stroke or coronary artery disease (CAD). B) Pedigree of a family with *MYH11* mutation similarly showing stroke and CAD in mutation carriers or obligate carriers. Van Tran Fadulu et al unpublished data, reprinted with permission.

The same mutations in *ACTA2* appeared to cause aneurysm formation in some carriers and occlusive arterial lesions in others, although the pathogenic processes driving the diseases seemed unrelated (**Figure 5.1a**). Occlusive lesions observed in *ACTA2* patients appeared similar to the Moyamoya lesions described above: they were comprised of proliferating SMCs with little to no lipid deposition. SMCs explanted from *ACTA2* patients indeed proliferate more rapidly in culture, and further work using the *Acta2* knockout mouse model has elucidated a complex mechanism involving a number of cancer-related pathways that drive hyperplasia of SMCs [62].

Although less abundant, there is genetic evidence to support a similar dual effect of mutations in *MYH11*. Families with *MYH11* mutations have affected members who develop Moyamoya disease or coronary artery disease in addition to TAAD, although the penetrance of occlusive vascular diseases is reduced compared with *ACTA2* families (**Figure 5.1b**). SMCs isolated from these patients are hyperplastic, similar to *ACTA2* mutant SMCs [68]. As we began investigating rare variants in the *MYH11* gene, we therefore asked not only whether these variants might contribute to aneurysm formation but also whether they might increase risk for occlusive diseases. The R247C rare variant studied in this dissertation is found both in patients with TAAD and in patients with occlusive disease. An *in vivo* model of vascular injury, the ligation of a single carotid artery, did lead to an enhanced *in vivo* proliferative response in *Myh11*^{R247C/R247C} mice, and the cells explanted from the knockin mouse model proliferated more rapidly in culture.

Unlike *Acta2*^{-/-} cells, which completely lack actin and therefore do not have pools of monomeric actin sequestering MRTF in the cytoplasm, the *Myh11*^{R247C/R247C} SMCs

were dedifferentiated via the canonical MRTF:SRF axis. Increased proliferation in these cells was accompanied by decreased contractile gene and protein expression, loss of actin polymerization, and the movement of MRTFA into the cytoplasm. We identified a novel pathway linking altered force generation by the mutant myosin to this dedifferentiated phenotype via loss of focal adhesion maturation and resultant decreases in RhoA activation. However, dedifferentiation was not observed in *Myh11*^{R247C/R247C} SMCs within the intact aorta. Within the aortic wall, elastin fibers act as a natural brake on SMC proliferation [144]. In addition, SMCs in developed, intact arteries are typically quiescent and nonproliferative; stimuli downstream of vascular injury including release of growth factors from reserves in the extracellular matrix, loss of contact inhibition at the site of injury, and generation of reactive oxygen species induce a proliferative phenotype in these cells [34]. We hypothesize that *Myh11*^{R247C/R247C} SMCs are more prone to dedifferentiation after injury and/or less responsive to signals to re-differentiate than wild-type cells.

Our study therefore supports a role for *MYH11* mutations in vascular occlusive disease, and further suggests that any rare variant in the myosin head domain that affects force generation may predispose carriers to vascular occlusive diseases via this same pathway.

Decreased contractility and aneurysm formation

Early descriptive studies of the pathology of aortic aneurysms showed fragmentation of elastin fibers and loss or dysfunction of supporting fibrils in the extracellular matrix [145,146]. Loss of elastin integrity was predicted to drive aneurysm

formation as the ability of the vessel to resist biomechanical forces would be impaired, leading to dilation and eventually rupture. The first genetic mutations identified to cause aortic aneurysm were mutations in *Fbn1* leading to Marfan syndrome, lending credence to the hypothesis that defective structure or function of extracellular fibers underlies the disease [147]. However, fibrillin-1, encoded by *Fbn1*, also plays a key role in modulating growth factor signaling by sequestering the latent TGF- β complex within the matrix [148]. Loss of functional fibrillin-1 would thus not only alter the response of the aorta to biomechanical forces, but would also increase bioavailability of TGF- β ligand. A mouse model of hypomorphic expression of *Fbn1* suggested a critical role for excessive TGF- β signaling in a pulmonary defect associated with Marfan syndrome [149].

The potential role of TGF- β signaling in Marfan-associated aortic aneurysms was first investigated in *Fbn1* C1039G heterozygous knockin mice, which develop aortic root aneurysms as early as two months of age. Pathology showed both increased collagen expression and increased nuclear phosphorylated Smad2, suggesting that TGF- β signaling is increased in this model. Further, treatment of the mice with a TGF- β neutralizing antibody partially attenuated aortic dilation and medial degeneration [54].

Mutations in *TGFBR1* and *TGFBR2* were identified to cause aortic disease, and the role of TGF- β in aneurysm pathogenesis became controversial [56]. Despite evidence of enhanced Smad signaling, as well as increased fibrotic signaling downstream of TGF- β , in the aortic wall of patients with *TGFBR2* mutations, the mutations proved to encode kinase-deficient receptors leading to a loss of signaling function [64]. SMCs explanted from the aortas of *TGFBR2* patients were significantly

less differentiated than control SMCs, showing decreased expression of all contractile markers tested, as well as loss of contractile filament formation *in vitro*, both at baseline and with exposure to TGF- β (**Figure 5.2a**). Similarly, immunohistochemical staining of aortic sections from these patients showed a decrease of contractile protein signal in the SMCs of the aortic medial layer *in vivo* (**Figure 5.2b**). Additionally, recently identified mutations in *TGFB2*, encoding the ligand TGF- β 2, are clearly loss-of-function mutations resulting in haploinsufficiency for TGF- β 2. Explanted SMCs from *TGFB2* patients clearly show reduced TGF- β 2 protein; however levels of TGF- β 2 are actually increased in the disease aortic tissue, and there are further signs of excessive signaling activity *in vivo* [58]. The role of TGF- β signaling in aortic disease remains controversial [150]. The most likely explanation is that TGF- β signaling becomes secondarily increased in later stages of aortic disease, but the primary defect driving the disease in these patients is related to the loss of TGF- β signaling.

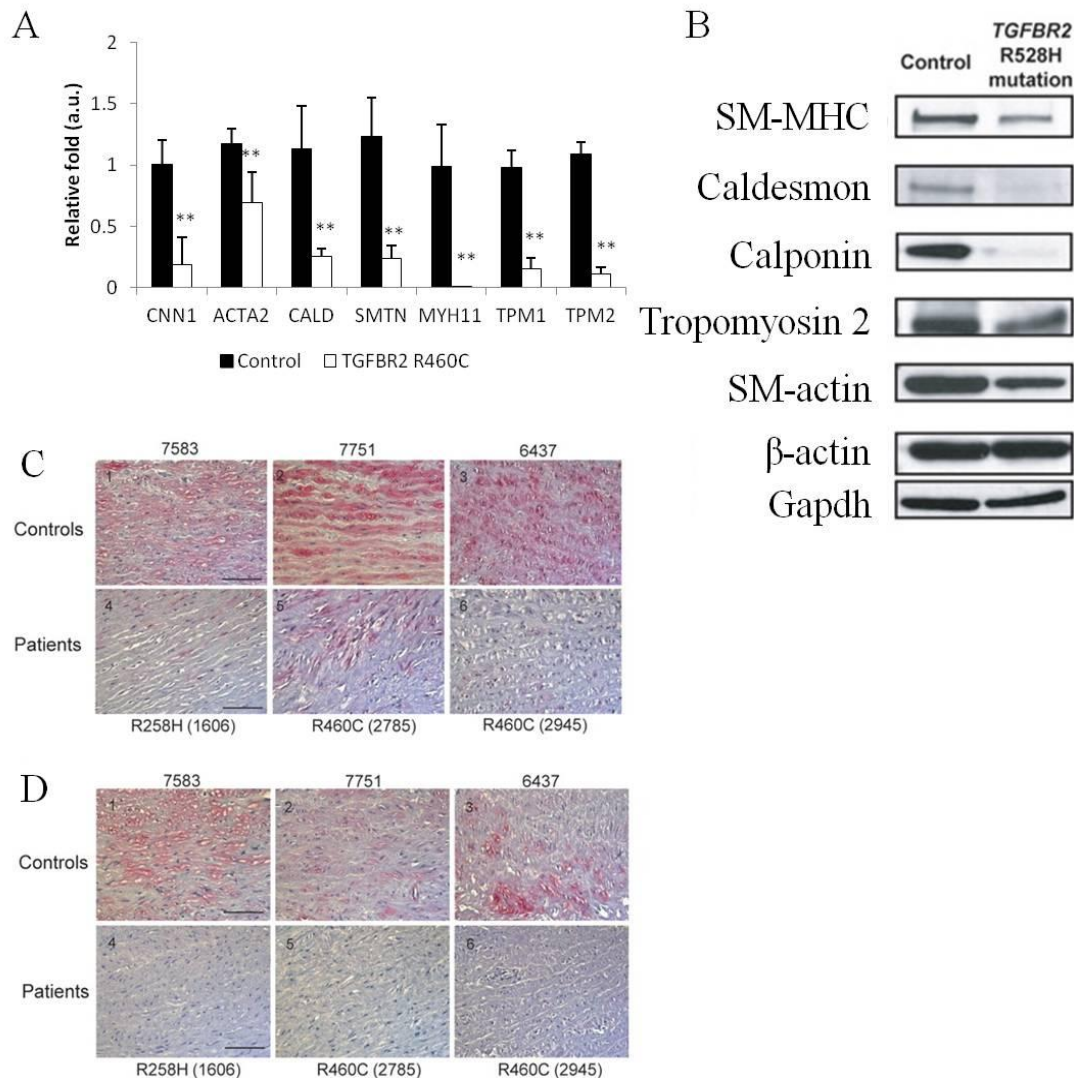


Figure 5.2 Loss of SMC differentiation with *TGFBR2* mutations. A, B) Decreased expression of contractile gene (A) and proteins (B) in SMCs explanted from patients with *TGFBR2* mutations. C, D) Immunohistochemistry on tissue from *TGFBR2* patients shows decreased signal for calponin (C) and SM-MHC (D). Reprinted with permission from Oxford University Press [*TGFBR2* mutations alter smooth muscle cell phenotype and predispose to thoracic aortic aneurysms and dissections. Inamoto S, Kwartler CS, Lafont AL, Liang YY, Fadulu VT, Duraisamy S, Willing M, Estrera A, Safi H, Hannibal MC, Carey J, Wiktorowicz J, Tan FK, Feng XH, Pannu H, Milewicz DMM. *Cardiovascular Research*. 2010]

The discovery of mutations in the contractile genes *ACTA2* and *MYH11* around the same time as evidence accumulated to support SMC dedifferentiation due to *TGFBR2* mutations suggested that loss of SMC contractility was potentially a universal factor underlying all genetically triggered aortic disease [59,61]. The *Fbn1* hypomorphic mouse model also shows loss of aortic contractility and alterations in SMC phenotype, confirming that these pathways are affected both by mutations in contractile protein genes and genes encoding proteins involved in TGF- β signaling [48,151].

In this study, however, the R247C rare variant decreases aortic contractility but does not induce spontaneous aortic disease. Therefore, these data indicate that decreased contractility alone is insufficient to drive disease. Introducing the R247C variant into another mouse model of contractile protein dysfunction, the *Acta2*^{-/-} model, worsens disease without worsening the contractile defect. Therefore, the relationship between decreased contractility and development of aortic disease is nonlinear, but at the same time, decreased contractility is the most direct result of the genetic lesions so it must play some role in the disease process.

Recent studies investigating other pathways that might drive disease have shown that signaling downstream of the angiotensin type I receptor (*Agtr1*) is responsible for many of the pathologic changes accompanying aneurysm formation. A commonly used model of aneurysm formation in the mouse is accomplished by infusion of angiotensin-II, suggesting that angiotensin-related signaling alone is sufficient to drive aneurysm formation [152]. Furthermore, the *Agtr1* blocker, Losartan, has been used to successfully prevent pathologic changes in a number of mouse models of aneurysm formation. The most well-studied of these models is the Marfan *Fbn1*^{C1039G/+} mouse; aneurysm

formation is accompanied by loss of aortic contractility, but also loss of elastin, thickening of the medial layer, and evidence of increased TGF- β signaling, all of which are prevented by treatment with losartan [54]. Our own lab has recently confirmed that losartan similarly blocks many aspects of pathologic remodeling that accompany increased biomechanical forces in the model of aneurysm development after transverse aortic banding, and that losartan prevents aneurysm formation in *Acta2*^{-/-} mice (unpublished data).

Significantly, studies in both abdominal aneurysms and thoracic aneurysms have shown a protective role for the angiotensin type II receptor (Agtr2). Knockout of the receptor worsens aortic disease in the Marfan *Fbn1*^{C1039G/+} mouse, and pharmacologic block of Agtr2 accelerates disease in the abdominal aorta after angiotensin II infusion [153,154]. These same studies showed that treatment with losartan, an Agtr1-specific blocker, but not with angiotensin converting enzyme inhibitors (ACE inhibitors) ameliorates disease. ACE inhibitors may be ineffective treatments for aneurysm progression because they block both the deleterious effects of Agtr1 and also the protective effects of Agtr2. Alternatively, ACE inhibitors may be unable to prevent disease because activation of Agtr1 is ligand-independent. Evidence of mechanical stress-induced, ligand-independent activation of Agtr1 has been shown in cardiomyocytes, and this activation can be blocked with specific blockers of Agtr1 [155,156]. If mechanical stretch can cause ligand-independent activation of Agtr1 in smooth muscle cells, and if cells deficient in contractile function experience greater mechanical stretch, this pathway could provide a link between mutations in the contractile proteins and signaling known to drive aortic disease.

Aortic dissection: the black box

A “typical” TAAD patient develops an aortic aneurysm that over time becomes less stable and eventually progresses to dissection. However, careful examination of families with TAAD indicates that some genetic mutations lead to stable aneurysm formation with no history of dissection, and others lead to dissection with no evidence of prior aortic enlargement [52]. Patients with mutations in *MYH11* or *MLCK* tend to fall into the latter category and dissect with little enlargement of the ascending aorta, as do patients with 16p13.1 duplications [60,88]. Although aneurysm formation has been extensively studied using mouse models, the molecular mechanisms that distinguish aneurysm formation from aortic dissection have not been established.

There are two established mouse models of Marfan syndrome mentioned above: the *Fbn1*^{C1039G/+} missense mutant mouse and the hypomorphic mouse *Fbn1*^{mgR/mgR}. The missense mutant mouse develops aneurysms that do not progress to dissection, while the hypomorphic mouse progresses to dissection without aneurysm [157,158]. As described above, aortic dilation and pathologic changes in the *Fbn1*^{C1039G/+} mouse can be blocked by losartan. Similarly, treatment of the *Fbn1*^{mgR/mgR} mouse with either a metalloproteinase blocker, doxycycline, or with losartan prevents fragmentation of elastin fibers and significantly delays death due to dissection [159,160]. Combinatorial treatment with both doxycycline and losartan results in a synergistic effect on survival, and in fact almost completely prevented deaths during through the length of the study (**Figure 5.3**) [160]. These results tell us that elastin fragmentation may be critical for preserving aortic integrity, as matrix metalloproteinases (MMPs) are extracellular

proteases and elastin is one of their targets [50]. However, as both Marfan mouse models have significant fragmentation of elastic fibers, these data do not inform us on the differences in molecular events leading to stable aneurysms versus dissections.

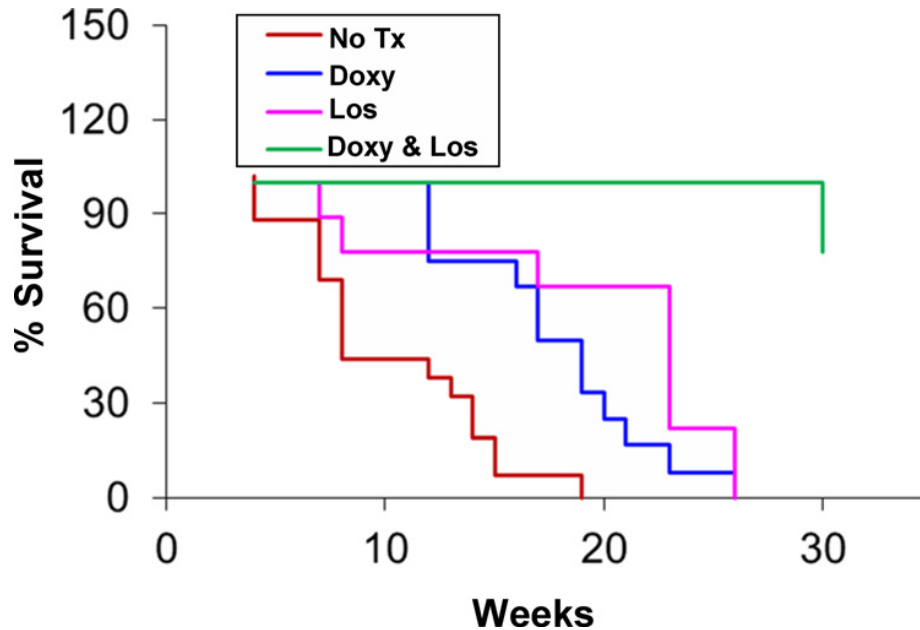


Figure 5.3 Treatment with doxycycline, losartan, or a combination improves survival in *Fbn1^{mgR/mgR}* mice. Survival curve showing improvements in survival with single treatment of *Fbn1^{mgR/mgR}* mice with doxycycline or losartan, and synergistic survival improvements with combinatorial treatment. Reprinted with permission from Wolters Kluwer Health. [MMP-2 Regulates Erk1/2 Phosphorylation and Aortic Dilatation in Marfan Syndrome. Xiong W, Meisinger T, Knispel R, Worth JM, Baxter BT. *Circulation Research*. 2012.]

Unpublished *in silico* data using a sophisticated computer model to study the effects of biomechanical forces on the aorta suggest a model whereby pools of proteoglycans in the aortic wall may lead to disruption of the elastin fibers. As proteoglycans accumulate and focally displace elastin, SMCs, and collagens, the tensile strength of the wall decreases at that spot. Simultaneously, the discontinuity in the patterning of elastin and cells in the wall locally increases wall stress. The combination of decreased strength and increased stress could logically increase predisposition to

rupture at that precise location. In the *Acta2*^{-/-} *Myh11*^{R247C/R247C} model, proteoglycan deposition does appear to precede elastin fragmentation. However, there is no change in survival and no signs of dissection in the *Acta2*^{-/-} *Myh11*^{R247C/R247C} mice out to one year of age. An alternative hypothesis is that inflammatory cell infiltration underlies the pathology of aortic dissection. Inflammation, particularly in the adventitia but also extending into the medial layer, is common in the pathology of TAAD patients, however its direct contribution to pathogenesis remains unclear [161].

Interestingly, while the addition of the R247C allele on the *Acta2*^{-/-} background does not induce dissections, preliminary data suggests that induction of hypertension in *Myh11*^{R247C/R247C} mice drives dissection without enlargement of the aorta. A combination of L-NG-Nitroarginine methyl ester (L-NAME) in the drinking water and an 8% NaCl diet increased average systolic blood pressure in *Myh11*^{R247C/R247C} mice from 140mmHg to 180mmHg, and this increase is sustained for at least three months. Three of thirteen mice started on the hypertensive regimen died spontaneously during the four-month trial, and upon dissection and fixation a fourth mouse was found to have a stable aortic dissection. None of the thirteen *Myh11*^{R247C/R247C} mice on the typical nonhypertensive regimen died during the trial. Continued work on this model will begin to elucidate the pathology associated with aneurysms versus dissections and determine if proteoglycan deposition precedes dissection.

Hypertension is the most important risk factor driving aortic dissection, and all patients with 16p13.1 duplications present with both hypertension and dissection. Individuals with the duplications have an 11-fold increased risk of disease, and 1% of all TAAD patients have the duplication, making this the most common genetic variant

predisposing to TAAD identified to date. Because the duplication is a rare variant rather than a Mendelian mutation, hypertension likely represents the “second hit” that leads to disease in these patients.

The phenotypic data presented in Chapter 4 from the SM1 mouse establishes that SMCs overexpressing myosin have a unique phenotype involving accelerated contractile protein turnover. Furthermore, the pathway responsible for driving the protein turnover is autophagic degradation downstream of ER stress. In addition to autophagy, ER stress triggers calcium release from the ER, which leads to increased activity of myosin light chain kinase and increased contractility of the SM1 cells. *In vivo* data from the SM1 transgenic mouse model also shows increased contractility of the aorta. SM1 myosin generates more force than SM2 myosin, so it is possible the increased contractility is due to a change in isoform expression. However, no change in the ratio of SM1:SM2 isoforms is observable on Western blots using lysates from the aortic tissue. Increased contractility rather than decreased contractility has not previously been associated with aortic disease; therefore, additional studies and a more complete disease model will be required to establish the mechanism of disease downstream of protein turnover.

Currently, we are working with collaborators to generate patient-specific stem cells from peripheral blood mononuclear cells collected from 16p13 duplication patients. The goal would then be to transform those stem cells into smooth muscle cells and validate the pathways identified in SM1 SMCs. An *in vivo* model would further help to study the effects of increased biomechanical forces on myosin overexpressing SMCs would help clarify the causative link between the cellular changes and the disease. One possibility is that increased contractile function as well as the inefficient metabolic

energy usage by the SM1 SMCs combines to generate significantly more reactive oxygen species. Relevant to the role of angiotensin signaling in the etiology of TAAD, reactive oxygen species have been shown to potentiate angiotensin-driven pathologic processes in SMCs [162]. Alternatively, metabolic stress could uniquely predispose these SMCs to contractile dysfunction in response to additional perturbations of the system. Thus, while the cells appear more contractile under typical circumstances, decreased contractility may still underlie the predisposition to disease.

Conclusion

The work presented in this dissertation establishes the importance of two different rare variants in *MYH11*, the R247C missense mutation and chromosomal duplication of the locus, in regulating SMC phenotype and increasing risk for vascular diseases. Genomic duplications are a poorly understood cause of human disease, as the mechanisms linking an extra copy of a gene to a disease process are not intuitively obvious. The work presented here on the 16p13.1 duplications suggests a mechanism of increased protein turnover that results from overexpression of a tightly regulated protein. This novel mechanism may be more broadly applicable to other cases of disease-causing genomic duplications.

The models established by this study provide a framework for future studies on rare variants in vascular disease, and also provide strong preliminary evidence for the mechanisms of vascular disease associated with these particular rare variants. Most critically, the *in vivo* models involving *Myh11*^{R247C/R247C} mice will allow us through

future studies to examine the differences in pathology associated with stable aneurysm formation versus dissection.

References

1. Milewicz, D.M., Guo, D.C., Tran-Fadulu, V., Lafont, A.L., Papke, C.L., Inamoto, S., Kwartler, C.S., Pannu, H. Genetic basis of thoracic aortic aneurysms and dissections: focus on smooth muscle cell contractile dysfunction. *Annu Rev Genomics Hum Genet.* 9, 283-302 (2008).
2. Milewicz, D.M., Kwartler, C.S., Papke, C.L., Regalado, E.S., Cao, J., Reid, A.J. Genetic variants promoting smooth muscle cell proliferation can result in diffuse and diverse vascular diseases: evidence for a hyperplastic vasculomyopathy. *Genet Med.* 12, 196-203 (2010).
3. Wolinsky, H., Glagov, S. Nature of species differences in the medial distribution of aortic vasa vasorum in mammals. *Circ Res.* 20, 409-21 (1967).
4. El-Hamamsy, I., Yacoub, M.H. Cellular and molecular mechanisms of thoracic aortic aneurysms. *Nat Rev Cardiol.* 6, 771-86 (2009).
5. Wolinsky, H., Glagov, S. A lamellar unit of aortic medial structure and function in mammals. *Circ Res.* 20, 99-111 (1967).
6. Berry, C.L., Sosa-Melgarejo, J.A., Greenwald, S.E. The relationship between wall tension, lamellar thickness, and intercellular junctions in the fetal and adult aorta: its relevance to the pathology of dissecting aneurysm. *J Pathol.* 169, 15-20 (1993).
7. Wagenseil, J.E., Mecham, R.P. Vascular extracellular matrix and arterial mechanics. *Physiol Rev.* 89, 957-89 (2009).
8. Davis, E.C. Smooth muscle cell to elastic lamina connections in developing mouse aorta. Role in aortic medial organization. *Lab Invest.* 68, 89-99 (1993).

9. Guilford, W.H., Warshaw, D.M. The molecular mechanics of smooth muscle myosin. *Comp Biochem Physiol B Biochem Mol Biol.* 119, 451-8 (1998).
10. Seow, C.Y. Myosin filament assembly in an ever-changing myofilament lattice of smooth muscle. *Am J Physiol Cell Physiol.* 289, C1363-8 (2005).
11. Gillis, J.M., Cao, M.L., Godfraind-De Becker, A. Density of myosin filaments in the rat anococcygeus muscle, at rest and in contraction. II. *J Muscle Res Cell Motil.* 9, 18-29 (1988).
12. Xu, J.Q., Gillis, J.M., Craig, R. Polymerization of myosin on activation of rat anococcygeus smooth muscle. *J Muscle Res Cell Motil.* 18, 381-93 (1997).
13. Sellers, J.R., Spudich, J.A., Sheetz, M.P. Light chain phosphorylation regulates the movement of smooth muscle myosin on actin filaments. *J Cell Biol.* 101, 1897-902 (1985).
14. Ding, H.L., Ryder, J.W., Stull, J.T., Kamm, K.E. Signaling processes for initiating smooth muscle contraction upon neural stimulation. *J Biol Chem.* 284, 15541-8 (2009).
15. Somlyo, A.P., Somlyo, A.V. Signal transduction and regulation in smooth muscle. *Nature.* 372, 231-6 (1994).
16. Hartshorne, D.J., Ito, M., Erdödi, F. Myosin light chain phosphatase: subunit composition, interactions and regulation. *J Muscle Res Cell Motil.* 19, 325-41 (1998).
17. Ito, M., Nakano, T., Erdodi, F., Hartshorne, D.J. Myosin phosphatase: structure, regulation and function. *Mol Cell Biochem.* 259, 197-209 (2004).

18. Houdusse, A., Kalabokis, V.N., Himmel, D., Szent-Györgyi, A.G., Cohen, C. Atomic structure of scallop myosin subfragment S1 complexed with MgADP: a novel conformation of the myosin head. *Cell*. 97, 459-70 (1999).
19. Rayment, I., Rypniewski, W.R., Schmidt-Bäse, K., Smith, R., Tomchick, D.R., Benning, M.M., Winkelmann, D.A., Wesenberg, G., Holden, H.M. Three-dimensional structure of myosin subfragment-1: a molecular motor. *Science*. 261, 50-8 (1993).
20. Dominguez, R., Freyzon, Y., Trybus, K.M., Cohen, C. Crystal structure of a vertebrate smooth muscle myosin motor domain and its complex with the essential light chain: visualization of the pre-power stroke state. *Cell*. 94, 559-71 (1998).
21. Fisher, A.J., Smith, C.A., Thoden, J.B., Smith, R., Sutoh, K., Holden, H.M., Rayment, I. X-ray structures of the myosin motor domain of *Dictyostelium discoideum* complexed with MgADP.BeFx and MgADP.AIF₄⁻. *Biochemistry*. 34, 8960-72 (1995).
22. Yount, R.G., Lawson, D., Rayment, I. Is myosin a "back door" enzyme? *Biophys J*. 68, 44S-47S; discussion 47S-49S (1995).
23. Coureux, P.D., Wells, A.L., Ménétrey, J., Yengo, C.M., Morris, C.A., Sweeney, H.L., Houdusse, A. A structural state of the myosin V motor without bound nucleotide. *Nature*. 425, 419-23 (2003).
24. Berry, C.L., Greenwald, S.E., Rivett, J.F. Static mechanical properties of the developing and mature rat aorta. *Cardiovasc Res*. 9, 669-78 (1975).
25. Cox, R.H. Comparison of arterial wall mechanics in normotensive and spontaneously hypertensive rats. *Am J Physiol*. 237, H159-67 (1979).

26. Fridez, P., Makino, A., Miyazaki, H., Meister, J.J., Hayashi, K., Stergiopoulos, N. Short-Term biomechanical adaptation of the rat carotid to acute hypertension: contribution of smooth muscle. *Ann Biomed Eng.* 29, 26-34 (2001).
27. Babu, G.J., Pyne, G.J., Zhou, Y., Okwuchukuasanya, C., Brayden, J.E., Osol, G., Paul, R.J., Low, R.B., Periasamy, M. Isoform switching from SM-B to SM-A myosin results in decreased contractility and altered expression of thin filament regulatory proteins. *Am J Physiol Cell Physiol.* 287, C723-9 (2004).
28. Babu, G.J., Loukianov, E., Loukianova, T., Pyne, G.J., Huke, S., Osol, G., Low, R.B., Paul, R.J., Periasamy, M. Loss of SM-B myosin affects muscle shortening velocity and maximal force development. *Nat Cell Biol.* 3, 1025-9 (2001).
29. Aikawa, M., Sivam, P.N., Kuro-o, M., Kimura, K., Nakahara, K., Takewaki, S., Ueda, M., Yamaguchi, H., Yazaki, Y., Periasamy, M. Human smooth muscle myosin heavy chain isoforms as molecular markers for vascular development and atherosclerosis. *Circ Res.* 73, 1000-12 (1993).
30. Kuro-o, M., Nagai, R., Nakahara, K., Katoh, H., Tsai, R.C., Tsuchimochi, H., Yazaki, Y., Ohkubo, A., Takaku, F. cDNA cloning of a myosin heavy chain isoform in embryonic smooth muscle and its expression during vascular development and in arteriosclerosis. *J Biol Chem.* 266, 3768-73 (1991).
31. Rovner, A.S., Fagnant, P.M., Lowey, S., Trybus, K.M. The carboxyl-terminal isoforms of smooth muscle myosin heavy chain determine thick filament assembly properties. *J Cell Biol.* 156, 113-23 (2002).

32. Chi, M., Zhou, Y., Vedamoorthyrao, S., Babu, G.J., Periasamy, M. Ablation of smooth muscle myosin heavy chain SM2 increases smooth muscle contraction and results in postnatal death in mice. *Proc Natl Acad Sci U S A.* 105, 18614-8 (2008).
33. Martin, A.F., Bhatti, S., Pyne-Geithman, G.J., Farjah, M., Manaves, V., Walker, L., Franks, R., Strauch, A.R., Paul, R.J. Expression and function of COOH-terminal myosin heavy chain isoforms in mouse smooth muscle. *Am J Physiol Cell Physiol.* 293, C238-45 (2007).
34. Owens, G.K., Kumar, M.S., Wamhoff, B.R. Molecular regulation of vascular smooth muscle cell differentiation in development and disease. *Physiol Rev.* 84, 767-801 (2004).
35. Owens, G.K. Regulation of differentiation of vascular smooth muscle cells. *Physiol Rev.* 75, 487-517 (1995).
36. Mack, C.P., Hinson, J.S. Regulation of smooth muscle differentiation by the myocardin family of serum response factor co-factors. *J Thromb Haemost.* 3, 1976-84 (2005).
37. Miano, J.M., Long, X., Fujiwara, K. Serum response factor: master regulator of the actin cytoskeleton and contractile apparatus. *Am J Physiol Cell Physiol.* 292, C70-81 (2007).
38. Parmacek, M.S. Myocardin-related transcription factors: critical coactivators regulating cardiovascular development and adaptation. *Circ Res.* 100, 633-44 (2007).
39. Cen, B., Selvaraj, A., Prywes, R. Myocardin/MKL family of SRF coactivators: key regulators of immediate early and muscle specific gene expression. *J Cell Biochem.* 93, 74-82 (2004).

40. Hoofnagle, M.H., Nepl, R.L., Berzin, E.L., Teg Pipes, G.C., Olson, E.N., Wamhoff, B.W., Somlyo, A.V., Owens, G.K. Myocardin is differentially required for the development of smooth muscle cells and cardiomyocytes. *Am J Physiol Heart Circ Physiol.* 300, H1707-21 (2011).
41. Nakamura, S., Hayashi, K., Iwasaki, K., Fujioka, T., Egusa, H., Yatani, H., Sobue, K. Nuclear import mechanism for myocardin family members and their correlation with vascular smooth muscle cell phenotype. *J Biol Chem.* 285, 37314-23 (2010).
42. Mack, C.P., Somlyo, A.V., Hautmann, M., Somlyo, A.P., Owens, G.K. Smooth muscle differentiation marker gene expression is regulated by RhoA-mediated actin polymerization. *J Biol Chem.* 276, 341-7 (2001).
43. Ramanath, V.S., Oh, J.K., Sundt, T.M., Eagle, K.A. Acute aortic syndromes and thoracic aortic aneurysm. *Mayo Clin Proc.* 84, 465-81 (2009).
44. *IRAD Online, International Registry of Acute Aortic Dissection.*
45. LeMaire, S.A., Russell, L. Epidemiology of thoracic aortic dissection. *Nat Rev Cardiol.* 8, 103-13 (2011).
46. Milewicz, D.M. Stopping a killer: improving the diagnosis, treatment, and prevention of acute ascending aortic dissections. *Circulation.* 124, 1902-4 (2011).
47. Castellano, J.M., Kovacic, J.C., Sanz, J., Fuster, V. Are we ignoring the dilated thoracic aorta? *Ann N Y Acad Sci.* 1254, 164-74 (2012).
48. Bunton, T.E., Biery, N.J., Myers, L., Gayraud, B., Ramirez, F., Dietz, H.C. Phenotypic alteration of vascular smooth muscle cells precedes elastolysis in a mouse model of Marfan syndrome. *Circ Res.* 88, 37-43 (2001).

49. Elefteriades, J.A. Thoracic aortic aneurysm: reading the enemy's playbook. *Yale J Biol Med.* 81, 175-86 (2008).
50. Zhang, X., Shen, Y.H., LeMaire, S.A. Thoracic aortic dissection: are matrix metalloproteinases involved? *Vascular.* 17, 147-57 (2009).
51. Elefteriades, J.A., Farkas, E.A. Thoracic aortic aneurysm clinically pertinent controversies and uncertainties. *J Am Coll Cardiol.* 55, 841-57 (2010).
52. Milewicz, D.M., Regalado, E.S., Guo, D.C. Treatment guidelines for thoracic aortic aneurysms and dissections based on the underlying causative gene. *J Thorac Cardiovasc Surg.* 140, S2-4; discussion S45-51 (2010).
53. Brooke, B.S., Habashi, J.P., Judge, D.P., Patel, N., Loeys, B., Dietz, H.C. Angiotensin II blockade and aortic-root dilation in Marfan's syndrome. *N Engl J Med.* 358, 2787-95 (2008).
54. Habashi, J.P., Judge, D.P., Holm, T.M., Cohn, R.D., Loeys, B.L., Cooper, T.K., Myers, L., Klein, E.C., Liu, G., Calvi, C., Podowski, M., Neptune, E.R., Halushka, M.K., Bedja, D., Gabrielson, K., Rifkin, D.B., Carta, L., Ramirez, F., Huso, D.L., Dietz, H.C. Losartan, an AT1 antagonist, prevents aortic aneurysm in a mouse model of Marfan syndrome. *Science.* 312, 117-21 (2006).
55. Kalra, V.B., Gilbert, J.W., Malhotra, A. Loeys-Dietz syndrome: cardiovascular, neuroradiological and musculoskeletal imaging findings. *Pediatr Radiol.* 41, 1495-504; quiz 1616 (2011).
56. Loeys, B.L., Schwarze, U., Holm, T., Callewaert, B.L., Thomas, G.H., Pannu, H., De Backer, J.F., Oswald, G.L., Symoens, S., Manouvrier, S., Roberts, A.E., Faravelli, F., Greco, M.A., Pyeritz, R.E., Milewicz, D.M., Coucke, P.J., Cameron, D.E.,

- Braverman, A.C., Byers, P.H., De Paepe, A.M., Dietz, H.C. Aneurysm syndromes caused by mutations in the TGF-beta receptor. *N Engl J Med.* 355, 788-98 (2006).
57. Regalado, E.S., Guo, D.C., Villamizar, C., Avidan, N., Gilchrist, D., McGillivray, B., Clarke, L., Bernier, F., Santos-Cortez, R.L., Leal, S.M., Bertoli-Avella, A.M., Shendure, J., Rieder, M.J., Nickerson, D.A., Milewicz, D.M. Exome sequencing identifies SMAD3 mutations as a cause of familial thoracic aortic aneurysm and dissection with intracranial and other arterial aneurysms. *Circ Res.* 109, 680-6 (2011).
58. Boileau, C., Guo, D.C., Hanna, N., Regalado, E.S., Detaint, D., Gong, L., Varret, M., Prakash, S.K., Li, A.H., d'Indy, H., Braverman, A.C., Grandchamp, B., Kwartler, C.S., Gouya, L., Santos-Cortez, R.L., Abifadel, M., Leal, S.M., Muti, C., Shendure, J., Gross, M.S., Rieder, M.J., Vahanian, A., Nickerson, D.A., Michel, J.B., Jondeau, G., Milewicz, D.M. TGFB2 mutations cause familial thoracic aortic aneurysms and dissections associated with mild systemic features of Marfan syndrome. *Nat Genet.* 44, 916-21 (2012).
59. Guo, D.C., Pannu, H., Tran-Fadulu, V., Papke, C.L., Yu, R.K., Avidan, N., Bourgeois, S., Estrera, A.L., Safi, H.J., Sparks, E., Amor, D., Ades, L., McConnell, V., Willoughby, C.E., Abuelo, D., Willing, M., Lewis, R.A., Kim, D.H., Scherer, S., Tung, P.P., Ahn, C., Buja, L.M., Raman, C.S., Shete, S.S., Milewicz, D.M. Mutations in smooth muscle alpha-actin (ACTA2) lead to thoracic aortic aneurysms and dissections. *Nat Genet.* 39, 1488-93 (2007).
60. Wang, L., Guo, D.C., Cao, J., Gong, L., Kamm, K.E., Regalado, E., Li, L., Shete, S., He, W.Q., Zhu, M.S., Offermanns, S., Gilchrist, D., Elefteriades, J., Stull, J.T.,

Milewicz, D.M. Mutations in myosin light chain kinase cause familial aortic dissections. *Am J Hum Genet.* 87, 701-7 (2010).

61. Zhu, L., Vranckx, R., Khau Van Kien, P., Lalande, A., Boisset, N., Mathieu, F., Wegman, M., Glancy, L., Gasc, J.M., Brunotte, F., Bruneval, P., Wolf, J.E., Michel, J.B., Jeunemaitre, X. Mutations in myosin heavy chain 11 cause a syndrome associating thoracic aortic aneurysm/aortic dissection and patent ductus arteriosus. *Nat Genet.* 38, 343-9 (2006).

62. Guo, D.C., Papke, C.L., Tran-Fadulu, V., Regalado, E.S., Avidan, N., Johnson, R.J., Kim, D.H., Pannu, H., Willing, M.C., Sparks, E., Pyeritz, R.E., Singh, M.N., Dalman, R.L., Grotta, J.C., Marian, A.J., Boerwinkle, E.A., Frazier, L.Q., LeMaire, S.A., Coselli, J.S., Estrera, A.L., Safi, H.J., Veeraraghavan, S., Muzny, D.M., Wheeler, D.A., Willerson, J.T., Yu, R.K., Shete, S.S., Scherer, S.E., Raman, C.S., Buja, L.M., Milewicz, D.M. Mutations in smooth muscle alpha-actin (ACTA2) cause coronary artery disease, stroke, and Moyamoya disease, along with thoracic aortic disease. *Am J Hum Genet.* 84, 617-27 (2009).

63. Milewicz, D.M., Østergaard, J.R., Ala-Kokko, L.M., Khan, N., Grange, D.K., Mendoza-Londono, R., Bradley, T.J., Olney, A.H., Adès, L., Maher, J.F., Guo, D., Buja, L.M., Kim, D., Hyland, J.C., Regalado, E.S. De novo ACTA2 mutation causes a novel syndrome of multisystemic smooth muscle dysfunction. *Am J Med Genet A.* 152A, 2437-43 (2010).

64. Inamoto, S., Kwartler, C.S., Lafont, A.L., Liang, Y.Y., Fadulu, V.T., Duraisamy, S., Willing, M., Estrera, A., Safi, H., Hannibal, M.C., Carey, J., Wiktorowicz, J., Tan, F.K., Feng, X.H., Pannu, H., Milewicz, D.M. TGFBR2 mutations alter smooth muscle

cell phenotype and predispose to thoracic aortic aneurysms and dissections. *Cardiovasc Res.* 88, 520-9 (2010).

65. Kawabata, M., Miyazono, K. Signal transduction of the TGF-beta superfamily by Smad proteins. *J Biochem.* 125, 9-16 (1999).

66. Sinha, S., Hoofnagle, M.H., Kingston, P.A., McCanna, M.E., Owens, G.K. Transforming growth factor-beta1 signaling contributes to development of smooth muscle cells from embryonic stem cells. *Am J Physiol Cell Physiol.* 287, C1560-8 (2004).

67. Deaton, R.A., Su, C., Valencia, T.G., Grant, S.R. Transforming growth factor-beta1-induced expression of smooth muscle marker genes involves activation of PKN and p38 MAPK. *J Biol Chem.* 280, 31172-81 (2005).

68. Pannu, H., Tran-Fadulu, V., Papke, C.L., Scherer, S., Liu, Y., Presley, C., Guo, D., Estrera, A.L., Safi, H.J., Brasier, A.R., Vick, G.W., Marian, A.J., Raman, C.S., Buja, L.M., Milewicz, D.M. MYH11 mutations result in a distinct vascular pathology driven by insulin-like growth factor 1 and angiotensin II. *Hum Mol Genet.* 16, 2453-62 (2007).

69. Lemaire, S.A., McDonald, M.L., Guo, D.C., Russell, L., Miller, C.C., Johnson, R.J., Bekheirnia, M.R., Franco, L.M., Nguyen, M., Pyeritz, R.E., Bavaria, J.E., Devereux, R., Maslen, C., Holmes, K.W., Eagle, K., Body, S.C., Seidman, C., Seidman, J.G., Isselbacher, E.M., Bray, M., Coselli, J.S., Estrera, A.L., Safi, H.J., Belmont, J.W., Leal, S.M., Milewicz, D.M. Genome-wide association study identifies a susceptibility locus for thoracic aortic aneurysms and aortic dissections spanning FBN1 at 15q21.1. *Nat Genet.* 43, 996-1000 (2011).

70. Prakash, S.K., LeMaire, S.A., Guo, D.C., Russell, L., Regalado, E.S., Golabbakhsh, H., Johnson, R.J., Safi, H.J., Estrera, A.L., Coselli, J.S., Bray, M.S., Leal, S.M., Milewicz, D.M., Belmont, J.W. Rare copy number variants disrupt genes regulating vascular smooth muscle cell adhesion and contractility in sporadic thoracic aortic aneurysms and dissections. *Am J Hum Genet.* 87, 743-56 (2010).
71. Roopnarine, Leinwand Functional analysis of myosin mutations that cause familial hypertrophic cardiomyopathy. *Biophysical Journal.* 75, 3023-3030 (1998).
72. Sata, M., Ikebe, M. Functional analysis of the mutations in the human cardiac beta-myosin that are responsible for familial hypertrophic cardiomyopathy. Implication for the clinical outcome. *J Clin Invest.* 98, 2866-73 (1996).
73. Kuang, S.Q., Kwartler, C.S., Byanova, K.L., Pham, J., Gong, L., Prakash, S.K., Huang, J., Kamm, K.E., Stull, J.T., Sweeney, H.L., Milewicz, D.M. Rare, nonsynonymous variant in the smooth muscle-specific isoform of myosin heavy chain, MYH11, R247C, alters force generation in the aorta and phenotype of smooth muscle cells. *Circ Res.* 110, 1411-22 (2012).
74. Kuo, J.C., Han, X., Hsiao, C.T., Yates, J.R., Waterman, C.M. Analysis of the myosin-II-responsive focal adhesion proteome reveals a role for β -Pix in negative regulation of focal adhesion maturation. *Nat Cell Biol.* 13, 383-93 (2011).
75. Geiger, B., Tokuyasu, K.T., Dutton, A.H., Singer, S.J. Vinculin, an intracellular protein localized at specialized sites where microfilament bundles terminate at cell membranes. *Proc Natl Acad Sci U S A.* 77, 4127-31 (1980).

76. Parsons, J.T., Martin, K.H., Slack, J.K., Taylor, J.M., Weed, S.A. Focal adhesion kinase: a regulator of focal adhesion dynamics and cell movement. *Oncogene*. 19, 5606-13 (2000).
77. Hendzel, M.J., Wei, Y., Mancini, M.A., Van Hooser, A., Ranalli, T., Brinkley, B.R., Bazett-Jones, D.P., Allis, C.D. Mitosis-specific phosphorylation of histone H3 initiates primarily within pericentromeric heterochromatin during G2 and spreads in an ordered fashion coincident with mitotic chromosome condensation. *Chromosoma*. 106, 348-60 (1997).
78. Geiger, B., Spatz, J.P., Bershadsky, A.D. Environmental sensing through focal adhesions. *Nat Rev Mol Cell Biol*. 10, 21-33 (2009).
79. Parsons, J.T., Horwitz, A.R., Schwartz, M.A. Cell adhesion: integrating cytoskeletal dynamics and cellular tension. *Nat Rev Mol Cell Biol*. 11, 633-43 (2010).
80. Liu, B., Itoh, H., Louie, O., Kubota, K., Kent, K.C. The signaling protein Rho is necessary for vascular smooth muscle migration and survival but not for proliferation. *Surgery*. 132, 317-25 (2002).
81. Shen, D., Li, J., Lepore, J.J., Anderson, T.J., Sinha, S., Lin, A.Y., Cheng, L., Cohen, E.D., Roberts, J.D., Dedhar, S., Parmacek, M.S., Gerszten, R.E. Aortic aneurysm generation in mice with targeted deletion of integrin-linked kinase in vascular smooth muscle cells. *Circ Res*. 109, 616-28 (2011).
82. Morano, I., Chai, G.X., Baltas, L.G., Lamounier-Zepter, V., Lutsch, G., Kott, M., Haase, H., Bader, M. Smooth-muscle contraction without smooth-muscle myosin. *Nat Cell Biol*. 2, 371-5 (2000).

83. Isotani, E., Zhi, G., Lau, K.S., Huang, J., Mizuno, Y., Persechini, A., Geguchadze, R., Kamm, K.E., Stull, J.T. Real-time evaluation of myosin light chain kinase activation in smooth muscle tissues from a transgenic calmodulin-biosensor mouse. *Proc Natl Acad Sci U S A*. 101, 6279-84 (2004).
84. Mizuno, Y., Isotani, E., Huang, J., Ding, H., Stull, J.T., Kamm, K.E. Myosin light chain kinase activation and calcium sensitization in smooth muscle in vivo. *Am J Physiol Cell Physiol*. 295, C358-64 (2008).
85. Schildmeyer, L.A., Braun, R., Taffet, G., Debiasi, M., Burns, A.E., Bradley, A., Schwartz, R.J. Impaired vascular contractility and blood pressure homeostasis in the smooth muscle alpha-actin null mouse. *FASEB J*. 14, 2213-20 (2000).
86. Kim, T.E., Smith, D.D. Thoracic aortic dissection in an 18-year-old woman with no risk factors. *J Emerg Med*. 38, e41-4 (2010).
87. Pannu, H., Fadulu, V.T., Chang, J., Lafont, A., Hasham, S.N., Sparks, E., Giampietro, P.F., Zaleski, C., Estrera, A.L., Safi, H.J., Shete, S., Willing, M.C., Raman, C.S., Milewicz, D.M. Mutations in transforming growth factor-beta receptor type II cause familial thoracic aortic aneurysms and dissections. *Circulation*. 112, 513-20 (2005).
88. Kuang, S.Q., Guo, D.C., Prakash, S.K., McDonald, M.L., Johnson, R.J., Wang, M., Regalado, E.S., Russell, L., Cao, J.M., Kwartler, C., Fraivillig, K., Coselli, J.S., Safi, H.J., Estrera, A.L., Leal, S.M., Lemaire, S.A., Belmont, J.W., Milewicz, D.M., GenTAC Investigators Recurrent chromosome 16p13.1 duplications are a risk factor for aortic dissections. *PLoS Genet*. 7, e1002118 (2011).

89. Ingason, A., Rujescu, D., Cichon, S., Sigurdsson, E., Sigmundsson, T., Pietiläinen, O.P., Buizer-Voskamp, J.E., Strengman, E., Francks, C., Muglia, P., Gylfason, A., Gustafsson, O., Olason, P.I., Steinberg, S., Hansen, T., Jakobsen, K.D., Rasmussen, H.B., Giegling, I., Möller, H.J., Hartmann, A., Crombie, C., Fraser, G., Walker, N., Lonnqvist, J., Suvisaari, J., Tuulio-Henriksson, A., Bramon, E., Kiemene, L.A., Franke, B., Murray, R., Vassos, E., Toulopoulou, T., Mühleisen, T.W., Tosato, S., Ruggeri, M., Djurovic, S., Andreassen, O.A., Zhang, Z., Werge, T., Ophoff, R.A., Rietschel, M., Nöthen, M.M., Petursson, H., Stefansson, H., Peltonen, L., Collier, D., Stefansson, K., St Clair, D.M. Copy number variations of chromosome 16p13.1 region associated with schizophrenia. *Mol Psychiatry*. 16, 17-25 (2011).
90. Liu, J.Y., Kasperavičiūtė, D., Martinian, L., Thom, M., Sisodiya, S.M. Neuropathology of 16p13.11 deletion in epilepsy. *PLoS One*. 7, e34813 (2012).
91. Ramalingam, A., Zhou, X.G., Fiedler, S.D., Brawner, S.J., Joyce, J.M., Liu, H.Y., Yu, S. 16p13.11 duplication is a risk factor for a wide spectrum of neuropsychiatric disorders. *J Hum Genet*. 56, 541-4 (2011).
92. Babu, G.J., Warshaw, D.M., Periasamy, M. Smooth muscle myosin heavy chain isoforms and their role in muscle physiology. *Microsc Res Tech*. 50, 532-40 (2000).
93. Barral, J.M., Hutagalung, A.H., Brinker, A., Hartl, F.U., Epstein, H.F. Role of the myosin assembly protein UNC-45 as a molecular chaperone for myosin. *Science*. 295, 669-71 (2002).
94. Price, M.G., Landsverk, M.L., Barral, J.M., Epstein, H.F. Two mammalian UNC-45 isoforms are related to distinct cytoskeletal and muscle-specific functions. *J Cell Sci*. 115, 4013-23 (2002).

95. Landsverk, M.L., Li, S., Hutagalung, A.H., Najafov, A., Hoppe, T., Barral, J.M., Epstein, H.F. The UNC-45 chaperone mediates sarcomere assembly through myosin degradation in *Caenorhabditis elegans*. *J Cell Biol.* 177, 205-10 (2007).
96. Croons, V., Martinet, W., Herman, A.G., Timmermans, J.P., De Meyer, G.R. Selective clearance of macrophages in atherosclerotic plaques by the protein synthesis inhibitor cycloheximide. *J Pharmacol Exp Ther.* 320, 986-93 (2007).
97. Croons, V., Martinet, W., Herman, A.G., De Meyer, G.R. Differential effect of the protein synthesis inhibitors puromycin and cycloheximide on vascular smooth muscle cell viability. *J Pharmacol Exp Ther.* 325, 824-32 (2008).
98. Martin, A.F., Rabinowitz, M., Blough, R., Prior, G., Zak, R. Measurements of half-life of rat cardiac myosin heavy chain with leucyl-tRNA used as precursor pool. *J Biol Chem.* 252, 3422-9 (1977).
99. Zak, R., Martin, A.F., Prior, G., Rabinowitz, M. Comparison of turnover of several myofibrillar proteins and critical evaluation of double isotope method. *J Biol Chem.* 252, 3430-5 (1977).
100. McLeland, C.B., Rodriguez, J., Stern, S.T. Autophagy monitoring assay: qualitative analysis of MAP LC3-I to II conversion by immunoblot. *Methods Mol Biol.* 697, 199-206 (2011).
101. Bjørkøy, G., Lamark, T., Pankiv, S., Øvervatn, A., Brech, A., Johansen, T. Monitoring autophagic degradation of p62/SQSTM1. *Methods Enzymol.* 452, 181-97 (2009).
102. Jung, C.H., Ro, S.H., Cao, J., Otto, N.M., Kim, D.H. mTOR regulation of autophagy. *FEBS Lett.* 584, 1287-95 (2010).

103. Egan, D., Kim, J., Shaw, R.J., Guan, K.L. The autophagy initiating kinase ULK1 is regulated via opposing phosphorylation by AMPK and mTOR. *Autophagy*. 7, 643-4 (2011).
104. Meijer, A.J., Dubbelhuis, P.F. Amino acid signaling and the integration of metabolism. *Biochemical and Biophysical Research Communications*. 313, 397-403 (2004).
105. Salazar, M., Hernández-Tiedra, S., Torres, S., Lorente, M., Guzmán, M., Velasco, G. Detecting autophagy in response to ER stress signals in cancer. *Methods Enzymol*. 489, 297-317 (2011).
106. Schröder, M., Kaufman, R.J. The mammalian unfolded protein response. *Annu Rev Biochem*. 74, 739-89 (2005).
107. Ron, D., Walter, P. Signal integration in the endoplasmic reticulum unfolded protein response. *Nat Rev Mol Cell Biol*. 8, 519-29 (2007).
108. Kuznetsov, G., Chen, L.B., Nigam, S.K. Several endoplasmic reticulum stress proteins, including ERp72, interact with thyroglobulin during its maturation. *J Biol Chem*. 269, 22990-5 (1994).
109. Tabas, I., Ron, D. Integrating the mechanisms of apoptosis induced by endoplasmic reticulum stress. *Nat Cell Biol*. 13, 184-90 (2011).
110. Ayala, P., Montenegro, J., Vivar, R., Letelier, A., Urroz, P.A., Copaja, M., Pivet, D., Humeres, C., Troncoso, R., Vicencio, J.M., Lavandero, S., Díaz-Araya, G. Attenuation of endoplasmic reticulum stress using the chemical chaperone 4-phenylbutyric acid prevents cardiac fibrosis induced by isoproterenol. *Exp Mol Pathol*. 92, 97-104 (2012).

111. Mimori, S., Okuma, Y., Kaneko, M., Kawada, K., Hosoi, T., Ozawa, K., Nomura, Y., Hamana, H. Protective effects of 4-phenylbutyrate derivatives on the neuronal cell death and endoplasmic reticulum stress. *Biol Pharm Bull.* 35, 84-90 (2012).
112. Park, C.S., Cha, H., Kwon, E.J., Sreenivasaiah, P.K., Kim, d.o. .H. The chemical chaperone 4-phenylbutyric acid attenuates pressure-overload cardiac hypertrophy by alleviating endoplasmic reticulum stress. *Biochem Biophys Res Commun.* 421, 578-84 (2012).
113. Sandri, M. Autophagy in health and disease. 3. Involvement of autophagy in muscle atrophy. *Am J Physiol Cell Physiol.* 298, C1291-7 (2010).
114. Yang, Y.P., Liang, Z.Q., Gu, Z.L., Qin, Z.H. Molecular mechanism and regulation of autophagy. *Acta Pharmacol Sin.* 26, 1421-34 (2005).
115. Longatti, A., Tooze, S.A. Vesicular trafficking and autophagosome formation. *Cell Death Differ.* 16, 956-65 (2009).
116. Heng, M.Y., Duong, D.K., Albin, R.L., Tallaksen-Greene, S.J., Hunter, J.M., Lesort, M.J., Osmand, A., Paulson, H.L., Detloff, P.J. Early autophagic response in a novel knock-in model of Huntington disease. *Hum Mol Genet.* 19, 3702-20 (2010).
117. Jia, G., Cheng, G., Gangahar, D.M., Agrawal, D.K. Insulin-like growth factor-1 and TNF-alpha regulate autophagy through c-jun N-terminal kinase and Akt pathways in human atherosclerotic vascular smooth cells. *Immunol Cell Biol.* 84, 448-54 (2006).
118. Wei, H., Wei, S., Gan, B., Peng, X., Zou, W., Guan, J.L. Suppression of autophagy by FIP200 deletion inhibits mammary tumorigenesis. *Genes Dev.* 25, 1510-27 (2011).

119. Wei, H., Guan, J.L. Pro-tumorigenic function of autophagy in mammary oncogenesis. *Autophagy*. 8, 129-31 (2012).
120. Nobukuni, T., Kozma, S.C., Thomas, G. hvps34, an ancient player, enters a growing game: mTOR Complex1/S6K1 signaling. *Curr Opin Cell Biol*. 19, 135-41 (2007).
121. She, P., Zhang, Z., Marchionini, D., Diaz, W.C., Jetton, T.J., Kimball, S.R., Vary, T.C., Lang, C.H., Lynch, C.J. Molecular characterization of skeletal muscle atrophy in the R6/2 mouse model of Huntington's disease. *Am J Physiol Endocrinol Metab*. 301, E49-61 (2011).
122. Avruch, J., Long, X., Ortiz-Vega, S., Rapley, J., Papageorgiou, A., Dai, N. Amino acid regulation of TOR complex 1. *Am J Physiol Endocrinol Metab*. 296, E592-602 (2009).
123. Narita, M., Inoki, K. Rags connect mTOR and autophagy. *Small GTPases*. 3, 111-4 (2012).
124. Sancak, Y., Peterson, T.R., Shaul, Y.D., Lindquist, R.A., Thoreen, C.C., Bar-Peled, L., Sabatini, D.M. The Rag GTPases bind raptor and mediate amino acid signaling to mTORC1. *Science*. 320, 1496-501 (2008).
125. Sancak, Y., Bar-Peled, L., Zoncu, R., Markhard, A.L., Nada, S., Sabatini, D.M. Ragulator-Rag complex targets mTORC1 to the lysosomal surface and is necessary for its activation by amino acids. *Cell*. 141, 290-303 (2010).
126. Young, A.R., Narita, M., Narita, M. Spatio-temporal association between mTOR and autophagy during cellular senescence. *Autophagy*. 7, 1387-8 (2011).

127. Rayavarapu, S., Coley, W., Nagaraju, K. Endoplasmic reticulum stress in skeletal muscle homeostasis and disease. *Curr Rheumatol Rep.* 14, 238-43 (2012).
128. Sarkar, S., Rubinsztein, D.C. Inositol and IP3 levels regulate autophagy: biology and therapeutic speculations. *Autophagy.* 2, 132-4 (2006).
129. Williams, A., Sarkar, S., Cuddon, P., Ttofi, E.K., Saiki, S., Siddiqi, F.H., Jahreiss, L., Fleming, A., Pask, D., Goldsmith, P., O'Kane, C.J., Floto, R.A., Rubinsztein, D.C. Novel targets for Huntington's disease in an mTOR-independent autophagy pathway. *Nat Chem Biol.* 4, 295-305 (2008).
130. Ejiri, J., Inoue, N., Tsukube, T., Munezane, T., Hino, Y., Kobayashi, S., Hirata, K., Kawashima, S., Imajoh-Ohmi, S., Hayashi, Y., Yokozaki, H., Okita, Y., Yokoyama, M. Oxidative stress in the pathogenesis of thoracic aortic aneurysm: protective role of statin and angiotensin II type 1 receptor blocker. *Cardiovasc Res.* 59, 988-96 (2003).
131. Xiong, W., Mactaggart, J., Knispel, R., Worth, J., Zhu, Z., Li, Y., Sun, Y., Baxter, B.T., Johanning, J. Inhibition of reactive oxygen species attenuates aneurysm formation in a murine model. *Atherosclerosis.* 202, 128-34 (2009).
132. Lichter-Konecki, U., Diaz, G.A., Merritt, J.L., Feigenbaum, A., Jomphe, C., Marier, J.F., Beliveau, M., Mauney, J., Dickinson, K., Martinez, A., Mokhtarani, M., Scharschmidt, B., Rhead, W. Ammonia control in children with urea cycle disorders (UCDs); phase 2 comparison of sodium phenylbutyrate and glycerol phenylbutyrate. *Mol Genet Metab.* 103, 323-9 (2011).
133. Fauci, A.S.1. *Harrison's principles of internal medicine* . 2754 (McGraw-Hill Medical: New York , 2008).

134. Stary, H.C., Chandler, A.B., Dinsmore, R.E., Fuster, V., Glagov, S., Insull, W., Rosenfeld, M.E., Schwartz, C.J., Wagner, W.D., Wissler, R.W. A definition of advanced types of atherosclerotic lesions and a histological classification of atherosclerosis. A report from the Committee on Vascular Lesions of the Council on Arteriosclerosis, American Heart Association. *Circulation*. 92, 1355-74 (1995).
135. Topol, E.J., Smith, J., Plow, E.F., Wang, Q.K. Genetic susceptibility to myocardial infarction and coronary artery disease. *Hum Mol Genet*. 15 Spec No 2, R117-23 (2006).
136. Wang, Q. Molecular genetics of coronary artery disease. *Curr Opin Cardiol*. 20, 182-8 (2005).
137. Fukui, M. Guidelines for the diagnosis and treatment of spontaneous occlusion of the circle of Willis ('moyamoya' disease). Research Committee on Spontaneous Occlusion of the Circle of Willis (Moyamoya Disease) of the Ministry of Health and Welfare, Japan. *Clin Neurol Neurosurg*. 99 Suppl 2, S238-40 (1997).
138. Haltia, M., Iivanainen, M., Majuri, H., Puranen, M. Spontaneous occlusion of the circle of Willis (moyamoya syndrome). *Clin Neuropathol*. 1, 11-22 (1982).
139. Aoyagi, M., Fukai, N., Yamamoto, M., Nakagawa, K., Matsushima, Y., Yamamoto, K. Early development of intimal thickening in superficial temporal arteries in patients with moyamoya disease. *Stroke*. 27, 1750-4 (1996).
140. Masuda, J., Ogata, J., Yutani, C. Smooth muscle cell proliferation and localization of macrophages and T cells in the occlusive intracranial major arteries in moyamoya disease. *Stroke*. 24, 1960-7 (1993).

141. Ikeda, K., Watanabe, K., Suzuki, H., Oshima, T., Tanno, N., Shimomura, A., Sunose, H., Takasaka, T., Ikeda, H., Yoshimoto, T. Nasal airway resistance and olfactory acuity following transsphenoidal pituitary surgery. *Am J Rhinol.* 13, 45-8 (1999).
142. Inoue, T.K., Ikezaki, K., Sasazuki, T., Matsushima, T., Fukui, M. Linkage analysis of moyamoya disease on chromosome 6. *J Child Neurol.* 15, 179-82 (2000).
143. Sakurai, K., Horiuchi, Y., Ikeda, H., Ikezaki, K., Yoshimoto, T., Fukui, M., Arinami, T. A novel susceptibility locus for moyamoya disease on chromosome 8q23. *J Hum Genet.* 49, 278-81 (2004).
144. Karnik, S.K., Brooke, B.S., Bayes-Genis, A., Sorensen, L., Wythe, J.D., Schwartz, R.S., Keating, M.T., Li, D.Y. A critical role for elastin signaling in vascular morphogenesis and disease. *Development.* 130, 411-23 (2003).
145. Perejda, A.J., Abraham, P.A., Carnes, W.H., Coulson, W.F., Uitto, J. Marfan's syndrome: structural, biochemical, and mechanical studies of the aortic media. *J Lab Clin Med.* 106, 376-83 (1985).
146. Scheck, M., Siegel, R.C., Parker, J., Chang, Y.H., Fu, J.C. Aortic aneurysm in Marfan's syndrome: changes in the ultrastructure and composition of collagen. *J Anat.* 129, 645-57 (1979).
147. Dietz, H.C., Cutting, G.R., Pyeritz, R.E., Maslen, C.L., Sakai, L.Y., Corson, G.M., Puffenberger, E.G., Hamosh, A., Nanthakumar, E.J., Curristin, S.M. Marfan syndrome caused by a recurrent de novo missense mutation in the fibrillin gene. *Nature.* 352, 337-9 (1991).

148. Isogai, Z., Ono, R.N., Ushiro, S., Keene, D.R., Chen, Y., Mazzieri, R., Charbonneau, N.L., Reinhardt, D.P., Rifkin, D.B., Sakai, L.Y. Latent transforming growth factor beta-binding protein 1 interacts with fibrillin and is a microfibril-associated protein. *J Biol Chem.* 278, 2750-7 (2003).
149. Neptune, E.R., Frischmeyer, P.A., Arking, D.E., Myers, L., Bunton, T.E., Gayraud, B., Ramirez, F., Sakai, L.Y., Dietz, H.C. Dysregulation of TGF-beta activation contributes to pathogenesis in Marfan syndrome. *Nat Genet.* 33, 407-11 (2003).
150. Jones, J.A., Spinale, F.G., Ikonomidis, J.S. Transforming growth factor-beta signaling in thoracic aortic aneurysm development: a paradox in pathogenesis. *J Vasc Res.* 46, 119-37 (2009).
151. Marque, V., Kieffer, P., Gayraud, B., Lartaud-Idjouadiene, I., Ramirez, F., Atkinson, J. Aortic Wall Mechanics and Composition in a Transgenic Mouse Model of Marfan Syndrome. *Arteriosclerosis, Thrombosis, and Vascular Biology.* 21, 1184-1189 (2001).
152. Lu, H., Rateri, D.L., Cassis, L.A., Daugherty, A. The role of the renin-angiotensin system in aortic aneurysmal diseases. *Curr Hypertens Rep.* 10, 99-106 (2008).
153. Daugherty, A., Rateri, D.L., Charo, I.F., Owens, A.P., Howatt, D.A., Cassis, L.A. Angiotensin II infusion promotes ascending aortic aneurysms: attenuation by CCR2 deficiency in apoE^{-/-} mice. *Clin Sci (Lond).* 118, 681-9 (2010).
154. Habashi, J.P., Doyle, J.J., Holm, T.M., Aziz, H., Schoenhoff, F., Bedja, D., Chen, Y., Modiri, A.N., Judge, D.P., Dietz, H.C. Angiotensin II type 2 receptor signaling

- attenuates aortic aneurysm in mice through ERK antagonism. *Science*. 332, 361-5 (2011).
155. Rakesh, K., Yoo, B., Kim, I.M., Salazar, N., Kim, K.S., Rockman, H.A. beta-Arrestin-biased agonism of the angiotensin receptor induced by mechanical stress. *Sci Signal*. 3, ra46 (2010).
156. Zou, Y., Akazawa, H., Qin, Y., Sano, M., Takano, H., Minamino, T., Makita, N., Iwanaga, K., Zhu, W., Kudoh, S., Toko, H., Tamura, K., Kihara, M., Nagai, T., Fukamizu, A., Umemura, S., Iiri, T., Fujita, T., Komuro, I. Mechanical stress activates angiotensin II type 1 receptor without the involvement of angiotensin II. *Nat Cell Biol*. 6, 499-506 (2004).
157. Judge, D.P., Biery, N.J., Keene, D.R., Geubtner, J., Myers, L., Huso, D.L., Sakai, L.Y., Dietz, H.C. Evidence for a critical contribution of haploinsufficiency in the complex pathogenesis of Marfan syndrome. *J Clin Invest*. 114, 172-81 (2004).
158. Pereira, L., Lee, S.Y., Gayraud, B., Andrikopoulos, K., Shapiro, S.D., Bunton, T., Biery, N.J., Dietz, H.C., Sakai, L.Y., Ramirez, F. Pathogenetic sequence for aneurysm revealed in mice underexpressing fibrillin-1. *Proc Natl Acad Sci U S A*. 96, 3819-23 (1999).
159. Xiong, W., Knispel, R.A., Dietz, H.C., Ramirez, F., Baxter, B.T. Doxycycline delays aneurysm rupture in a mouse model of Marfan syndrome. *J Vasc Surg*. 47, 166-72; discussion 172 (2008).
160. Xiong, W., Meisinger, T., Knispel, R., Worth, J.M., Baxter, B.T. MMP-2 regulates Erk1/2 phosphorylation and aortic dilatation in Marfan syndrome. *Circ Res*. 110, e92-e101 (2012).

161. Tieu, B.C., Lee, C., Sun, H., Lejeune, W., Recinos, A., Ju, X., Spratt, H., Guo, D.C., Milewicz, D., Tilton, R.G., Brasier, A.R. An adventitial IL-6/MCP1 amplification loop accelerates macrophage-mediated vascular inflammation leading to aortic dissection in mice. *J Clin Invest.* 119, 3637-51 (2009).
162. Weber, D.S., Rocic, P., Mellis, A.M., Laude, K., Lyle, A.N., Harrison, D.G., Griending, K.K. Angiotensin II-induced hypertrophy is potentiated in mice overexpressing p22phox in vascular smooth muscle. *Am J Physiol Heart Circ Physiol.* 288, H37-42 (2005).
163. Bauvy, C., Meijer, A.J., Codogno, P. Assaying of Autophagic Protein Degradation. *Methods in Enzymology.* 452, 47-61 (2009).
164. Ngo, P., Ramalingam, P., Phillips, J.A., Furuta, G.T. Collagen Gel Contraction Assay. *Methods in Molecular Biology.* 341: 103-109 (2006).
165. Trepakova, E.S., Gericke, M., Hirakawa, Y., Weisbrod, R.M., Cohen, R.A., Bolotina, V.M. Properties of a Native Cation Channel Activated by Ca²⁺ Store Depletion in Vascular Smooth Muscle Cells. *Journal of Biological Chemistry.* 276: 7782-7790 (2001).

Vita

Callie Savannah Kwartler was born in Houston, TX on February 22, 1985 and is the daughter of Murray Jules Fogler and Teresa Wiggins Fogler. After graduating successfully from St. John's School in Houston, TX in May 2003, she went on to attend Amherst College in Amherst, MA, from which she earned the degree of Bachelor of Arts in Biology and Women's and Gender Studies *cum laude* in May 2007. Callie married Eric Glen Kwartler in January 2008 before enrolling at the University of Texas Graduate School of Biomedical Sciences in August 2008. She will graduate with a Doctor of Philosophy in May 2013.

Permanent address:

3610 Sunset Blvd
Houston, TX 77005

Email: callie.fogler@gmail.com